STABILIZATION OF ELECTRODYNAMIC BEARINGS WITH ACTIVE MAGNETIC DAMPERS

PAR

Qingwen CUI

acceptée sur proposition du jury:

Prof. Y. Perriard, président du jury
Prof. H. Bleuler, directeur de thèse
Prof. B. Dehez, rapporteur
Prof. A. Tonoli, rapporteur
Prof. J. Schiffmann, rapporteur

Acknowledgements

Lausanne, August 2016   Qingwen CUI

Abstract

Electrodynamic Bearings (EDBs) are a kind of passive magnetic bearings that exploit the interaction between the induced eddy currents in a conductor and a magnetic field to provide restoring forces. They have been regarded as an appealing alternative to Active Magnetic Bearings (AMBs), having the ability to provide positive stiffness passively without introducing negative stiffness in any direction. Compared to AMBs, EDBs present advantages such as lower cost and higher reliability due to simplicity of configurations. One of the most interesting features of EDBs is the possibility to obtain stable levitation using standard conductive materials at room temperature, requiring no control systems, power electronics or sensors. Thus EDBs could be suitable solutions for high–speed rotating machinery such as flywheels, small size compressors, centrifuges and vaccum pumps.

Despite these promising characteristics of EDBs, applications are still limited because of instability issues. The main problem is that the effect of the rotating damping force in EDBs causes unstable behavior of the rotor. In existing solutions, stabilization is achieved mainly by introducing non-rotating damping to the rotor with passive ways. Although stable levitation is possible, the effectiveness of the existing methods is still limited. A hybrid solution has been proposed in this thesis, where EDBs are combined with active magnetic dampers (AMDs). Using similar magnetic actuators as those used in classical active magnetic bearings (AMBs), non–rotating damping forces are applied on the rotor supported by EDBs to obtain stable operation. This system is designed to exploit the high reliability of EDBs, overcoming the stability problem by means of controllable AMDs. It results in increased global system reliability. In case of AMBs failure, the EDBs are able to guarantee a stable levitation down to a certain speed considered safe for touch–down. During the operation speed range, the AMDs provide non–rotating damping to stabilize the rotor. This non–rotating damping can be easily tuned during rotor operation phase. At low speeds when the EDB forces are not sufficient to support the rotor, the active magnetic actuators work as AMBs to guarantee stable levitation of the rotor in a wide speed range. Besides, the EDB–AMD configuration also allows characterizing in dynamic condition, which opens the possibility to establish damping strategy that can in perspective be implemented by totally passive means, such as eddy currents, elastomeric mounts.

The combination of EDB and AMD forces are studied both analytically and experimentally. An analytical model of the system, as well as a test rig, has been built. Simulations and experimental tests validate the model and characterize the system. The effectiveness of the proposed solution is confirmed. The control strategy of AMDs and stabilizing alternatives of EDBs are discussed consequently. The combination of EDB and AMD can be exploited to investigate easily different damping strategies.

Keywords

Sommario

I cuscinetti elettrodinamici (in inglese "Electrodynamic Bearings" da cui la sigla EDBs) sono una tipologia di cuscinetti magnetici passivi che sfruttano l'interazione fra le correnti parassite indotte in un conduttore ed un campo magnetico al fine di ottenere forze di stabilizzazione. Sono considerati una possibile alternativa ai cuscinetti magnetici attivi ("Active Magnetic Bearings", AMBs) per la loro capacità di fornire una rigidezza positiva al sistema in modo passivo, senza introdurre una rigidezza negativa in nessuna direzione. In confronto agli AMBs, gli EDBs risultano vantaggiosi per il costo ridotto e la maggiore affidabilità dovuta alla semplicità delle configurazioni. Una delle caratteristiche più interessanti degli EDBs è la possibilità di ottenere una levitazione stabile usando materiali conduttori standard a temperatura ambiente, senza richiedere sistemi di controllo, elettronica di potenza o sensori. Perciò gli EDBs possono essere una soluzione adatta per macchine rotanti ad alta velocità come volani, compressori di piccole dimensioni,centrifughe e pompe a vuoto.

Nonostante queste caratteristiche promettenti degli EDBs, le applicazioni sono ancora limitate per problemi di instabilità. Il problema principale è dato dal fatto che l'effetto della forza rotante di smorzamento negli EDBs causa un comportamento instabile del rotore. Nelle soluzioni esistenti, la stabilizzazione è ottenuta principalmente introducendo uno smorzamento non rotante al rotore in modo passivo. Nonostante la levitazione stabile sia possibile, l'efficacia dei metodi esistenti è ancora limitata. In questa tesi si propone una soluzione ibrida, dove l'azione degli EDBs è combinata con quella di smorzatori magnetici attivi ("Active Magnetic Dampers", AMDs). Usando degli attuatori magnetici simili a quelli utilizzati nei classici cuscinetti magnetici attivi (AMBs), delle forze non rotanti di smorzamento sono applicate al rotore supportato dagli EDBs per ottenere una operazione stabile. Tale sistema è progettato al fine di sfruttare l'alta affidabilità degli EDBs, superando i problemi di instabilità attraverso AMDs controllabili. Questo metodo permette di ottenere in definitiva una maggiore affidabilità del sistema globale. Nel caso di guasto degli AMBs, gli EDBs sono capaci di garantire una levitazione stabile fino a determinate basse velocità considerate sicure per lo spegnimento del sistema (indicato con il termine "touch-down"). All'interno dell'intervallo di velocità di funzionamento, gli AMDs conferiscono uno smorzamento non rotante per stabilizzare il rotore. Questo smorzamento non rotante può facilmente essere calibrato durante la fase di operazione del rotore. A basse velocità quando le forza degli EDBs non sono sufficienti per supportare il rotore, gli attuatori magnetici attivi lavorano come AMBs per garantire una levitazione stabile del rotore in un ampio intervallo di velocità. Inoltre la configurazione EDB-AMD permette anche una caratterizzazione delle condizioni dinamiche, fatto che apre la possibilità di stabilire una strategia di smorzamento che può in prospettiva essere implementata da soluzioni completamente passive, come supporti a correnti parassite o elastomerici.

Lo studio della combinazione delle forze di EDBs e AMDs è condotto sia analiticamente che sperimentalmente mediante la costruzione sia di un modello analitico che di un banco prova dedicato. Simulazioni e test sperimentali sono utilizzati per validare il modello e caratterizzare il sistema. L'efficacia della soluzione proposta è confermata. Si discutono infine la strategia di controllo degli AMDs e alcune alternative di stabilizzazione per gli EDBs.

Keywords

Cuscinetti elettrodinamici, Smorzatori magnetici attivi, Forze non rotanti di smorzamento, Rotordynamics, stabilità del sistema

Contents

List of Figures

Chapter 1 Introduction

Magnetic bearings (MBs) are able to provide contactless suspension for rotors exploiting magnetic forces. Compared to conventional mechanical bearings, MBs present several advantages including elimination of lubrication, friction-free operation and absence of mechanical wear [1]. Therefore they are attractive for applications with high rotating speeds and high power density. Active magnetic bearings (AMBs) are the classical magnetic bearings that have been under research for years and have reached the level of industrial applications. However, the system complexity and resulting high costs due to power electronics and control units limit the applications of AMBs, although the controllability of rotordynamics in AMB systems is indeed an advantage. Therefore, Passive magnetic bearings (PMBs) have drawn plenty of attentions. Permanent magnet bearings, as most common kind of PMBs, have also reached a good level of development. They are attractive for applications with constraints of cost and size. But as well known from Earnshaw's theorem [2], stable levitation cannot be obtained with solely permanent magnets. Thus permanent magnetic bearings are always used together with other kinds of bearings. For example, in the field of vacuum technologies, permanent magnetic bearings are used in combination with conventional ball bearings or AMBs. The main drawbacks of permanent magnetic bearings are the negative stiffness which needs to be compensated and the lack of real time control and monitoring.

1.1   Electrodynamic bearings

Electrodynamic bearings (EDBs), as another kind of passive magnetic bearings, have been regarded as an appealing alternative, having the ability to provide stiffness passively without introducing negative stiffness in any direction. EDBs provide restoring force on the rotor exploiting the interaction between the induced eddy currents in the conductor with relative motion in the magnetic field. They have the possibility to obtain stable levitation using standard conductive materials at room temperature, requiring no control systems, power electronics or sensors. Despite promising characteristics, rotors supported by EDBs are subject to different types of instabilities [3] [4]. The cooresponding stabilization solution is highly demanded.

1.2   Motivation

Similar to hydrodynamic bearings, EDB systems provide levitation only when the rotating speed is above a threshold. Besides, the effect of the rotating damping force arising in the conductor on the rotor also causes unstable behavior of the rotor. Two main solutions based on passive systems have been proposed in literature. Filatov et al. [5] presented a solution with eddy current dampers to introduce non-rotating damping between the rotor and the stator. Tonoli et al. [6] proposed to introduce an elastic and dissipative element between the statoric part of the bearing and the base

of the machine. Although stable levitation is possible, the effectiveness of the existing methods is still limited [7]. They do not allow fully levitating the rotor at low rotating speeds. Besides, the amount of damping could only be modified during the design phase. These issues limit the applications of EDBs and require more efforts to find an optimal solution.

The advantage of AMBs over PMBs, as stated in the previous section, is the real time controllability. The feedback control feature of AMBs can be an ideal solution to stabilize the rotor supported by EDBs. Therefore, a hybrid solution has been presented in this thesis, where EDBs are combined with Active Magnetic Dampers (AMDs). In this configuration, AMB systems are introduced together with EDBs in order to provide non-rotating damping to the rotor instead of acting as bearings. Thus the system will be called EDB−AMD system.

This system is designed to exploit the high reliability of EDBs overcoming the stability problem by means of controllable AMDs. It could be a promising configuration to exploit the key features of both. The proposed hybrid configuration is attractive for high speed rotating machineries due to the following advantages:

- Compared to standard AMBs:

  ■ With the stiffness contribution of EDB at high speeds, the AMB can be downsized.

  ■ In case of AMB failure, the EDB could allow a smooth run down and a soft landing.

  ■ The rotor landing on the landing bearings can occur at a relatively low rotating speed, which allows increasing significantly the life of landing bearings. In this case, it is possible to discard the traditional ceramic landing bearings.

  ■ Since EDB acts as the role of bearing in nominal operation speed, the system's reliability can be increased.

- Compared to existing EDB systems:

  ■ During the operation speed, the AMD supplies the amount of damping that is required to keep the rotor in stable operation, which is controllable.

  ■ The AMD also provides levitation and stabilization from zero speed up to EDB's working speed range, which can avoid complex mechanical structure to allow rotor take off as used in other EDB systems.

Another purpose of the EDB−AMD study is to investigate different damping strategies for EDB systems to reach fully passive levitation.

1.3   Objectives

The goal of this thesis is to study the EDB−AMD combination system both analytically and experimentally. This has never been done in details to our knowledge. An analytical model of the system

has been built by coupling a four degrees-of-freedom rotor model together with EDBs and AMD models. This model is crucial to study the rotordynamic stability and to determine the control strategies for the AMD actuators in the operation speed range. A dedicated test rig has been built to validate the analytical model and to characterize the system.

The effectiveness of the hybrid solution is demonstrated. Based on the results from dynamic analysis, stabilization of the rotor supported by EDBs is discussed. Finally, the damping strategy of EDB systems is also discussed to find possible alternative damping solutions.

1.4 Outline of the thesis

The thesis is structured in the following way:

Chapter 2 provides an introduction to state of the art of EDBs. The different types of EDB configurations, the potential applications and limitations as well as the performance of existing EDB stabilizing methods are presented.

Chapter 3 introduces the hybrid solution of EDB—AMD system. AMBs are used as dampers to provide non-rotating damping force to the rotor supported by EDBs. The configuration is described thoroughly. To validate the proposed solution, a dedicated test rig is designed and built. A detailed description of this test rig is also presented.

Chapter 4 deals with modeling of the system. The system is composed of three subsystems: rotor, EDB and AMD. The analytical model of each subsystem has been built and then coupled together. Consequently, the dynamic model of the rotor coupled to electrodynamic forces and AMDs is obtained. The system's performance is also modeled with Simulink® for simulations.

Chapter 5 presents results from experimental tests and simulations. The tests start with validation of the analytical model both with quasi-static EDB force tests and frequency response measurements in AMDs. The results demonstrate the effectiveness of the EDB—AMD system.

Chapter 6 focuses on the control strategies of AMDs. Rotordynamics analysis is presented. Stability analysis of the system is made with the validated analytical model. The controller in AMDs is decided with simulations. Control parameters are optimized.

Chapter 7 discusses about the damping strategies for EDB systems. The required damping force for the stable operation of the rotor is investigated, which could also be used to find possible alternative solutions.

Chapter 8 concludes this thesis with a summary and outlook.

Chapter 2   Electrodynamic bearings

A brief introduction of EDBs and their characteristics is presented in this chapter. It is followed by state of the art of EDB technologies attempting to make a clear and organized review of the existing works. Finally, the limitations and critical issues that still preclude the applications of EDBs in the industry are discussed.

2.1   Background

Early work on electrodynamic suspension (EDS) started in the 1930s [8]. The working principle of an EDS system is to exploit repulsive forces due to eddy currents to produce levitation. Since the eddy currents can be induced either by using alternating current driven electromagnets or by the relative motion between a conductor and a constant magnetic field, the research on EDS has developed many different configurations for different applications. In the configuration by Bedford et al. from 1939 [9], an aluminum plate can be levitated stably above two concentric cylindrical coils that are driven with an AC current. Later on, similar concept has been used for linear induction motor and also in the field of metal melting. Known as levitation melting, this technique exploits a coil driven by high frequency AC current to levitate a metal part and achieve melting of the material with induction heating [9]. The second concept for EDS requires relative motion between the conductor and the magnetic field. It means the stable levitation is obtained when the velocity of the relative motion is beyond a certain threshold value. This concept has been used in maglev trains, such as the Japanese SCMaglev [10].

(a)
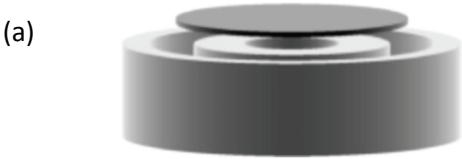
(a) Example of a levitator similar to Bedford's configuration: "TEAM problem 28"on www.compumag.org.

(b)
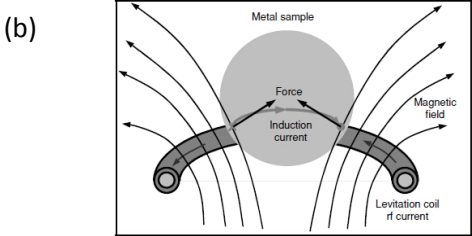
(b) Mechanism of levitation melting.

Figure 2:1 Applications of Electrodynamic Suspension.
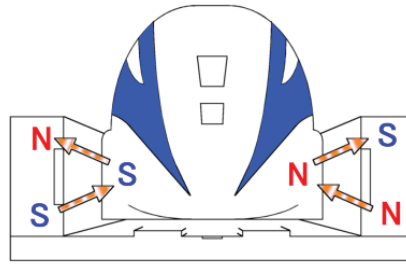
Figure 2:2 A scheme of Japanese SCMaglev train, using Electrodynamic Suspension.

Magnetic bearings exploiting Lorentz forces that are introduced by the induced eddy currents are called electrodynamic bearings (EDBs). EDBs are a special case of EDS, where the same mechanism is applied to levitate rotors, controlling either the axial degree of freedom or the radial ones of a rotor. Although EDBs can be actively controlled, in general thery are passive. It is with passive EDBs that the present thesis is concerned, especially on radial EDBs.

Existing EDB configurations can be divided into two main categories according to the degrees of freedom of the rotor that EDBs control: radial EDBs and axial EDBs. They are dicussed respectively in the following sections. Most recent works of different configurations are presented to obtain the state of the art in this field and to highlight the limitaions and existing isues of EDBs.

2.2   Radial EDBs

Radial EDBs refer to EDBs that support the radial degrees of freedom of a rotor. Firstly, same as EDS, radial EDBs can be made with an active AC supplied coil or a passive magnetic field with a conductor inside it. Several research groups have made some invesitgation on the AC supplied EDBs [11] [12], which shows a big drawback of them that is the large amount of heat loss due to eddy currents in the conductor. Thus the feasibility and application of AC supplied EDBs are quite limited [13]. Passive EDB configurations are more feasible and thus more attractive.

In passive EDBs, the restoring forces on the rotor arise from the interaction between the induced eddy currents in the conductor and the magnetic field made of Permanent Magnets (PMs). Most of them are null flux configurations to reduce the Joule losses and obtain a higher power efficiency, which means when the rotor is in the equilibriumn position it experience no varying magnetic flux therefore no unnecessary eddy currents and losses are produced. The null flux concept was first introduced by Powell and Danby [14] for maglev train applications.

Passive EDBs can be further classified into two groups according to the number of inversions of the magnetic field that the conductor experiences during one turn of rotation, that is, heteropolar bearings presenting *n* inversions of the magnetic field and homopolar bearings presenting no inversions of the magnetic field [15]. Figure 2:3 shows the representive configurations of the two concepts.
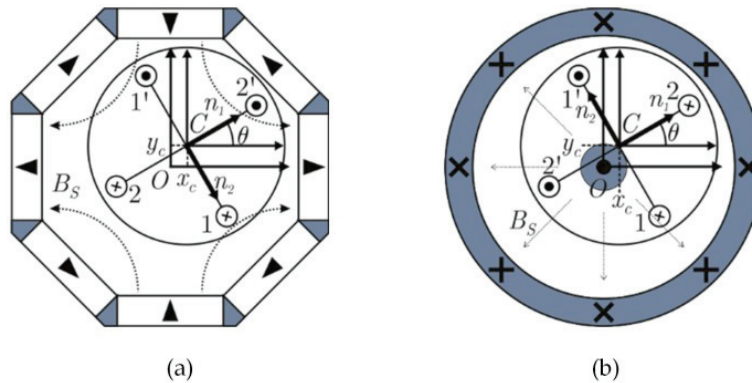
Figure 2:3 Configurations of EDBs: (a) heteropolar configuration; (b) homopolar configuration.

2.2.1 Heteropolar EDBs

Early work on passive EDBs started in 1980s with Bosore's investigation on both homopolar and heteropolar EDBs for the application of energy storage flywheels [3]. The null-flux configuration of heteropolar EDB that he presented is illustrated in Figure 2:4 a. It is composed with a ring of conductor placed in the middle of a magnetic field generated by permanent magnets in repulsion. In the nominal position, the flux is in the direction of rotation, thus virtually no currents are induced during rotation. When the rotor is off-centered, restoring forces are introduced due to the induced eddy currents. But the rotational losses produced when the rotor is not perfectly centered is too high, which makes the configuration not feasible. It is also quite sensitive to the geometry precision of the conductor, which means thermal or centrifugal expansion does affect.
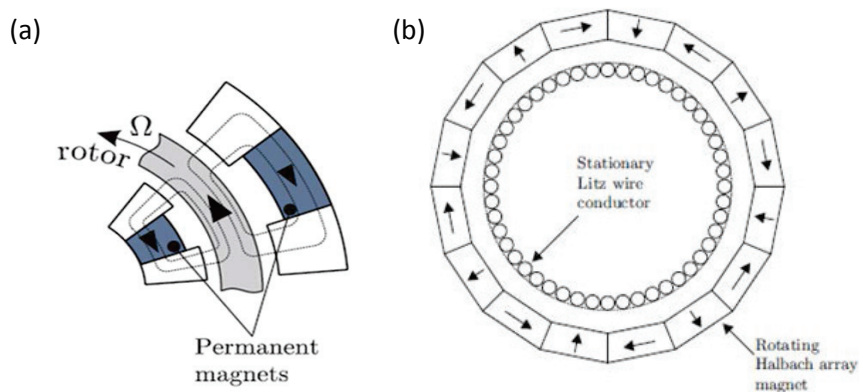
Figure 2:4 Heteropolar EDBs. (a) Null-flux configuration proposed in [3]. (b) Radial flux heteropolar configuration using a Halbach array of permanent magnets [16].

Post and his colleagues at the Lawrence Livermore National Laboratory (LLNL) made intensive research in the field of EDB. Post and Ryutov [16] proposed a configuration of heteropolar electro-dynamic bearings including Halbach arrays. In this configuration, as shown in Figure 2:4 b, the magnetic field was produced by a rotating Halbach array of magnets whereas the Litz wire conduc-

tors were placed in the stator. It ensures flux cancellation at centered position thus unwanted energy losses can be strongly reduced. The stationary conductor also allows easier cooling. The modeling of the system was built, coupling a simplified electromechanical model of the EDB with a Jeffcott rotor model, to study the stability of the rotor. The introduction of non-rotating electromagnetic damping associated to the relative speed of motion between rotor and stator was identified as a possible solution to stabilize the rotor.

Eichenberg et al. [17] also built an analytical model of the same EDB configuration. The currents and forces are calculated under quasi-static conditions, considering a fixed position of the rotor and neglecting its lateral speed. Experimental results were used to validate the model showing good agreement for force and rotational loss measurements. However, the results show clearly the limitation in the lift and drag forces caused by the introduction of external inductively loaded circuits in series with the stator coils.

2.2.2 Homopolar EDBs

The working principle of homopolar EDBs replies on the presence of relative motion between a conductor and a magnetic field, which is similar to heteropolar EDBs. However, the homopolar concept exploits a magnetic field that has no inversion in the circumferential direction of the rotor.
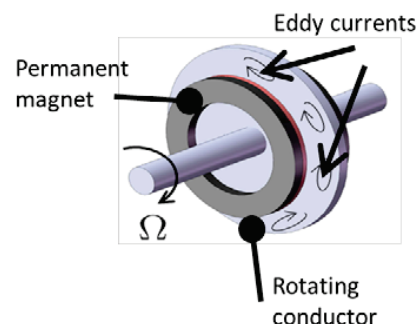
Figure 2:5 Configuration of a homopolar EDB

The magnetic field is axisymmetric and the conductor should also be axisymmetricly shaped such as a disc or a cylinder. The working condition is that the conductor is mounted on the rotor, which rotates in a stationary magnetic field.

Homopolar EDBs provide restoring force on the rotor exploiting the interaction between the induced eddy currents in the rotating conductor and the static magnetic field. As illustrated in Figure 2:6, if the rotor is centered in the magnetic field and rotating, no eddy currents are induced. If the rotor is off-centered, eddy currents will be induced due to the relative motion between the conductor and the magnetic field.
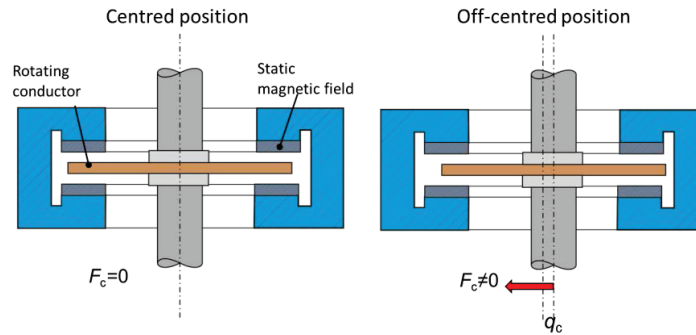
Figure 2:6 Working principle of homopolar EDBs

When a conductor has relative motion in a magnetic field, the variation of magnetic flux linked to the conductor generates an electromotive force which induces eddy currents in the conductor. The induced currents with motion in the magnetic field produce electromagnetic forces. This mechanical effect is a function of the frequency. When the frequency is lower than the R–L dynamics of the eddy currents, the force provides viscous damping, which could be applied for eddy current dampers. On the contrary, at higher frequency, it behaves as elastic force. This force could be exploited to obtain levitation.
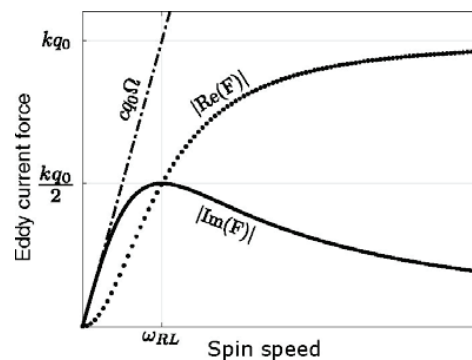
Figure 2:7 Eddy current forces developed in homopolar EDBs in the spin speed range [18]

The theory of homopolar EDBs have drawn a lot of interests in the past decade. It shows the possibility to obtain stable levitation with simple shaped conductor and permanent magnets at room temperature, presenting the advantages of passive magnetic bearings without introducing negative stiffness in any direction. Two common possible configurations of homopolar EDBs are shown in Figure 2:8. In the first configuration, the magnetic flux goes through the conductor in the direction parallel to the rotation axis, thus being called axial flux configuration. The second one exploits the magnetic flux that goes through the conductor along the radial direction, which is called radial flux configuration. So far all the configurations presented in literature are based on these two basic concepts.
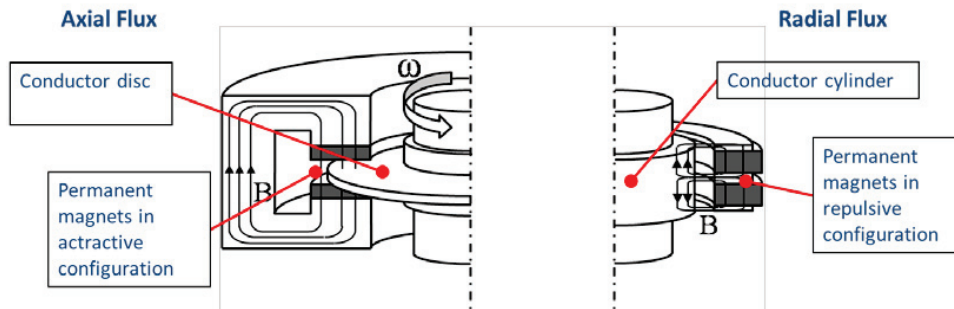
Figure 2:8 Axial flux and radial flux homopolar EDBs

Compared with AC driven EDBs, homopolar structures are advantagenous in terms of rotational losses, because they introduce virtually no drag torque when the rotor's rotation axis is centered in the axisymmetric magnetic field. In this case, the tolerance requirement of fabrication of the conductor is not as critical as in the case of heteropolar bearings.

Another key feature of homopolar EDBs is the possibility of synchronous excitation filtering. Synchronous vibration caused by residual rotor unbalance has a remarkable influence on rotordynamics and stability of the whole system in rotating machineries. This issue requires dedicated damping strategy to achieve stable operation. For example, in AMB systems, Herzog [19] introduced General Notch Filter (GNF) algorithm for synchronous vibration control. Homopolar EDBs are able to overcome this issue because if the excitation force is synchronous to the rotation of the rotor, the conductor still experience the same area of magnetic flux (Figure 2:9) provided that the conductor is isotropic and the magnetic field of the stator is constant and axisymmetric. Therefore, no reaction force will be produced and the dynamics of rotor is not disturbed. It means that the homopolar EDBs behave as a narrow notch filter for a force excitation synchronous with the rotating speed ($\frac{\omega}{\Omega} = 1$). This is an advantage of this type of passive bearing with respect to active magnetic bearings. The heteropolar EDBs behave as a regular elastic support reacting to every input frequency.
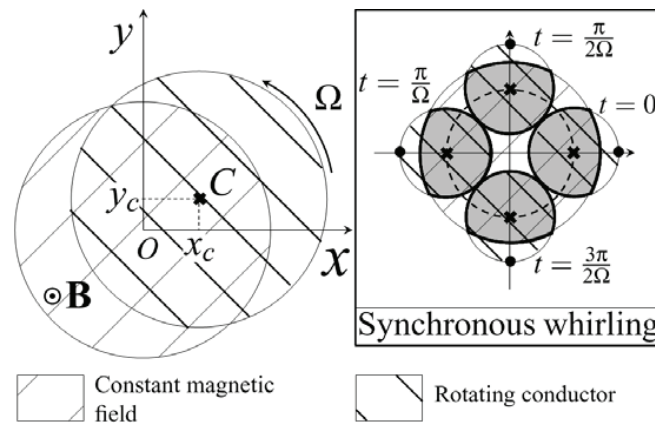
Figure 2:9 Scheme of a conductor rotating in a magnetic field. Synchronous whirling is illustrated.

The first work on homopolar configurations was performed by Basore [3]. In his configuration, radial homopolar EDB was combined with axial permanent magnet bearing. The EDB consisted of a thin conducting cylinder attached to the rotor utilizing the radial homopolar magnetic field generated by the permanent magnet bearing. The EDB's forces were modeled considering constant spin speed and fixed position of the rotor relative to the stator. This analytical model could be used to predict the bearing's performance in terms of load capacity and losses but not suitable to predict the stability of the rotor.

Later, Murakami and Satoh [20] presented some experimental results on the properties of axial flux homopolar EDBs which showed a linear relation between bearing forces and radial displacement of the rotor for constant spin speed. However the relatively small range of speed limited the validity of the obtained conclusions.

During last decade, several groups of researchers have made intensive work in this field. Filatov and Maslen [21] designed a homopolar EDB configuration which combined Basore's homopolar concept with Pinkerton's [22] rotating conducting loop. They made a new analytical model to investigate the EDB's performance. In successive work, Filatov et al. [23] used their model to design a homopolar EDB for a flywheel energy storage system, where eddy current damper was introduced to obtain stable operation.

2.3 Axial EDBs

Axial EDBs exploits null flux coils to provide electrodynamic forces for levitation, similar to the mechanism of maglev trains [24]. Post [25] presented the configuration using stationary conductors and rotating Halbach arrays of permanent magnets. This configuration was later studied by Eichenberg et al. and Storm with numerical models and experimental tests which were used to validate the models.

A more recent work of axial EDB was presented by Sandtner and Bleuler [26]. The configuration of their test rig is based on that previously proposed by Post [25]. This system was able to achieve stable levitation of a spindle rotor for rotational speeds above 4800 rpm. Later, Sandtner and Bleuler [27] investigated strategies to improve the bearings performance at constant spin speed. An electromechanical model of this test rig was built by Impinna et al. [28] to study the dynamic behaviors.

2.4   Modeling of EDBs

In all works of EDBs, modeling is necessary to understand the performances of different configurations. Validated models are also useful to design a bearing and improve its performance.

Recently, amounts of efforts have also been devoted to modeling of EDBs. The first work to be mentioned is the contribution by Lembke [29] [30].He studied accurate FE models of EDBs and obtained the relationship of EDB mechanical properties and its geometrical parameters, which allows improve the bearing performance. With the help of FE modeling, he developed several different layouts of EDBs for applications in the field of turbopumps. In addition to the FE modeling, the rotordynamic stability was investigated using the previous proposed model by Filatov and Maslen [5].

Kluyskens and Dehez [31] [32] have made intensive work on modeling of EDBs. In their work, a dynamic electromechanical model was built to describe the interaction between the rotor and stator on homopolar bearings. The rotating damping is clearly identified as the cause of instability. The model was refined later [33] taking account of the influence of skin effect occurring in the rotating conductor on the rotordynamic stability. They also studied the power consumption in EDBs showing the influence of the rotating damping on the dissipated power [34]. This work is essential regarding the applications of EDBs in flywheels or vacuum fields.

Amati et al. [35] presented a new modeling approach to describe the electromechanical interaction between the rotating conductor and stationary magnetic field of homopolar EDBs. The equations were derived using complex notations and considering the equivalence between the state equation of a voice coil and that of a spring in series with a viscous damper. This model is more general than those previously presented in literature. The model was validated under both quasi-static and dynamic conditions in their following work [6].

2.5   Technical challenges

Although a lot of work has been done by several research groups especially in the past decade, the applications of EDBs are still quite limited. It can be noticed that, so far attempts have been made to implement EDBs in the systems of energy storage flywheels and turbomolecular pumps, basically small sized machines. According to their features, EDBs are suitable for high speed applications where stiffness requirement is relatively low but cost critical, which means there're other different potential applications that could be investigated.

Before promoting EDBs for more applications, there is still big room of improvement in this technology. Compared to AMBs, the stiffness-to-volume ratio and specific load capacity of EDBs are lower. Besides, similar to fluid bearings, EDBs work when the rotating speed of rotor goes above a certain threshold. Thus it is necessary to support the rotor and keep it centered before reaching the threshold speed which allows the EDB to work properly. The present main solution of low speed rotor supporting is using mechanical centering structure including mechanical bearing. It is acceptable for research prototypes, but not convenient for industrial applications since the centering structure needs to be disengaged manually.

However, the main issue that precludes the application of EDBs is the instability due to rotating damping arising in the conductor. It is well known that rotating damping causes instability in supercritical speed range. Different methods have been presented to introduce non-rotating damping to compensate the rotating damping and to stabilize the rotor during operation. First damping mechanism was presented in the flywheel energy storage system by Filatov [21], where eddy current damper was used together with EDB. He made improvement of the eddy current damper that used in his system to achieve sufficient damping for his system and stated the effectiveness [23], where stable operation occurred above 3400 RPM. This approach has at least the following drawbacks: first, the magnets are attached on the rotor, which changes rotordynamic behavior; second, the high performance magnets are usually quite brittle, which limits the rotational speed to avoid magnets failure due to centrifugal stresses.

Later, Tonoli et al. [6] proposed another passive solution for the stabilization of EDBs. Instead of introducing a damping between the rotor and the statoric part of the bearing, they proposed to introduce an elastic and dissipative element between the statoric part of the bearing and the base of the machine. In this reference paper, a comparative analysis of the proposed solution and the eddy current damping method by Filatov is also presented based on a Jeffcott rotor model. It shows the possibility of effectiveness and allows a reduction of the rotor mass and complexity. However, the effectiveness of this approach still needs better investigation.

Detoni et al. [7] performed stability analysis of a homopolar EDB system with a 4 degree of freedom rotor model. The two existing stabilization methods are modeled and their effects are analyzed. Compared to formerly presented studies, the presented one allowed analyzing not only the well-known cylindrical whirl instability but also an unstable conical whirl mode. The results showed that the stabilization method where damping is introduced directly between rotor and casing is particularly effective to stabilize the conical mode, whereas it is not so effective in stabilizing the forward cylindrical mode. The second stabilization method, based on the introduction of damping between the stator of the bearing and the base of machine showed to be less effective to stabilize the conical mode. However it is more effective to stabilize the cylindrical mode.

Chapter 3   EDB−AMD system

As has been stated in the previous section, so far the existing EDB stabilization methods are both implemented in passive ways. Although the eddy current damper in Filatov's system could be active, in other words current driven, to increase the amount of damping, the controllability of rotordynamics was not presented.

The main advantage of AMBs is the controllability. They could be an ideal solution to control the instability of rotors supported by other types of bearings, where the AMB functions as an active magnetic damper (AMD). The concept of AMD has been applied in combination with bearings that present instability issues. For example, El-Shafei and Dimitri used AMDs to control journal bearing instability [36]. A recent work presented by Looser and Kolar [37] was to use AMDs to stabilize gas bearings in high speed operations.

A hybrid bearing concept employing AMDs to stabilize EDBs has been proposed and is presented in the present thesis. Using similar magnetic actuators as those used in classical AMBs, non−rotating damping forces are applied on the rotor supported by EDBs to obtain stable operation. This system is designed to exploit the high reliability of EDBs, overcoming the stability problem by means of controllable AMDs. Besides, the use of an active magnetic damping system could allow investigating in a controlled laboratory environment a damping strategy that could then find a passive implementation.

In the present chapter, the EDB−AMD configuration is presented. A dedicated test rig has been built to validate the proposed solution and characterize the system.

3.1   Configuration of EDB−AMD

The configuration of the EDB−AMD system is shown in Figure 3:1. It consists of two radial homopolar EDB units with two AMDs and one electric motor at the center of the rotor. The two EDBs are placed with the same distance to the center of the rotor. The same symmetry is presented by the two AMDs. The axial degree of freedom is controlled passively, using the magnetic flux closure of AMDs as reluctance bearing. If needed, there's also possibility to control the axial degree-of-freedom using the center motor, which is axial flux thus could act as an axial AMB.

During the operation speed range of EDBs, the AMDs provide non-rotating damping to stabilize the rotor. This non-rotating damping can be easily tuned during operation phase which is advantageous to the system operation. The AMDs also provides levitation from zero speed up to the EDB's

working speed as stiffness compensation to the rotor when EDB forces are not sufficient. It results in a feasible EDB system to guarantee stable levitation of the rotor in a wide speed range.
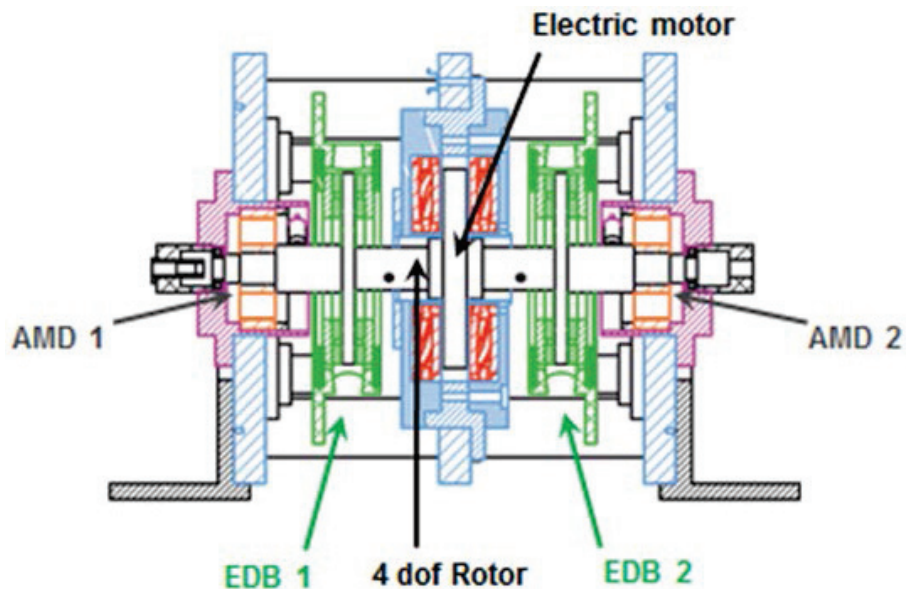
Figure 3:1 Configuration of the EDB-AMD system

3.2 Test rig description

A dedicated horizontal full sized test rig has been designed and built, as shown in Figure 3:2, to demonstrate the feasibility of the proposed magnetic suspension system and to validate the analytical model. The test rig follows the designed configuration and is composed of five main parts: (a) the frame supporting the stator of the bearings and the motor; (b) the AMDs and the sensors; (c) the EDB units; (d) the rotor including the rotating parts of EDBs and of the motor; (e) the electronics for driving the motor and the AMD actuators.
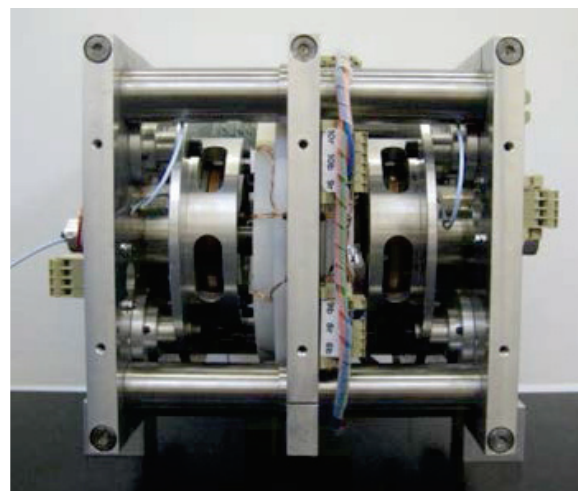
Figure 3:2 A picture of the test rig
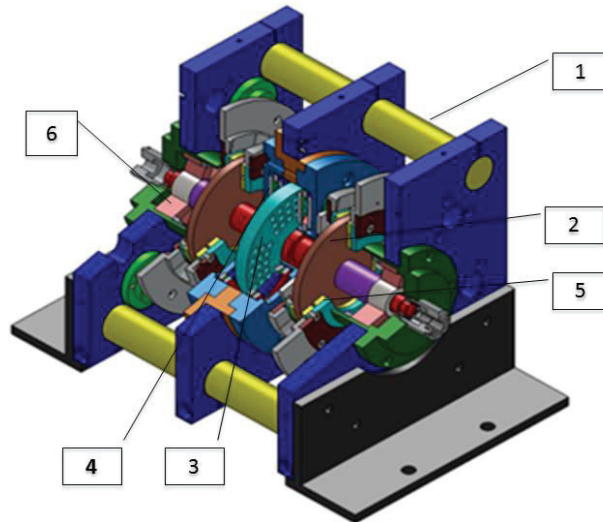
Figure 3:3 Isometric view of the test rig. 1) Test rig's structure; 2) EDB conductor disc; 3) Electric motor disc; 4) Electric motor windings; 5) EDB statoric magnetic circuit; 6) AMD.

Figure 3:3 shows the isometric view of the test rig, where the system components as well as the structure elements can be observed. The frame of the test rig is composed of four stainless steel columns, which ensure a stiff construction, connected to three aluminum alloy plates. The plates allow the different components to be assembled together. The statoric parts of both AMDs and the motor's stator are all fixed to the aluminum plates.

The middle plate integrates a permanent magnet motor. It is an axial flux electric motor which was custom designed with air wound coils (Figure 3:4) and no back iron to minimize the negative stiffness induced by it. The two sets of coils located at two sides of the rotor disc can be used to realize an integrated motor-axial bearing system. The main characteristics of the motor are listed in Table 3:1.

Table 3:1 Data of the electric motor

Description	Unit	Value
Number of poles	-	4
Number of phases	-	3
Number of winding per coil	-	24
Nominal current	A	2
Nominal voltage	V	380
Nominal speed Ω	Rev/min	20,000
Nominal torque	Nm	0.9

Five eddy current displacement sensors are implemented in the system for the axial degree of freedom and two radial AMDs (each AMD has two sensors for the *x* and *y* directions in its action plane).
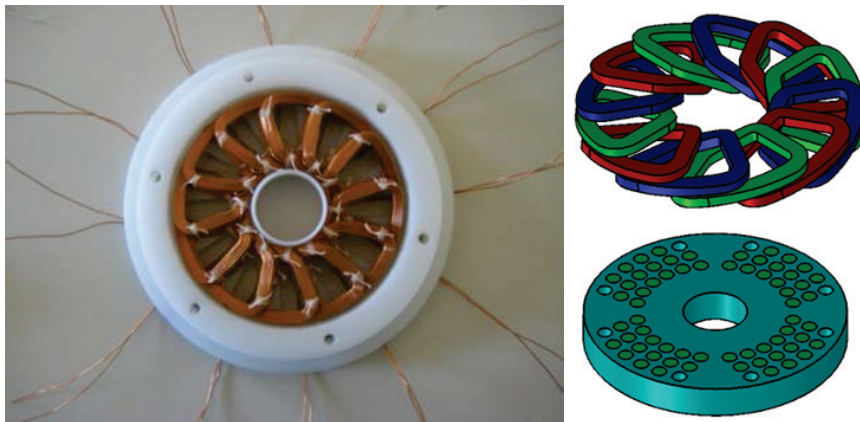
Figure 3:4 One set of stator coil of the electric motor. The 3D plot shows the coil and the disc of the motor.

The rotor, as illustrated in Figure 3:5, is composed of a solid steel shaft with the rotating parts of the electric motor, the EDB units and the AMDs mounted on it.
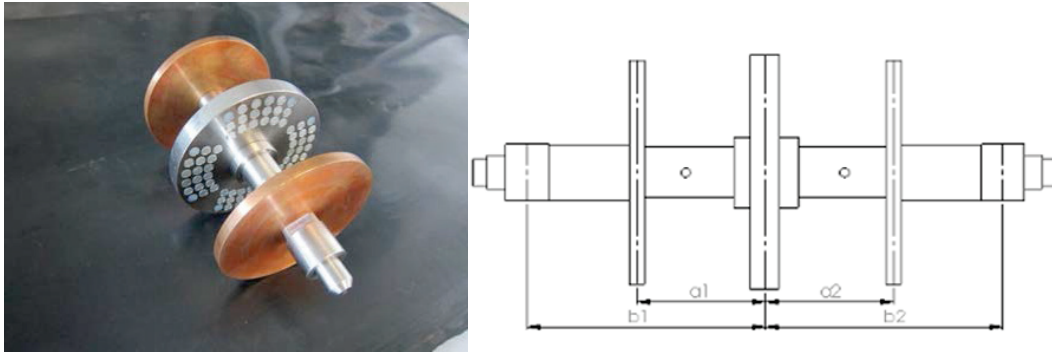
Figure 3:5 The rotor in the test rig.

Some parameters of the test rig are reported in Table 3:2.

Table 3:2 Parameters of the test rig.

Parameter	Description	Value
ω	Nominal speed	20000 rpm
m_r	Rotor mass	4.35 kg
l_r	Rotor length	305 mm
J_p	Polar moment of inertia	0.00572 kg·m^2
J_t	Transversal moment of inertia	0.01995 kg·m^2
a_1	EDB$_1$ arm	67 mm
a_2	EDB$_2$ arm	67 mm
b_1	AMB$_1$ arm	125 mm
b_2	AMB$_2$ arm	125 mm

3.2.1 Radial EDB units

Homopolar EDB concept is used in this system. To improve stiffness and minimize the power losses, the EDBs present a double flux configuration as shown in Figure 3:6 and 3:7. Each EDB is composed of four ring shaped permanent magnets magnetized axially and bonded to two back iron discs (two magnet rings on each back iron disc). The magnets are oriented in attraction so that the flux lines are closed as shown in Figure 3:7. The geometric parameters of the double flux EDB from the design procedure are listed in Table 3:3. The characterization of the EDB units will be presented in the following chapter concerning the modeling.
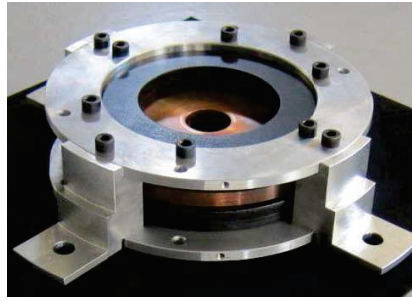
Figure 3:6 One homopolar EDB unit in the test rig
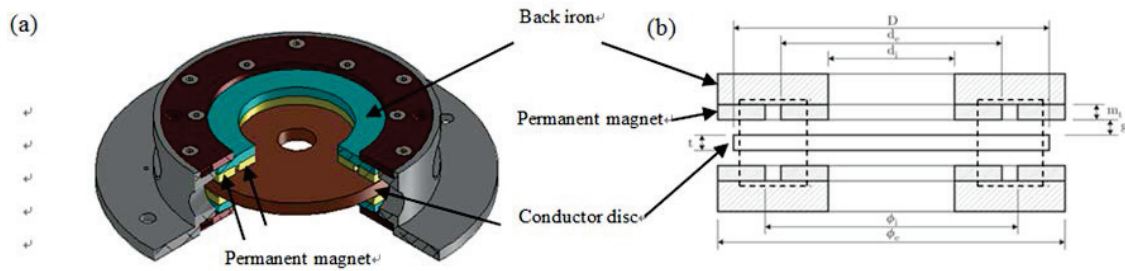
Figure 3:7 The double flux EDB

Table 3:3 Geometrical and physical data of the double flux EDB.

Parameter	Description	Value
D	Conductor outer diameter	120 mm
Φ_e	Outer permanent magnet outer diameter	120 mm
Φ_t	Outer permanent magnet outer diameter	95 mm
de	Inner permanent magnet outer diameter	89 mm
di	Inner permanent magnet inner diameter	64 mm
mt	Permanent magnet thickness	5.5 mm
t	Conductor disc thickness	8 mm
g	Axial air gap	0.75 mm
B_r	NiFeB residual magnetic flux density	1.4 T

3.2.2 Radial AMB/AMD units

8–pole actuators are used in the AMB/AMD units. The configuration is shown in Figure 3:8. In the test rig, the AMDs can be used as active magnetic bearings (AMBs) to guarantee suspension for

speeds below the EDB's stability threshold or for speeds where EDBs are not able to provide sufficient levitation forces. The AMDs act as pure damper for high speeds ensuring a stable levitation over a wide speed range.

Two eddy current displacement sensors (Bently Nevada 3300 XL series) are placed in the two orthogonal directions of each AMB/AMD plane. PID architecture is used in the position control of AMDs to provide proper stiffness and damping to the rotor. Different tuning of this controller is performed depending on the type of test. Integral action is activated just for quasi–static characterization. PI control is used in the current loop of the AMDs.

With properly tuned control parameters of the AMDs, the rotor is able to levitate and rotate within a stable speed range of 0 to 6000 rpm. Tests have been run within this speed range.
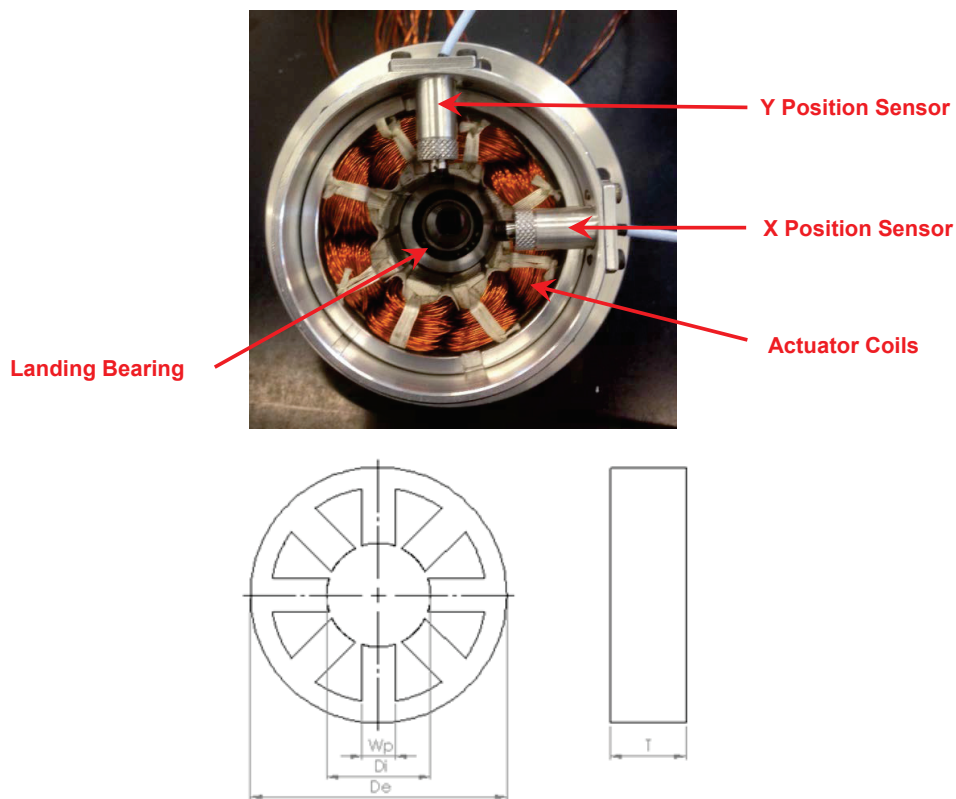
Figure 3:8 The AMB/AMD actuator

Some geometric parameters of AMD actuators are listed in Table 3:4.

Table 3:4 Geometric parameters of the AMDs.

Parameter	Description	Value
D_e	Outer diameter	76 mm
D_i	Inner diameter	31 mm
W_p	Pole width	10 mm
T	Actuator thickness	22.5 mm
N	Number of turns	53
W_d	Wire diameter	0.63 mm
g_0	Radial air gap	0.7 mm

Figure 3:9 shows the control units for the AMBs/AMDs. The blue cables and boxes are for the displacement sensors. The electronic architecture called Multi-Purpose Power Module (MPPM) [38] is used in the test rig.
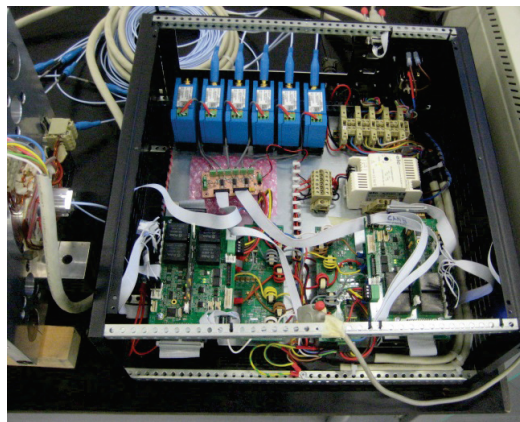
Figure 3:9 The control box of the AMBs/AMDs

Chapter 4   Modeling

In order to predict the performance of the EDB−AMD system, an analytical model is built in this chapter. The system is composed of three main subsystems: the rotor, EDBs and AMDs. The analytical model of each subsystem will be built and then they will be coupled together. Consequently, the dynamic model of the rotor coupled to electrodynamic forces and active magnetic dampers is obtained, which is crucial for rotordynamic analysis and stability research of the system. The system's performance will also be modelled with MATLAB Simulink for numerical simulations.

4.1   Four degree-of-freedom rotor model

Rotordynamics studies on the rotor supported by EDBs have been made by different researchers to understand the system stability and performance of EDBs. In these works, different electromechanical models of EDBs were built and coupled to rotordynamic models. However in most of these studies, Jeffcott rotor models were used, which neglects gyroscopic effects and only the instability of cylindrical whirling motion was considered [7]. In order to make a more complete rotordynamics study, especially for stability analysis, a four degree-of-freedom (4 DOF) rotor model is used in the present research. Therefore, both cylindrical and conical modes can be included in the dynamic study, which allows a more accurate dynamics study of the whole system.

Figure 4:1 shows the scheme of a 4 DOF rotor supported by two magnetic bearings at both ends. The rotor is composed of a gyroscopic rigid body described by its mass m, transversal moment of inertia J_t, and the polar moment of inertia J_p.

The shaft is assumed to be massless and rigid, which is based on the fact that the stiffness produced by magnetic bearings is much lower than the stiffness of the shaft. The reaction forces produced by magnetic bearings are represented with F_{b1} and F_{b2}. They are positioned respectively with distances of a and b from the mass center of the rotor, as shown in the figure. The rotor has six degrees of freedom. However to study the flexural behavior of the rotor, under the hypothesis of small transverse and angular displacements, it can be modeled with four degrees of freedom.
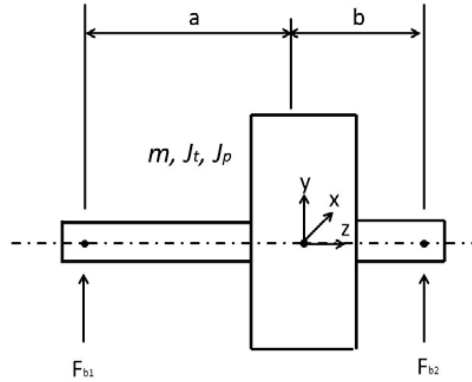
Figure 4:1 Scheme of the rotor supported by two magnetic bearings

The dynamic equations of the four degrees of freedom rotor are:

$$M\begin{Bmatrix} \ddot{q} \\ \ddot{\phi} \end{Bmatrix} - j\Omega G \begin{Bmatrix} \dot{q} \\ \dot{\phi} \end{Bmatrix} + \begin{Bmatrix} F_b \\ M_b \end{Bmatrix} = \begin{Bmatrix} F_{ext} \\ M_{ext} \end{Bmatrix}$$

(4:1)

where *M* and *G* are the mass and gyroscopic matrices respectively:

$$M = \begin{bmatrix} m & 0 \\ 0 & J_t \end{bmatrix}, G = \begin{bmatrix} 0 & 0 \\ 0 & J_p \end{bmatrix}$$

(4:2)

Here all the equations are written in two complex coordinates: *q* and *ϕ*, which represent the transverse and angular displacements respectively:

$$q = x + iy$$
$$\phi = \phi_y - j\phi_x$$

(4:3)

4.2   Modeling of EDBs

The modeling of EDBs here is based on the electromechanical dynamics of a conductor in translation in a constant magnetic field. In its simplest form, a motional eddy current damper is constituted by a linear voice coil whose electric terminals are shunted by a resistive and inductive load (Fig 4:2), where *R* and *L* are respectively the resistance and the self-inductance of the coil. It is the same as for a purely mechanical system made of a linear spring and a viscous damper in series. This approach was proposed by Amati et al. in [35].

4.2.1 Linear damper
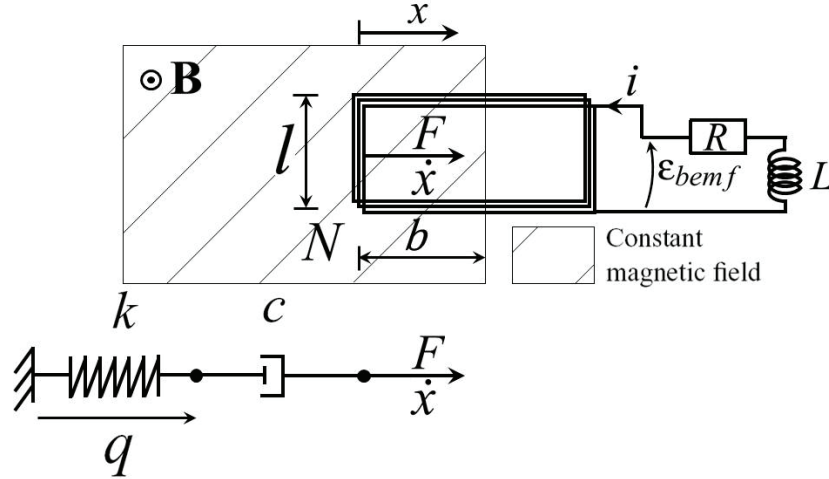
Figure 4:2 Electromechanical equivalence between a short-circuited rigid coil in motion in a constant magnetic field and a mechanical system made of a linear spring and a viscous damper connected in series.

Let us consider the simple form of a motional eddy current damper, as shown in Figure 4:2. It consists of a coil of wire that moves along the x direction inside a constant magnetic field with flux density $B.$ The total magnetic flux linked by the coil is

$$\lambda = Li + \Lambda \tag{4:4}$$

The first term gives the flux linkage due to the self-inductance of the coil whereas the second term gives the flux linked due to the external constant magnetic field. The magnetic flux generated by the constant field and linked by the coil is

$$\Lambda = N \int_s B \cdot n dS = K_m (b - x) \tag{4:5}$$

Where N is the number of turns of the coil and n represents the unit vector normal to the surface of integration S. The coefficient K_m is the coil constant and depends on the magnetic and geometrical parameters of the system.

$$K_m = NBl \tag{4:6}$$

Due to Faraday's law, the time dependence of the coil displacement x generates an electromotive force that induces eddy currents in the coil. These currents can be determined by Kirchoff's voltage law, considering the coil's resistance and self-inductance.

$$\frac{d\lambda}{dt} + Ri = 0 \tag{4:7}$$

which can be written as :

$$\frac{Ldi}{dt} + \frac{K_m d(b-x)}{dt} + Ri = 0 \tag{4:8}$$

Thus the state equation governing the currents can be obtained:

$$\frac{di}{dt} = \frac{K_m}{L}\dot{x} - \omega_{RL}i \tag{4:9}$$

where $\omega_{RL} = \frac{R}{L}$ is the frequency of the electrical pole of the conductor circuit.

The Lorentz force generated by the interaction between the induced eddy current and the magnetic field can be calculated as:

$$F = N\int i\overline{dl} \times B = K_m i \tag{4:10}$$

Substituting Equation 4:10 into Equation 4:9, we can get:

$$\dot{F} = \frac{K_m^2}{L}\dot{x} - \omega_{RL}F \tag{4:11}$$

The input velocity to output force transfer function can be obtained as:

$$F = \frac{K_m^2/R}{1 + s/\omega_{RL}}\dot{x} \tag{4:12}$$

It is the same as for a purely mechanical system made of a linear spring and a viscous damper in series. The stiffness and damping coefficients k and c of this mechanical analogue can be defined as [39]:

$$\begin{aligned} k &= K_m^2/L \\ c &= K_m^2/R \end{aligned} \tag{4:13}$$

In the simple mechanical system made of a linear spring and a viscous damper connected in series, the state equation is obtained considering that the velocity $\dot{x}$ is the sum of the spring deformation velocity $\dot{q}$ and the viscous damper velocity. Assuming the velocity $\dot{x}$ as the input and the resulting force F as the output, the system is governed by the following state and output equations:

$$\begin{aligned} \dot{q} &= -\omega_{RL}q + \dot{x} \\ F &= kq \end{aligned} \tag{4:14}$$

4.2.2 Eddy current forces due to radial motion and rotation

The general model of eddy current forces in a spinning conductor that moves radially inside an axisymmetric magnetic field is considered. The schematic representation of this physical system is shown in Figure 4:3. Points O and C give, respectively, the position of the axes of magnetic field and conductor. The reference frame (O, x, y) is fixed whereas (O, ξ, η) is a rotating reference frame that rotates with the same spin speed Ω as the conductor. The pairs (x_c, y_c) and (ξ_c, η_c) are the coordinates of point C in the fixed and rotating reference frames, respectively. The Lorentz force generated by the eddy currents in the conductor can be modeled as two orthogonal branches in

the rotating frame $\eta\xi$. Each branch is composed by the series connection of a linear spring and a viscous damper.
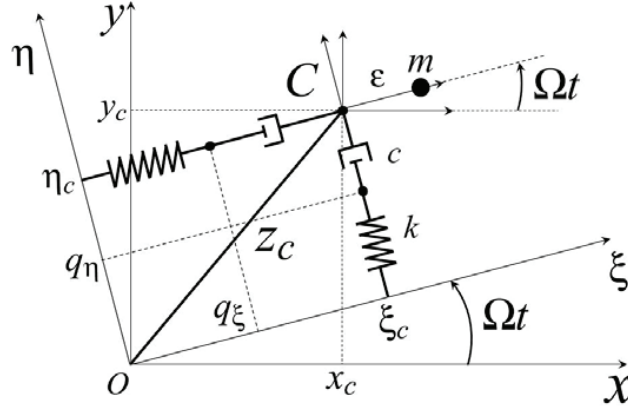
Figure 4:3 Schematic representation of EDB mechanical equivalence

Introducing the complex notation [35], the displacement of point C and the deformation of the equivalent spring in the frame (O, ξ, η) can be expressed as:

$$\zeta_c = \xi_c + j\eta_c$$
$$q_\zeta = q_\xi + jq_\eta$$

(4:15)

Thus the state and output equations (4:14) become:

$$\dot{q}_\zeta = -\omega_{RL}q_\zeta + \dot{\zeta}_c$$
$$F_\zeta = k_r q_\zeta$$

(4:16)

where the suffix r refers to the rotating reference frame.

Assuming that axes (O, x, y) and (O, ξ, η) coincide at $t = 0$ and that the spin speed is constant, the relation between the quantities in the rotating reference frame and those in the fixed reference frame can be written as:

$$\zeta_c = z_c e^{-j\Omega t}$$
$$\dot{\zeta}_c = -j\Omega z_c e^{-j\Omega t} + \dot{z}_c e^{-j\Omega t}$$

(4:17)

The dynamic behavior of the eddy current forces generated by the conductor's spin and relative motion can be expressed as:

$$\dot{F}_z = k(\dot{z}_c - j\Omega z_c) - F_z(\omega_{RL} - j\Omega)$$

(4:18)

where Ω is the spin speed of the conductor and z_c represents its complex displacement. Equation 4:18 is linear and has constant parameters. It allows modeling dynamically the resistive and induc-

27

tive effects on the eddy currents. Therefore the forces can be calculated provided that the equivalent electromechanical parameters k and c are known. These two coefficients can be identified both by means of finite element simulations and experimentally.

For quasi-static condition, which means constant relative displacement ($z_c=z_{c0}$=constant) and constant spin speed Ω, the force produced by eddy current becomes:

$$F = \frac{k}{1+(\frac{\omega_{RL}}{\Omega})^2} z_{c0} - j \frac{c\Omega}{1+(\frac{\Omega}{\omega_{RL}})^2} z_{c0} = F_{\parallel} + F_{\perp} \tag{4:19}$$

where $F_{\parallel}$ and $F_{\perp}$ are respectively the components of the force parallel and perpendicular to the displacement z_{c0}. It has to be noticed that the perpendicular component of the EDB force is a damping force. It is usually exploited in the field of eddy current dampers. In the case of homopolar EDBs, this component has destabilizing effect since it introduces rotating damping. The force parallel to the displacement is the restoring force that can be used to provide stiffness to the rotor.

The EDB force generated by the double flux configuration can be represented with two parallel sets of spring and damper (Figure 4:4). Thus the double flux EDB is characterized by the parameters k_1, c_1, k_2 and c_2 instead of k and c.
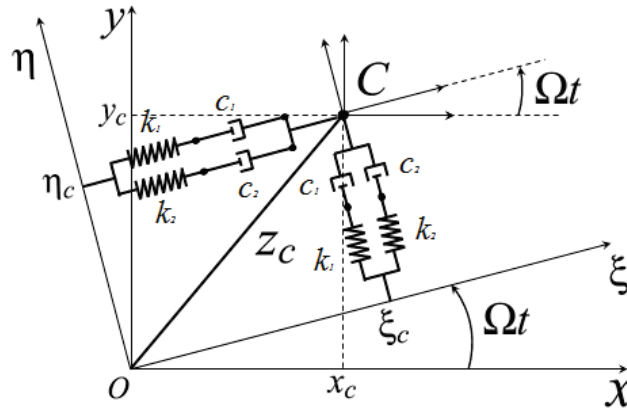
Figure 4:4 Mechanical equivalence of a double flux EDB

Therefore the force generated by the double flux EDB in quasi-static condition can be represented as:

$$F = (\frac{k_1}{1+(\frac{\omega_{RL1}}{\Omega})^2} + \frac{k_2}{1+(\frac{\omega_{RL2}}{\Omega})^2}) z_{c0} - j(\frac{c_1\Omega}{1+(\frac{\Omega}{\omega_{RL1}})^2} + \frac{c_2\Omega}{1+(\frac{\Omega}{\omega_{RL2}})^2}) z_{c0} = F_{\parallel} + F_{\perp} \tag{4:20}$$

The mechanical equivalent parameters of the EDB units can be identified numerically or experimentally in quasi-static condition. The approach is to impose a fixed eccentricity (static displace-

ment) to the conductor of EDB and measure the generated forces along the direction of the displacement and perpendicular to it. This procedure needs to be repeated for different rotating speed to obtain a plot of EDB forces in the parallel and perpendicular directions. The simulation or experimental results of EDB forces allow the identification of EDB coefficients by a best fitting procedure with the analytical model (Equation 4:20).

4.2.3 Quasi-static FE modeling of EDBs

The EDB forces can be obtained by Finite Element simulations. The FE simulation of eddy currents in moving conductors can be made with different formulations. The most general method is to simulate the relative motion between conductor and magnetic field using separate reference frames and moving mesh in time-stepping solutions. Although general and accurate, this type of calculation can be very time consuming. A simpler and much faster method is to make quasi-static simulation, using the analysis of moving conductors with invariant cross section perpendicular to the direction of motion. The stationary distribution of eddy currents can be calculated using a common reference frame for the rotor and the stator, using only one mesh, and by only one calculation. The validity of this approach has also been confirmed in [40].

For estimation of EDBs, FE method provides the capacity of calculating the distribution of flux density B for all domains and the current density distribution J inside the conductor. The movement of the conductor can be considered in the formulation by a term $v \times B$, where v is the velocity field of the conductor.

$$v = \begin{Bmatrix} v_x \\ v_y \\ v_z \end{Bmatrix} = \begin{Bmatrix} -y\Omega \\ x\Omega \\ 0 \end{Bmatrix} \tag{4:21}$$

Thus the produced Lorentz forces can be obtained with volume integration over $J \times B$ within the conductor domain.

$$F_{Ltz} = \iiint_{\Gamma_c} J \times B dV \tag{4:22}$$

For the present analysis, COMSOL Multiphysics® was used. Other FE softwares can also be used for the same purpose.
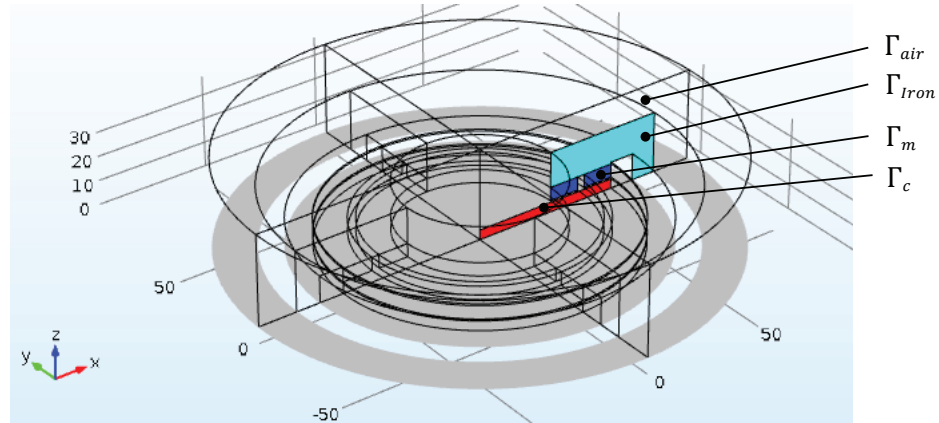
Figure 4:5 the three dimensional model built in COMSOL for the identification of the EDB unit.

Only half of the EDB unit was built due to the symmetry. The cross sections of the back iron, the two magnets and the conductor are coloured and marked to show the domains in the simulation. The symmetry plane is shown in grey. Γ_{air} is the surrounding air; Γ_{Iron} is the back iron; Γ_m are the magnets in the stator and Γ_c is the conductor disc.

The quasi-static simulation was performed for a given Ω and by introducing a small eccentricity ε between the EDB magnets domain Γ_m and conductor domain Γ_c in the x direction such that $z_{c0} = \varepsilon$. Here, z_{c0} is a real number, thus the Lorentz forces calculated by the FE can be directly compared to the forces of Equation 4:20. The real component gives the force along x direction whereas the imaginary component gives the force along y direction.

4.2.4 Quasi-static experimental identification of EDBs

Another method is to measure the EDB forces experimentally. A quasi-static test rig has been built as shown in Figure 4:6. The test rig was designed to measure the forces developed by the EDB at the fixed off-centered position of the rotor with respect to the stator. The structure of the rig is composed of two aluminum alloy plates rigidly connected by four vertical posts. A 2D micrometric xy positioning stage is fixed to the upper plate. The rotor is fixed to the moving plate of the xy positioning stage.

The rotor is supported by two ball bearings and is driven by an electric motor through a flexible coupling. The lower end of the rotor is connected to the copper disc of the EDB. The statoric parts of the EDB are fixed to the plate that is connected to the case of the rig by four compliant beams.
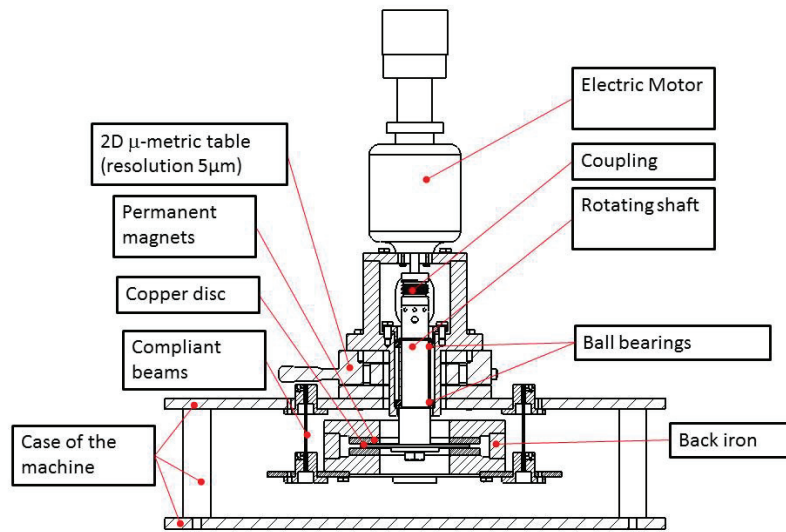
Figure 4:6 Quasi-static test rig for EDB identification.

Test bench characteristics and setup for quasi-static tests
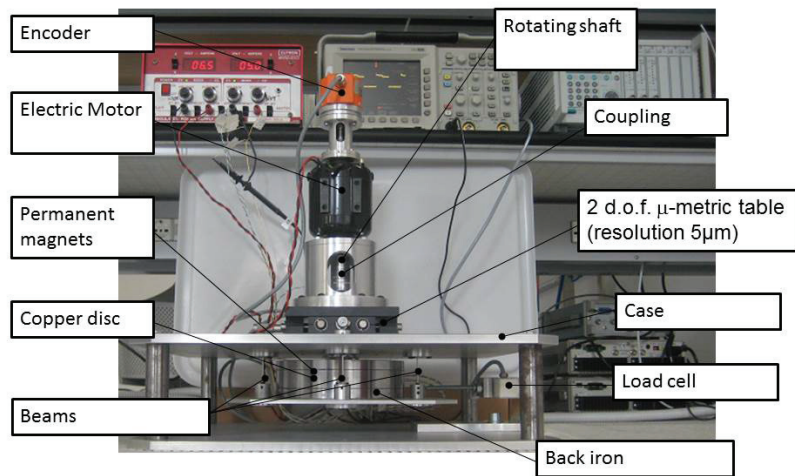
Figure 4:7 Test bench and setup for quasi-static tests

During the quasi-static tests, the conductor runs at a constant speed Ω by the electric motor. The motor is equipped with a Hohner H3363Z_4096 encoder, with five channels and 4096 pulse per revolution for an accurate measuring of the actual rotational speed.

The quasi-static testing procedure is as follows:

- Define a fixed radial displacement of the EDB copper disc by acting on the micrometric stage in one of the two degrees of freedom.

- Set a constant rotational speed Ω of the motor by voltage control and speed measuring with the encoder.

- Position two load cells between the statoric part of the EDB and the structure of the test rig in two orthogonal directions to measure the radial electromagnetic forces developed between the stator and the rotor of the bearing as a function of the rotating speed Ω.

Figure 4:8 shows the force developed by the EDB unit for different speeds with a constant eccentricity of 0.25 mm. The experimental results from quasi-static tests are plotted, where the circle markers refer to the force perpendicular to the eccentricity (damping force) and the cross markers refer to the force parallel to the eccentricity (restoring force). Full lines refer to the analytical results with curve fitting so that the mechanical parameters of the EDB are obtained.
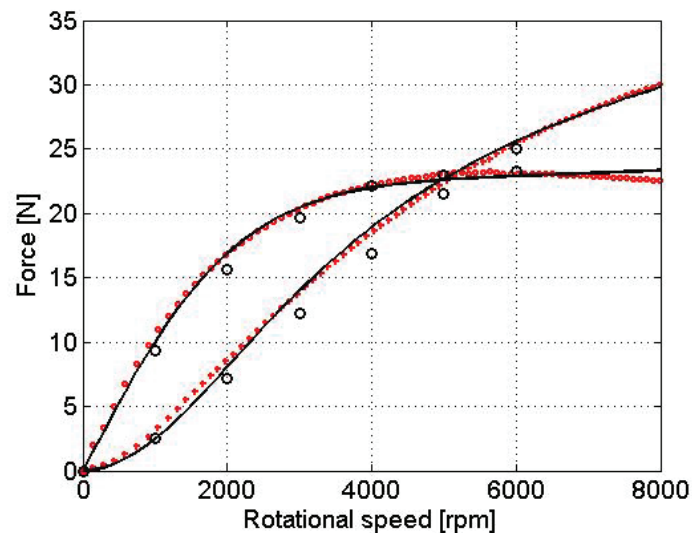
Figure 4:8 EDB forces according to the rotational speed with a constant eccentricity of 0.25 mm. Small circle markers refer to the measured forces perpendicular to the eccentricity while cross makers are the parallel components. Full lines refer to the analytical model. Bigger circles refer to FEM results.

The identified parameters of the mechanical equivalent for the double flux EDB are listed in Table 4:1.

Table 4:1 Parameters of the double flux EDB mechanical equivalent.

Parameter	Description	Value
ω_{EDB}	EDB electric pole	5000 rpm
k_1	EDB equivalent stiffness1	200010N/m
k_2	EDB equivalent stiffness2	123979 N/m
c_1	EDB equivalent damping1	57.7 Ns/m
c_2	EDB equivalent damping2	349.8 Ns/m

4.3   AMB/AMD model

Active magnetic bearings exploit the attractive forces generated by electromagnets to control the position of the rotor relative to the stator, with the feedback signals from position sensors. A general AMB configuration is illustrated in Figure 4:9. It is a complex mechatronic system. The interaction of different components like electromechanics, electronics and software is very high, so that the modeling of AMBs is not so straightforward. Analytical models of AMBs can be built based on linearized equations. But the parameters describing the electromechanical model need to be adjusted using experimental methods and the validity of the system model has to be confirmed experimentally. This work will be presented in the following chapter.

In the present section, the analytical model will be built first to be coupled with the rotor model and then to the EDB model.
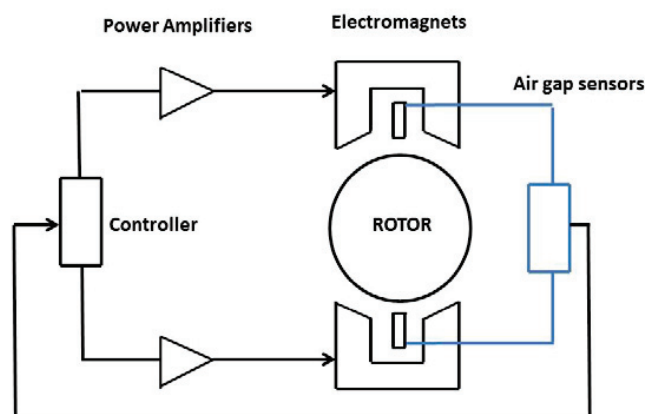
Figure 4:9 One degree of freedom AMB configuration

4.3.1 Chracterization of AMB/AMD actuators

The force/current relationship of AMBs is inherently nonlinear. For AMB rotors with small coil current variations under constant bias current, the nonlinear relationship can be effectively linearized about the rotor equilibrium position and nominal perturbation current. The force of an electromagnetic actuator at the operation point can be linearized as [1]:

$$f_x(\mathrm{x},\mathrm{i}) = k_i i + k_x x \qquad (4:23)$$

where k_x and k_i are respectively the negative displacement stiffness and the current stiffness of the actuator.

Their analytical equations are:

$$k_x = (2 \cdot N)^2 \cdot \mu_0 \cdot H \cdot I_b^{\ 2} / g_0^{\ 3} \cdot \cos(\mathrm{pi}/8)$$
$$k_i = (2 \cdot N)^2 \cdot \mu_0 \cdot H \cdot I_b / g_0^{\ 2} \cdot \cos(\mathrm{pi}/8) \qquad (4:24)$$

These linearized equations can be used for preliminary identification of AMB actuators, using the parameters of the actuator, as listed in Table 4:2.

<p align="center">Table 4:2   Parameters of the actuator.</p>

Parameter	Description	Value
D_e	Outer diameter	76 mm
D_i	Inner diameter	31 mm
W_p	Pole width	10 mm
H	Actuator thickness	22.5 mm
N	Number of turns	53
W_d	Wire diameter	0.63 mm
g_0	Radial air gap	0.7 mm
μ_0	Magnetic permeability of Vacuum	$4\pi \times 10^{-7}$H
I_b	Bias current	1.5 A

FE electromagnetic simulations were also used to model and identify the AMB actuators. The 2D model of the actuator was built with COMSOL Multiphysics®.
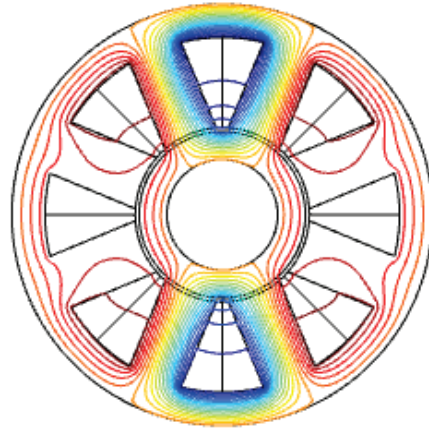
Figure 4:10 FE results of electromagnetic field of an AMB actuator.

The contour shows the magnetic vector potential, whereas the coloured surface shows the current density.

In COMSOL, the current stiffness was calculated considering a small variation in the control current, with the rotor kept centered. The displacement stiffness was calculated in COMSOL considering a virtual displacement of the rotor of 0.1mm. Figure 4:10 shows the electromagnetic distribution in the coils and rotor with coils activated in one degree of freedom.

Table 4:3 Parameters identification of AMBs.

Parameter	Description	Analytical results	FE results
k_x	Displacement stiffness	-19.2 N/mm	-16.8 N/mm
k_i	Current stiffness	9.0 N/A	8.5 N/A

The identified parameters of the AMB actuator are listed in Table 4:3. The comparison between analytical results and FE results shows good agreement. However, due to the complexity of AMB systems, the numerical values of these two parameters have to be verified experimentally.

4.3.2 Modeling of AMDs

The linearized equations of the AMD actuators in the fixed *x* and *y* directions can be represented as:

$$\begin{Bmatrix} F_{xAMD} \\ F_{yAMD} \end{Bmatrix} = \begin{bmatrix} k_x & 0 \\ 0 & k_x \end{bmatrix} \begin{Bmatrix} x_{AMD} \\ y_{AMD} \end{Bmatrix} + \begin{bmatrix} k_i & 0 \\ 0 & k_i \end{bmatrix} \begin{Bmatrix} i_{Cx} \\ i_{Cy} \end{Bmatrix}$$

(4:25)

where the variables x_{AMD}, i_{Cx}, y_{AMD} and i_{Cy} indicate respectively the displacements and the control currents in the two directions *x* and *y* of the actuator action plane.
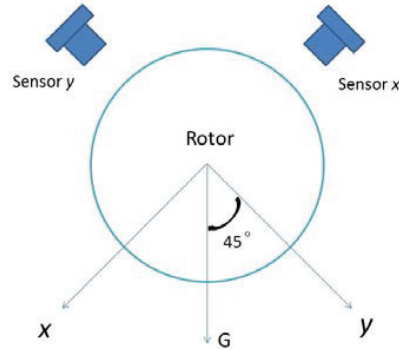
Figure 4:11 Cross section of the rotor, which shows an action plane of the AMB/AMD
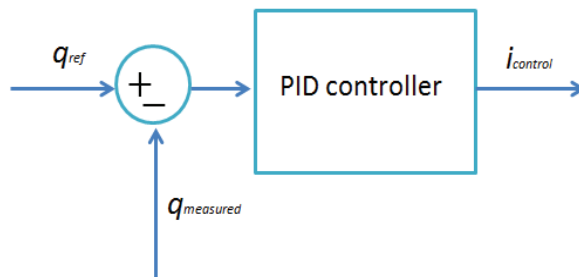
Figure 4:12 Block diagram of position control in the AMB/AMD

A PID architecture is used in the position control of AMDs to provide proper stiffness and damping. The transfer function between position error and reference control currents in each direction of the AMD is:

$$\frac{i_{c\_AMD}}{\varepsilon_{\_AMD}} = K_p(1 + \frac{1}{T_i \cdot s} + \frac{T_d \cdot s}{1 + \frac{T_d}{N} \cdot s})$$

(4:26)

where s is the Laplace variable. PID control is used just for quasi-static characterization, where the integral term is needed to keep the rotor at a reference position. While for the rest tests of the EDB–AMD system, PD control is used, because the EDBs will not provide levitation force if the rotor is centered. The corresponding stiffness k_{AMD} and non-rotating damping c_n can be obtained with the following equation:

$$k_{AMD} = K_p \cdot k_i + k_x$$
$$c_n = K_p \cdot T_d \cdot k_i$$

(4:27)

4.4   Complete model: rotor, EDB and AMD coupling

The dynamic equations of the rotor, the AMDs and the EDBs will be built and coupled together to obtain the complete model of the whole system.

4.4.1 State-space representation

State-space model is used here to represent the dynamics of the system. The most general state-space representation of a linear system with m inputs, p outputs and n state variables is written in the following form:

$$\dot{\underline{q}} = A\underline{q} + B\underline{u}$$
$$\underline{y} = C\underline{q} + D\underline{u}$$

(4:28)

where: $\underline{q}$ is the state vector, $\underline{u}$ is the input vector and $\underline{y}$ is the output vector.

4.4.2 State-space model of the rotor

The State Space model of the rotor with reference to the rotor center of gravity coordinates x, y, ϕ_y, ϕ_x could be written as following:

$$\begin{Bmatrix} \ddot{x} \\ \ddot{\phi}_y \\ \ddot{y} \\ \ddot{\phi}_x \\ \dot{x} \\ \dot{\phi}_y \\ \dot{y} \\ \dot{\phi}_x \end{Bmatrix} = \begin{bmatrix} -M^{-1}\Omega G & 0_{4\times4} \\ I_{4\times4} & 0_{4\times4} \end{bmatrix} \begin{Bmatrix} \dot{x} \\ \dot{\phi}_y \\ \dot{y} \\ \dot{\phi}_x \\ x \\ \phi_y \\ y \\ \phi_x \end{Bmatrix} + \begin{bmatrix} -M^{-1} \\ 0_{4\times4} \end{bmatrix} \begin{Bmatrix} F_x \\ M_y \\ F_y \\ M_x \end{Bmatrix}$$

(4:29)

$$\begin{Bmatrix} \dot{x} \\ \dot{\phi}_y \\ \dot{y} \\ \dot{\phi}_x \\ x \\ \phi_y \\ y \\ \phi_x \end{Bmatrix} = \begin{bmatrix} I_{8\times8} \end{bmatrix} \begin{Bmatrix} \dot{x} \\ \dot{\phi}_y \\ \dot{y} \\ \dot{\phi}_x \\ x \\ \phi_y \\ y \\ \phi_x \end{Bmatrix} + \begin{bmatrix} 0_{8\times4} \end{bmatrix} \begin{Bmatrix} F_x \\ M_y \\ F_y \\ M_x \end{Bmatrix}$$

(4:30)

Where *0* and *I* are null and identity matrices, *Ω* indicates the constant rotational speed of the rotor. The mass and gyroscopic matrices *M* and *G* are:

$$M = \begin{bmatrix} m & 0 & 0 & 0 \\ 0 & J_t & 0 & 0 \\ 0 & 0 & m & 0 \\ 0 & 0 & 0 & J_t \end{bmatrix}, G = \begin{bmatrix} 0 & 0 & 0 & 0 \\ 0 & 0 & 0 & -J_p \\ 0 & 0 & 0 & 0 \\ 0 & J_p & 0 & 0 \end{bmatrix} \qquad (4:31)$$

The outputs of the rotor model are displacements of the shaft. The inputs to the rotor are forces and torques due to EDB forces, AMD forces and general external forces (Equation 4:32).

$$\begin{Bmatrix} F_x \\ M_y \\ F_y \\ M_x \end{Bmatrix} = \begin{Bmatrix} F_{xAMB} + F_{xEDB} + F_{x\_ext} \\ M_{yAMB} + M_{yEDB} + M_{y\_ext} \\ F_{yAMB} + F_{yEDB} + F_{y\_ext} \\ M_{xAMB} + M_{xEDB} + M_{x\_ext} \end{Bmatrix} \qquad (4:32)$$

4.4.3 Transformation of coordinates

In the dynamic equations of the rotor (Equation 4:1), the reaction forces and moments generated by the two bearings are represented by F_b and M_b, while the external excitation forces and moments are F_{ext} and M_{ext}. Both the excitation forces and bearing forces are assumed to act on the center of mass of the rotor. However, in the real system, all the bearing reaction forces are applied away from the center of mass. For example, in the simple rotor model (Figure 4:1), the bearing forces are acted at the positions away from the center of mass by distances a and b.

Thus it is critical to clarify the relation between reaction forces at the bearing positions and force and moment at the center of mass of the rotor. Therefore, Figure 4:13 is plotted to show the transformation of reactions from bearing coordinates into the center of mass coordinates.
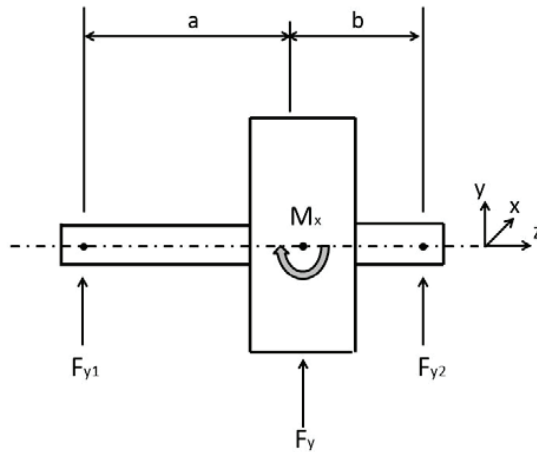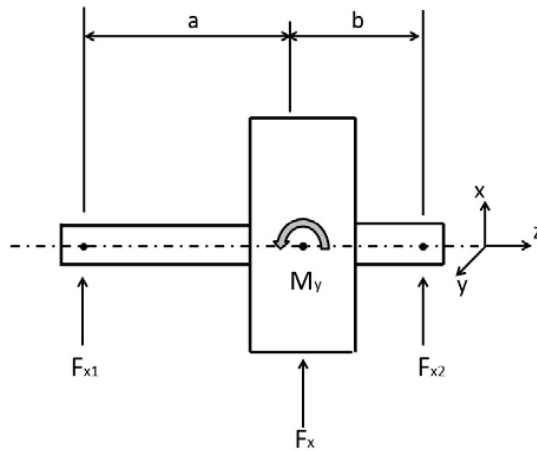
Figure 4:13 A 4 DOF rotor supported by two bearings.

It shows the transformation of reactions from bearing coordinates into the center of mass coordinates.

The forces and moments calculated at the center of mass of the rotor are:

$$
\begin{aligned}
F_x &= F_{x1} + F_{x2} \\
M_y &= -aF_{x1} + bF_{x2} \\
F_y &= F_{y1} + F_{y2} \\
M_x &= aF_{y1} - bF_{y2}
\end{aligned}
$$

(4:33)

Here the right hand rule is followed to define positive moments. Rearrange Equation 4:33 in matrix format:

$$
\begin{Bmatrix} F_x \\ M_y \\ F_y \\ M_x \end{Bmatrix} = T \begin{Bmatrix} F_{x1} \\ F_{y1} \\ F_{x2} \\ F_{y2} \end{Bmatrix}
$$

(4:34)

Where:

$$
T = \begin{bmatrix} 1 & 0 & 1 & 0 \\ -a & 0 & b & 0 \\ 0 & 1 & 0 & 1 \\ 0 & a & 0 & -b \end{bmatrix}
$$

(4:35)

The similar procedure is used to obtain the relation between the displacements at the center of mass of the rotor and those at the bearing positions. The transformation of displacements is expressed as following:

$$\begin{Bmatrix} x_1 \\ y_1 \\ x_2 \\ y_2 \end{Bmatrix} = R \begin{Bmatrix} x \\ \phi_y \\ y \\ \phi_x \end{Bmatrix}$$

(4:36)

Where *R* equals to the transpose of *T*:

$$R = \begin{bmatrix} 1 & -a & 0 & 0 \\ 0 & 0 & 1 & a \\ 1 & -b & 0 & 0 \\ 0 & 0 & 1 & b \end{bmatrix} = T^T$$

(4:37)

Utilizing the presented approach, the transformation matrices of coordinates can be obtained for the EDB-AMD system. The scheme of the bearing forces acting on the rigid rotor in the *XZ* and *YZ* planes are shown in Figure 4:14. It can be noticed that the two EDBs are positioned at both sides of the center of mass with distances a_{EDB} and b_{EDB}. The distances of the two AMBs/AMDs to the center of mass are a_{AMB} and b_{AMB}.
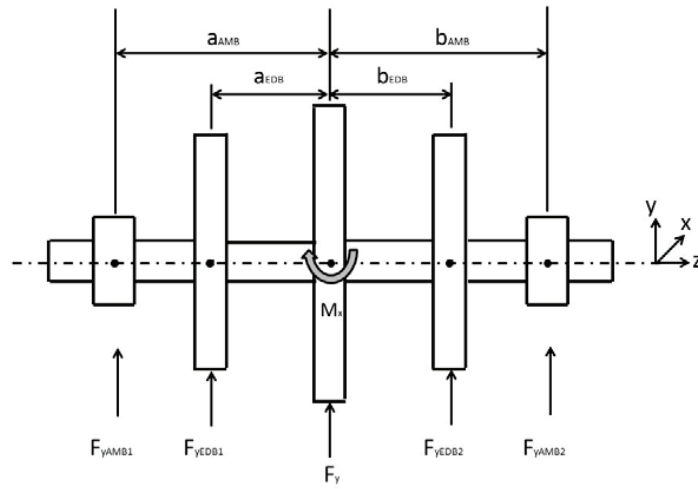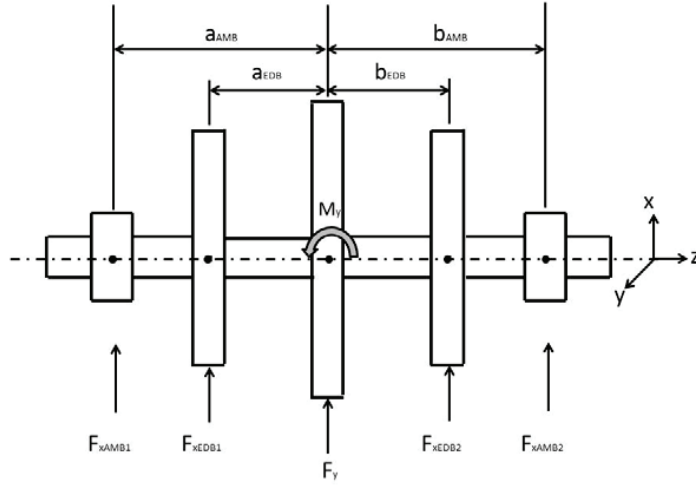
Figure 4:14 Scheme of the bearing forces acting on the rigid rotor in the XZ and YZ planes.

It shows the 4 DOF rotor model and the relative positions of EDBs and AMBs/AMDs.

Firstly, the transformation matrices of the AMBs/AMDs are obtained. R_{AMB} represents the transformation matrix linking the generalized displacements of the rotor center of mass to the AMB action planes. T_{AMB} is the transformation matrix linking the forces and moments acting on the rotor center of gravity to the AMB action planes.

$$
\begin{Bmatrix} x_{AMB1} \\ y_{AMB1} \\ x_{AMB2} \\ y_{AMB2} \end{Bmatrix} = \begin{bmatrix} 1 & -a_{AMB} & 0 & 0 \\ 0 & 0 & 1 & a_{AMB} \\ 1 & b_{AMB} & 0 & 0 \\ 0 & 0 & 1 & -b_{AMB} \end{bmatrix} \begin{Bmatrix} x \\ \phi_y \\ y \\ \phi_x \end{Bmatrix} = R_{AMB} \begin{Bmatrix} x \\ \phi_y \\ y \\ \phi_x \end{Bmatrix}
\tag{4:38}
$$

$$
\begin{Bmatrix} F_x \\ M_y \\ F_y \\ M_x \end{Bmatrix} = \begin{bmatrix} 1 & 0 & 1 & 0 \\ -a_{AMB} & 0 & b_{AMB} & 0 \\ 0 & 1 & 0 & 1 \\ 0 & a_{AMB} & 0 & -b_{AMB} \end{bmatrix} \begin{Bmatrix} F_{x1AMB} \\ F_{y1AMB} \\ F_{x2AMB} \\ F_{y2AMB} \end{Bmatrix} = T_{AMB} \begin{Bmatrix} F_{x1AMB} \\ F_{y1AMB} \\ F_{x2AMB} \\ F_{y2AMB} \end{Bmatrix}
\tag{4:39}
$$

Thus R_{AMB} and T_{AMB} are obtained:

$$
R_{AMB} = \begin{bmatrix} 1 & -a_{AMB} & 0 & 0 \\ 0 & 0 & 1 & a_{AMB} \\ 1 & b_{AMB} & 0 & 0 \\ 0 & 0 & 1 & -b_{AMB} \end{bmatrix}
\tag{4:40}
$$

$$T_{AMB} = \begin{bmatrix} 1 & 0 & 1 & 0 \\ -a_{AMB} & 0 & b_{AMB} & 0 \\ 0 & 1 & 0 & 1 \\ 0 & a_{AMB} & 0 & -b_{AMB} \end{bmatrix} \tag{4:41}$$

The same procedure has been made for EDBs. R_{EDB} represents the transformation matrix linking the generalized displacements of the rotor center of mass to the EDB planes.

$$R_{EDB} = \begin{bmatrix} 1 & -a_{EDB} & 0 & 0 \\ 0 & 0 & 1 & a_{EDB} \\ 1 & b_{EDB} & 0 & 0 \\ 0 & 0 & 1 & -b_{EDB} \end{bmatrix} \tag{4:42}$$

The transformation matrix linking the forces and moments acting on the rotor center of gravity to the EDB action planes is:

$$T_{EDB} = \begin{bmatrix} 1 & 0 & 1 & 0 \\ -a_{EDB} & 0 & b_{EDB} & 0 \\ 0 & 1 & 0 & 1 \\ 0 & a_{EDB} & 0 & -b_{EDB} \end{bmatrix} \tag{4:43}$$

4.4.4 State-space model of EDB

Equation 4:18 expressed the dynamic model of an EDB in complex coordinates. It can be written again here to show the real and imaginary parts:

$$\dot{F} = k(\dot{q} - j\Omega q) - F_q(\omega_{RL} - j\Omega)$$
$$q = x + jy \tag{4:44}$$
$$F_q = F_x + jF_y$$

Separating the real and imaginary parts, the dynamic behaviors of an EDB in both *x* and *y* directions are obtained:

$$\dot{F}_x = k(\dot{x} + \Omega y) - F_x \omega_{RL} - F_y \Omega$$
$$\dot{F}_y = k(\dot{y} - \Omega x) + F_x \Omega - F_y \omega_{RL} \tag{4:45}$$

The state-space representation of a single EDB can be expressed as:

$$\left\{\begin{matrix} \dot{F}_x \\ \dot{F}_y \end{matrix}\right\} = \begin{bmatrix} -\omega_{RL} & -\Omega \\ \Omega & -\omega_{RL} \end{bmatrix} \left\{\begin{matrix} F_x \\ F_y \end{matrix}\right\} + \begin{bmatrix} k & 0 & 0 & k\Omega \\ 0 & k & -k\Omega & 0 \end{bmatrix} \left\{\begin{matrix} \dot{x} \\ \dot{y} \\ x \\ y \end{matrix}\right\}$$

(4:46)

$$\left\{\begin{matrix} F_x \\ F_y \end{matrix}\right\} = I_{2\times2} \left\{\begin{matrix} F_x \\ F_y \end{matrix}\right\} + 0_{2\times4} \left\{\begin{matrix} \dot{x} \\ \dot{y} \\ x \\ y \end{matrix}\right\}$$

Therefore, the state-space representation of the double flux EDB unit in the system can be written as:

$$\left\{\begin{matrix} \dot{x}_{EDB} \\ \dot{y}_{EDB} \\ \dot{F}_{x1EDB} \\ \dot{F}_{y1EDB} \\ \dot{F}_{x2EDB} \\ \dot{F}_{y2EDB} \end{matrix}\right\} = \begin{bmatrix} 0 & 0 & 0 & 0 & 0 & 0 \\ 0 & 0 & 0 & 0 & 0 & 0 \\ 0 & k_1\Omega & -\omega_{RL1} & -\Omega & 0 & 0 \\ -k_1\Omega & 0 & \Omega & -\omega_{RL1} & 0 & 0 \\ 0 & k_2\Omega & 0 & 0 & -\omega_{RL2} & -\Omega \\ -k_2\Omega & 0 & 0 & 0 & \Omega & -\omega_{RL2} \end{bmatrix} \left\{\begin{matrix} x_{EDB} \\ y_{EDB} \\ F_{x1EDB} \\ F_{y1EDB} \\ F_{x2EDB} \\ F_{y2EDB} \end{matrix}\right\} + \begin{bmatrix} 1 & 0 \\ 0 & 1 \\ k_1 & 0 \\ 0 & k_1 \\ k_2 & 0 \\ 0 & k_2 \end{bmatrix} \left\{\begin{matrix} \dot{x}_{EDB} \\ \dot{y}_{EDB} \end{matrix}\right\}$$

(4:47)

where the suffix *EDB* indicates that the forces and displacements are referred to the plane of action of the EDB. The terms $\omega_{RL1}=k_1/c_1$ and $\omega_{RL2}=k_2/c_2$ are the poles of the two electric circuits arising in the rotating conductor. The state variables x_{EDB} and y_{EDB} in Equation 4:47 are added to couple the equation in the complete model of the whole system.

4.4.5 Complete model

The complete model of the system is built based on the rotor model coupled with EDBs and AMDs. The block diagram of the whole system is shown in Figure 4:15. Considering a reference frame where the *z*–axis represents the axial coordinate and the *x, y*–axes are the fixed radial coordinates, the rotor receives the forces in *x* and *y* directions by the EDBs and AMDs. The outputs of the rotor are the radial positions of the shaft referring to the EDBs and AMDs positions. The EDBs generate radial forces in function of the displacements and the rotating speed as inputs to the whole system. No axial force is produced by the EDBs. The AMDs react to the radial positions from the sensors and generate a force proportional to the first derivative of the position error thus adding non–rotating damping to the system.
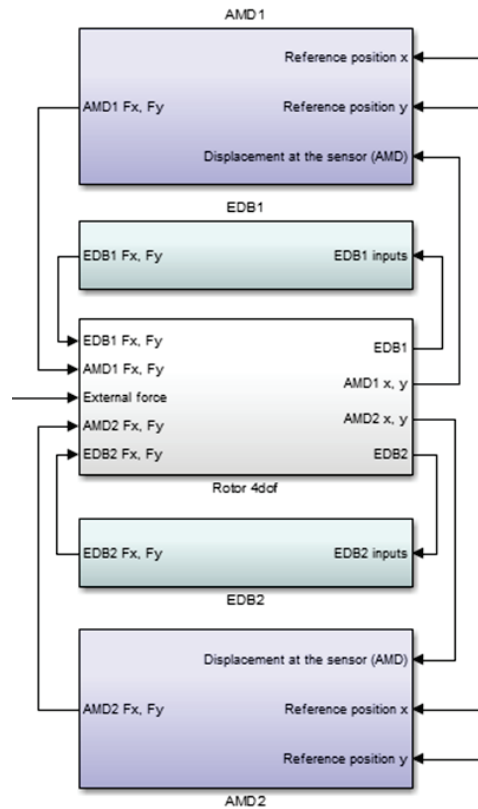
Figure 4:15 Block diagram of the complete model of the EDB-AMD system, showing the radial behavior of the system.

The analytical model of the whole system will be built in two steps. The first step is to build an open loop mechanical system including the rotor, EDBs and AMDs, based on the coupling of the three subsystems without close position loops.

The state-space representation of this system has been obtained (Equation 4:48 and 4:49), in which the inputs are the control currents to the AMBs/AMDs and outputs are the displacements at the two AMB planes. It is an open loop system. The second step is to close the position loops including PID controllers.

$$
\begin{Bmatrix}
\ddot{x} \\
\ddot{\phi}_y \\
\ddot{y} \\
\ddot{\phi}_x \\
\dot{x} \\
\dot{\phi}_y \\
\dot{y} \\
\dot{\phi}_x \\
\dot{F}_{x1EDB} \\
\dot{F}_{y1EDB} \\
\dot{F}_{x2EDB} \\
\dot{F}_{y2EDB} \\
\dot{F}^*_{x1EDB} \\
\dot{F}^*_{y1EDB} \\
\dot{F}^*_{x2EDB} \\
\dot{F}^*_{y2EDB}
\end{Bmatrix}
=
\begin{bmatrix}
-M^{-1}\Omega G & -k_d M^{-1} T_{AMB} R_{AMB} & -M^{-1} T_{EDB\_df} \\
I_{4\times4} & 0_{4\times4} & 0_{4\times8} \\
\begin{bmatrix} CC_{EDB} & 0_{4\times4} \\ 0_{4\times4} & CC_{EDB} \end{bmatrix} RR_{EDB} & & \begin{bmatrix} DD_{EDB} & 0_{4\times4} \\ 0_{4\times4} & DD_{EDB} \end{bmatrix}
\end{bmatrix}
\begin{Bmatrix}
\dot{x} \\
\dot{\phi}_y \\
\dot{y} \\
\dot{\phi}_x \\
x \\
\phi_y \\
y \\
\phi_x \\
F_{x1EDB} \\
F_{y1EDB} \\
F_{x2EDB} \\
F_{y2EDB} \\
F^*_{x1EDB} \\
F^*_{y1EDB} \\
F^*_{x2EDB} \\
F^*_{y2EDB}
\end{Bmatrix}
+
\begin{bmatrix}
-k_i M^{-1} T_{AMB} \\
0_{12\times4}
\end{bmatrix}
\begin{Bmatrix}
i_{x1} \\
i_{y1} \\
i_{x2} \\
i_{y2}
\end{Bmatrix}
$$

$$(4:48)$$

$$
\begin{Bmatrix}
x_{1AMB} \\
y_{1AMB} \\
x_{2AMB} \\
y_{2AMB}
\end{Bmatrix}
=
\begin{bmatrix} 0_{4\times4} & R_{AMB} & 0_{4\times8} \end{bmatrix}
\begin{Bmatrix}
\dot{x} \\
\dot{\phi}_y \\
\dot{y} \\
\dot{\phi}_x \\
x \\
\phi_y \\
y \\
\phi_x \\
F_{x1EDB} \\
F_{y1EDB} \\
F_{x2EDB} \\
F_{y2EDB} \\
F^*_{x1EDB} \\
F^*_{y1EDB} \\
F^*_{x2EDB} \\
F^*_{y2EDB}
\end{Bmatrix}
+
\begin{bmatrix} 0_{4\times4} \end{bmatrix}
\begin{Bmatrix}
i_{x1} \\
i_{y1} \\
i_{x2} \\
i_{y2}
\end{Bmatrix}
$$

$$(4:49)$$

where the notations are consistent with the analytical models of EDBs, AMBs and the rotor. It has to be mentioned that the suffix *x1*, *y1*, *x2* and *y2* in the EDB forces refer to the contribution from

two electric circuits in the same double flux EDB unit. The two EDB units are distinguished with * in the notations. It does not matter which EDB unit it is referred to, due to the symmetry in this case. Some more matrices have been introduced to simplify the state-space representation as follows.

RR_{EDB} is the transformation matrix that links the displacements and velocities of the rotor center of mass to the two EDB planes:

$$
\begin{Bmatrix} \dot{x}_1 \\ \dot{y}_1 \\ x_1 \\ y_1 \\ \dot{x}_2 \\ \dot{y}_2 \\ x_2 \\ y_2 \end{Bmatrix} =
\begin{bmatrix}
1 & -a_{EDB} & 0 & 0 & 0 & 0 & 0 & 0 \\
0 & 0 & 1 & a_{EDB} & 0 & 0 & 0 & 0 \\
0 & 0 & 0 & 0 & 1 & -a_{EDB} & 0 & 0 \\
0 & 0 & 0 & 0 & 0 & 0 & 1 & a_{EDB} \\
1 & b_{EDB} & 0 & 0 & 0 & 0 & 0 & 0 \\
0 & 0 & 1 & -b_{EDB} & 0 & 0 & 0 & 0 \\
0 & 0 & 0 & 0 & 1 & b_{EDB} & 0 & 0 \\
0 & 0 & 0 & 0 & 0 & 0 & 1 & -b_{EDB}
\end{bmatrix}
\begin{Bmatrix} \dot{x} \\ \dot{\phi}_y \\ \dot{y} \\ \dot{\phi}_x \\ x \\ \phi_y \\ y \\ \phi_x \end{Bmatrix} =
RR_{EDB}
\begin{Bmatrix} \dot{x} \\ \dot{\phi}_y \\ \dot{y} \\ \dot{\phi}_x \\ x \\ \phi_y \\ y \\ \phi_x \end{Bmatrix}
\tag{4:50}
$$

T_{EDB_df} is the transformation matrix linking the EDB forces in the two units to the forces and moments acting on the rotor center of mass:

$$
\begin{Bmatrix} F_x \\ M_y \\ F_y \\ M_x \end{Bmatrix} =
\begin{bmatrix}
1 & 0 & 1 & 0 & 1 & 0 & 1 & 0 \\
-a_{EDB} & 0 & -a_{EDB} & 0 & b_{EDB} & 0 & b_{EDB} & 0 \\
0 & 1 & 0 & 1 & 0 & 1 & 0 & 1 \\
0 & a_{EDB} & 0 & a_{EDB} & 0 & -b_{EDB} & 0 & -b_{EDB}
\end{bmatrix}
\begin{Bmatrix} F_{x1EDB} \\ F_{y1EDB} \\ F_{x2EDB} \\ F_{y2EDB} \\ F^*_{x1EDB} \\ F^*_{y1EDB} \\ F^*_{x2EDB} \\ F^*_{y2EDB} \end{Bmatrix} =
T_{EDB\_df}
\begin{Bmatrix} F_{x1EDB} \\ F_{y1EDB} \\ F_{x2EDB} \\ F_{y2EDB} \\ F^*_{x1EDB} \\ F^*_{y1EDB} \\ F^*_{x2EDB} \\ F^*_{y2EDB} \end{Bmatrix}
$$

(4:51)

$$
T_{EDB\_df} =
\begin{bmatrix}
1 & 0 & 1 & 0 & 1 & 0 & 1 & 0 \\
-a_{EDB} & 0 & -a_{EDB} & 0 & b_{EDB} & 0 & b_{EDB} & 0 \\
0 & 1 & 0 & 1 & 0 & 1 & 0 & 1 \\
0 & a_{EDB} & 0 & a_{EDB} & 0 & -b_{EDB} & 0 & -b_{EDB}
\end{bmatrix}
\tag{4:52}
$$

CC_{EDB} and DD_{EDB} are the two matrices in the dynamic equations of a double flux EDB unit:

$$
\begin{Bmatrix} \dot{F}_{x1EDB} \\ \dot{F}_{y1EDB} \\ \dot{F}_{x2EDB} \\ \dot{F}_{y2EDB} \end{Bmatrix} =
\begin{bmatrix}
k_1 & 0 & 0 & k_1\Omega \\
0 & k_1 & -k_1\Omega & 0 \\
k_2 & 0 & 0 & k_2\Omega \\
0 & k_2 & -k_2\Omega & 0
\end{bmatrix}
\begin{Bmatrix} \dot{x}_{EDB} \\ \dot{y}_{EDB} \\ x_{EDB} \\ y_{EDB} \end{Bmatrix} +
\begin{bmatrix}
-\omega_{RL1} & -\Omega & 0 & 0 \\
\Omega & -\omega_{RL1} & 0 & 0 \\
0 & 0 & -\omega_{RL2} & -\Omega \\
0 & 0 & \Omega & -\omega_{RL2}
\end{bmatrix}
\begin{Bmatrix} F_{x1EDB} \\ F_{y1EDB} \\ F_{x2EDB} \\ F_{y2EDB} \end{Bmatrix}
\tag{4:53}
$$

$$CC_{EDB} = \begin{bmatrix} k_1 & 0 & 0 & k_1\Omega \\ 0 & k_1 & -k_1\Omega & 0 \\ k_2 & 0 & 0 & k_2\Omega \\ 0 & k_2 & -k_2\Omega & 0 \end{bmatrix}$$

$$DD_{EDB} = \begin{bmatrix} -\omega_{RL1} & -\Omega & 0 & 0 \\ \Omega & -\omega_{RL1} & 0 & 0 \\ 0 & 0 & -\omega_{RL2} & -\Omega \\ 0 & 0 & \Omega & -\omega_{RL2} \end{bmatrix}$$

(4:54)

The complete close loop system is illustrated in Figure 4:16. The block "Rotor, AMD+EDB" has been built in the state-space representation (Equation 4:48 and 4:49). The block "PID controller" can be built using the transfer functions of the PID position controllers of the four degrees of freedom.
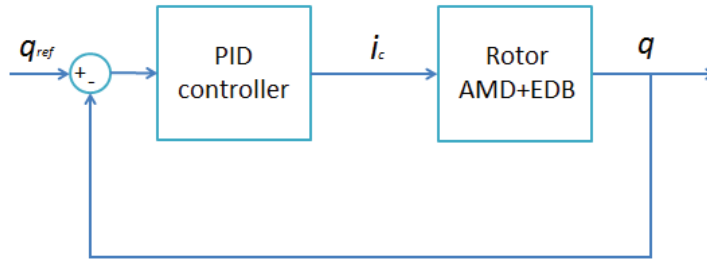
Figure 4:16 Block diagram of the close loop system

The transfer function between position error and reference control currents in each degree of freedom of the AMB/AMD is:

$$TF_{position\_loop} = K_p(1 + \frac{1}{T_i \cdot s} + \frac{T_d \cdot s}{1 + \frac{T_d}{N} \cdot s})$$

(4:55)

The two block systems can be consequently connected together to close the position loops. In MATLAB, the function append was used to connect the two blocks and to close the loop. The system's performance is also modelled with MATLAB Simulink® for simulations.

4.5 Rotordynamic stability

In the present section, the rotordynamic stability of the rotor supported by EDBs is investigated, using the obtained analytical models.

The first analysis is to see the stability of the EDB rotor without adding any additional damping, as shown in Figure 4:17.
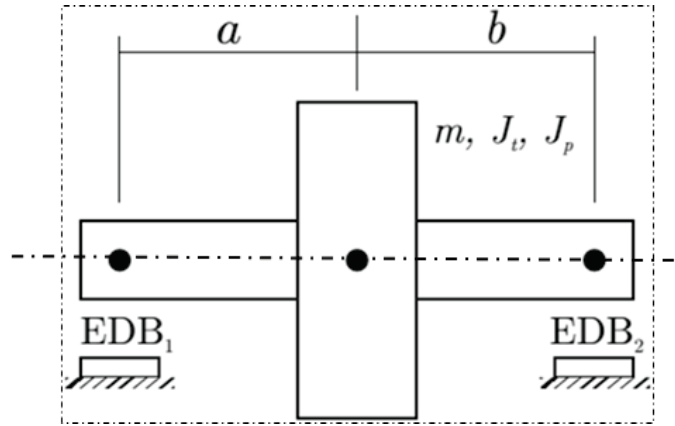
Figure 4:17 A four degrees of freedom rotor supported by two radial EDBs

Thus the AMDs are removed in the present study. The state-space representation of the system in this case becomes:

$$
\begin{Bmatrix}
\ddot{x} \\
\ddot{\phi}_y \\
\ddot{y} \\
\ddot{\phi}_x \\
\dot{x} \\
\dot{\phi}_y \\
\dot{y} \\
\dot{\phi}_x \\
\dot{F}_{x1EDB} \\
\dot{F}_{y1EDB} \\
\dot{F}_{x2EDB} \\
\dot{F}_{y2EDB} \\
\dot{F}^*_{x1EDB} \\
\dot{F}^*_{y1EDB} \\
\dot{F}^*_{x2EDB} \\
\dot{F}^*_{y2EDB}
\end{Bmatrix}
=
\begin{bmatrix}
-M^{-1}\Omega G & 0_{4\times4} & -M^{-1}T_{EDB\_df} \\
I_{4\times4} & 0_{4\times4} & 0_{4\times8} \\
\begin{bmatrix} CC_{EDB} & 0_{4\times4} \\ 0_{4\times4} & CC_{EDB} \end{bmatrix} \cdot RR_{EDB} & \begin{bmatrix} DD_{EDB} & 0_{4\times4} \\ 0_{4\times4} & DD_{EDB} \end{bmatrix}
\end{bmatrix}
\begin{Bmatrix}
\dot{x} \\
\dot{\phi}_y \\
\dot{y} \\
\dot{\phi}_x \\
x \\
\phi_y \\
y \\
\phi_x \\
F_{x1EDB} \\
F_{y1EDB} \\
F_{x2EDB} \\
F_{y2EDB} \\
F^*_{x1EDB} \\
F^*_{y1EDB} \\
F^*_{x2EDB} \\
F^*_{y2EDB}
\end{Bmatrix}
+
\begin{bmatrix} -M^{-1} \\ 0_{12\times4} \end{bmatrix}
\begin{Bmatrix} F_x \\ M_y \\ F_y \\ M_x \end{Bmatrix}
$$

(4:56)

Root locus plot is used to investigate the stability of the system. The real and imaginary parts of the calculated eigenvalues are plotted in the complex plane, where the sign of the real part decides stability. Negative real part confirms asymptotic stability whereas a non-negative value indicates instability.

The root locus as a function of spin speed (0 to 8000 rpm) is plotted in Figure 4:18. It evidences the presence of two poles having positive real parts.
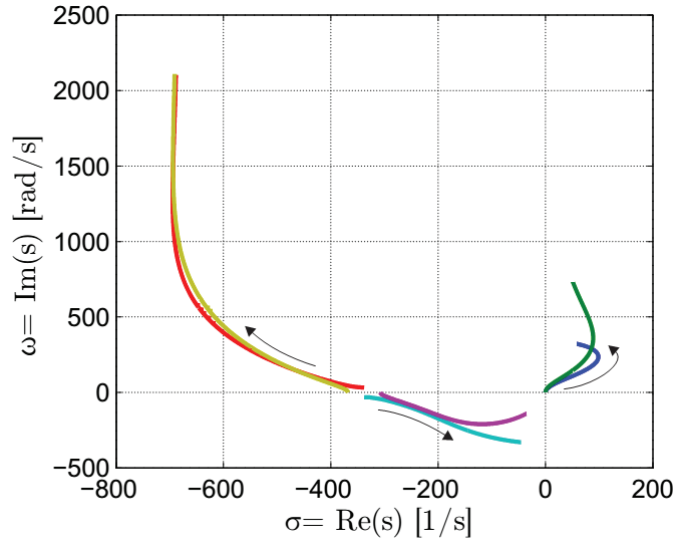
Figure 4:18 Root locus plot in function of rotational speed of a 4 DoF rotor supported by two radial EDBs

In the plot we can observe three pairs of curves. The first is given by two highly damped roots, represented with red and yellow lines, positioned far to left in the complex plane. A second pair of roots, represented in light blue and purple, lies in the lower part of the diagram. Finally, the third pair is located on the right half of the complex plane, and is represented with deep blue and green lines.
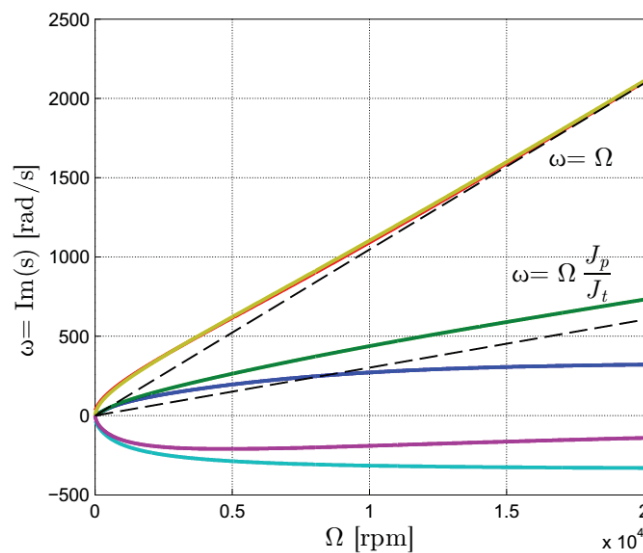
Figure 4:19 Campbell diagram of a 4 DoF rotor supported by two radial EDBs

The first set of curves represents two roots of the system that are associated to the dynamics of the eddy currents inside the conducting part of the EDB. These two roots are always stable. The

identification of the rotor mode associated to each root can be done with the support of the Campbell diagram shown in Figure 4:19. From this diagram we observe that the deep blue lines are associated to forward modes whereas the light blue lines are associated to backward modes. Both blue lines are related to cylindrical whirl modes, while green and purple lines are related to conical whirl modes.

Regarding the rotordynamic stability, Figure 4:18 shows that the rotor has two modes unstable. These modes are the forward cylindrical and conical whirl modes. In absence of external non-rotating damping the two modes are unstable for any value of spin speed different from zero.

Chapter 5   Measurements and results

Experimental results and simulations are presented in the present chapter. Firstly, the test bench will be set up properly allowing system operation. A PID controller is used for preliminary tests. The analytical model of the EDB–AMD rotor system will be validated both with quasi–static tests and with frequency response measurements. During this process, all the coefficients in the system will be confirmed.

Once the analytical model is validated, further calculations and simulations will be exploited to investigate the control parameters and feasibility of the system.

5.1   Test rig set up

Before any experimental tests, the test rig needs to be set up in a proper way. The whole test bench consists of the test rig, control electronics and power supplies for AMDs and the motor respectively. Figure 5:1 shows the test rig and the control electronics of AMDs.
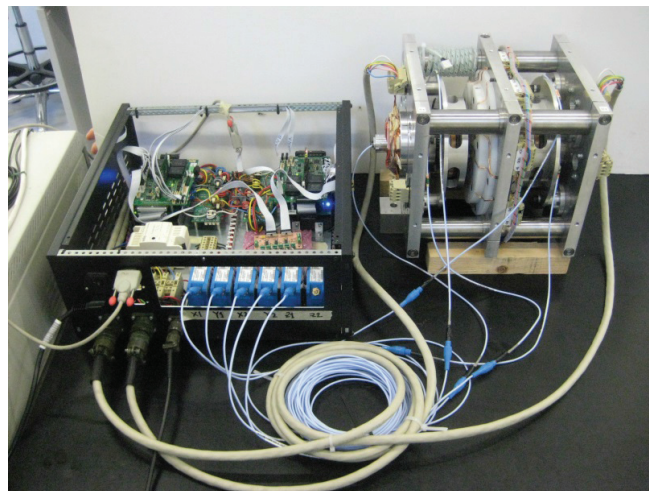
Figure 5:1 The test rig and control electronics of AMDs

A PID controller (Equation 5:1) in the position loop of AMDs is used for preliminary tests. In this system, radial EDBs provide stiffness when the rotor rotates with an eccentricity or under another disturbance force. If the rotor is levitated and perfectly centered in the magnetic field of EDBs by AMDs, EDBs will not make contribution to levitation.

With a PID position controller in AMDs, where AMDs are used as AMBs, it is possible to control the value of rotor eccentricity (between the geometry axis and the axis of the axisymmetric magnetic field). Consequently, the effect of EDBs in this system is controlled. Therefore, the system can be controlled dynamically using PID controller of the AMDs.

Firstly, different sets of control parameters have been obtained analytically and then tested experimentally to keep the rotor levitated and rotating stably in the speed range of 0 to 6000 rpm. Although in the setup phase the analytical model of the system had not yet been fully validated, the numerical stability analysis was applied to select proper control parameters to complete the setup.

$$\frac{i_{c\_AMB}}{\varepsilon_{\_AMB}} = K_p (1 + \frac{1}{T_i \cdot s} + \frac{T_d \cdot s}{1 + \frac{T_d}{N} \cdot s}) \tag{5:1}$$

The function of AMBs is eventually realized in the test bench, which is the first step and opens the possibility of further tests of the system. Table 5:1 lists a set of PID control parameters (for Equation 5:1) that allow stable and smooth operation.

Table 5:1 Parameters of PID controller.

Parameter	Description	Value
K_p	Controller proportional gain	10 A/mm
T_d	Derivative time constant	0.005 s
T_i	Integral time	0.1 s
N	Time constant of the first order derivative filter	5

5.1.1 Adjustment of magnetic center

As a hybrid bearing system, the nominal positions of both types of bearings must be considered and tuned properly. The offsets of displacement sensors should be set consistently with the center of the magnetic field of EDBs. This center should be also the nominal position for AMBs. If the reference center position of AMBs are different from the magnetic center of EDBs, when the rotor rotates EDBs produces restoring forces which will be compensated by AMBs. Thus the control currents in AMDs are influenced. Since the restoring forces of EDBs vary according to the spin speed, the control currents in AMBs will vary accordingly.

A scheme of this effect is illustrated in Figure 5:2. It shows the interaction of different force components in the radial plane of the rotor for a given rotational speed ($\Omega > 0$ to include the effect of EDBs). Here mg is the gravity force and δ is the offset between AMB nominal center and the magnetic center of EDB. The effect of δ on AMB force F_{AMB} is illustrated: if the offset of the two centers are zero, AMB forces only compensates the gravity, thus $F_{AMB} = mg$; when δ is positive, which

means the restoring force of EDB is cumulative to gravity force, F_{AMB} is increased. Contrastively, if δ is negative, F_{AMB} is reduced.
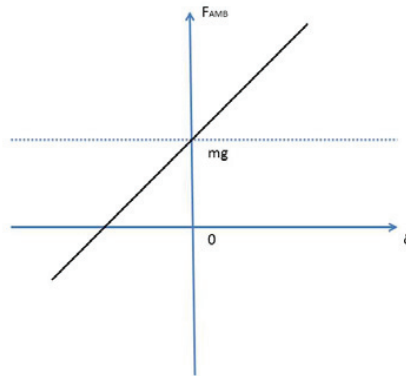
Here, *mg* is the gravity effect force and δ is the offset between AMB nominal center and the magnetic center of EDB. When δ is positive, which means the restoring force of EDB is cumulative to gravity force, F_{AMB} is increased. Contrastively, if δ is negative, F_{AMB} is reduced.

Figure 5:2 The effect of δ on AMB force F_{AMB}.

The adjustment of the magnetic center should be completed before any further tests to minimize the unwanted interaction between AMBs and EDBs. The approach is based on the effect illustrated in Figure 5:2. Run the rotor (levitated by AMBs) in the speed range of 0 to 6000 rpm and measure the control currents in AMBs: if the two bearing centers are perfectly coincided, the AMB control currents should not vary according to the rotational speed; the larger the offset is, the more AMB control currents will vary with increasing of the rotational speed.

Therefore, the experimental tests have been performed by tuning the reference positions of the two AMBs and reduce as much as possible the changing of control currents in the speed range. In the test rig, there are two EDBs and two AMBs positioned on the rotor shaft with different distances to the center of the rotor. This fact makes the present test not so easy, because of the interaction of different planes in terms of the radial positions.

The control currents in AMB_1 and AMB_2 with the rotor centered are measured in the test rig and plotted in Figure 5:3. It can be noticed different axes show different behaviors. The y-axis of AMB_2 (named y_2) shows the least effect of the offset while the x-axis of AMB_2 (named x_2) shows relative big offset compared to other three axes.
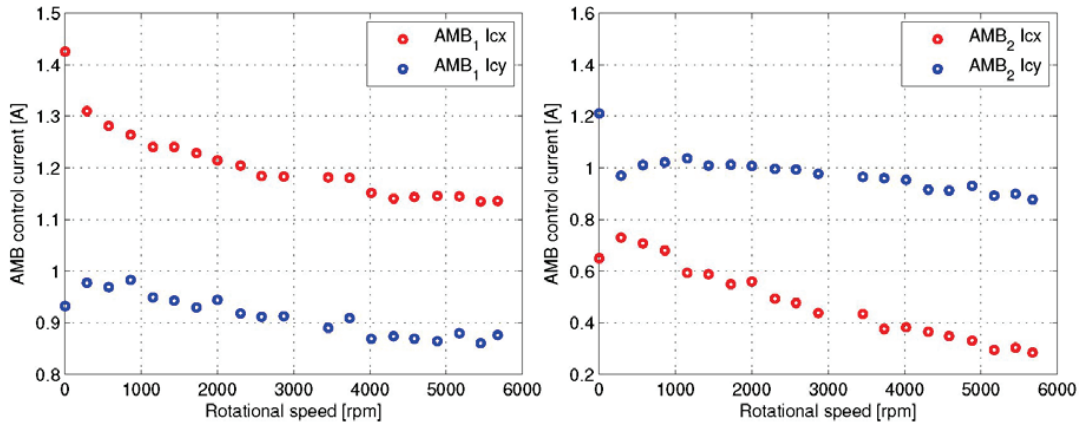
Figure 5:3 Control currents in the two AMBs with the rotor centered

The corresponding EDB center offsets in the four axes x_1 ,y_1 ,x_2 ,y_2 are obtained as listed in Table 5:2.

Table 5:2 EDB-AMB center offsets

Parameter	Description	Value
X_1	EDB center offset in x direction of AMB action plane 1	0.13 mm
Y_1	EDB center offset in y direction of AMB action plane 1	0.07 mm
X_2	EDB center offset in x direction of AMB action plane 2	0.04 mm
Y_2	EDB center offset in y direction of AMB action plane 2	0.24 mm

5.2   Quasi-static model validation

Quasi-static characterization is commonly used in the field of EDB parameters identification, where the rotor is fixed in an off-centered radial position and rotates at a certain speed. The parameters of the double flux EDB has been identified both with FE simulations and experimental tests in quasi-static condition. The reference results of EDB forces both along the direction of the eccentricity and perpendicular to it will be used in the present test to validate the analytical model of the system. The validation procedure is described in the following paragraph.

In the test rig, the rotor rotates with a fixed eccentricity, which is kept by PID control of the AMDs. The EDBs produce restoring forces due to the eccentricity, whereas the AMDs are required to provide the same amount of forces with opposite direction to keep the rotor in the off–centered position. Thus the values of EDB forces are obtained by measuring the AMD forces, which can be calculated from the measured control currents (Equation 5:2). With an eccentricity of 0.1 mm in +y direction, the control currents in AMDs are measured both in simulations and experimentally in the speed range of 0 to 6000 rpm.
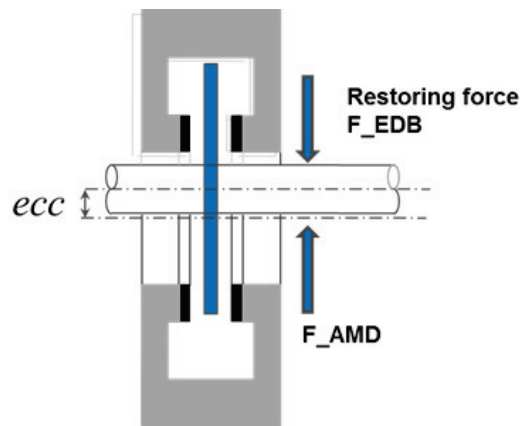
Figure 5:4 Scheme of the quasi-static tests, which show the force of EDB due to the rotor static eccentricity and the force of AMB/AMD to keep the rotor at the off-centered position
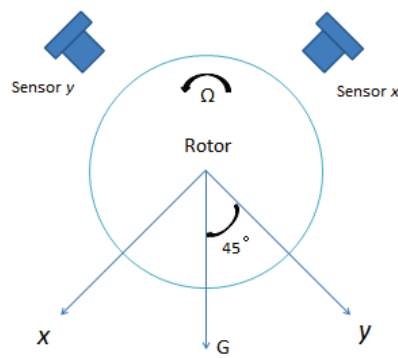
Figure 5:5 One action plane of AMDs, with the directions of the xy coordinates illustrated

$$F_{EDB} = -F_{AMD}$$
$$F_{AMD} = k_i i_c + k_x y$$

(5:2)

In simulations, gravity force is not considered to show the effect of EDBs. Whereas in experimental tests, two sets of control currents are measured respectively with the rotor centered and off-centered (Figure 5:6). Then the difference of the two sets of control currents are used to eliminate the influence of gravity and to compare with simulation results.

(a)   (b)
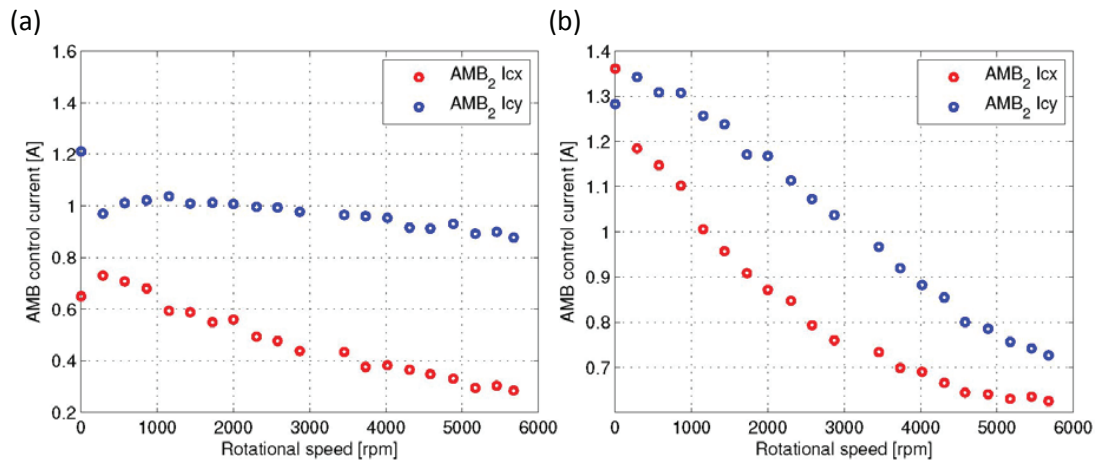
Figure 5:6 Control currents in the coils of AMB_2. (a) The rotor is in the centre position. (b) The rotor is off-centered with 0.1 mm eccentricity in +y direction.

Numerical and experimental results are plotted and compared in Figure 5:7, which show good agreements.
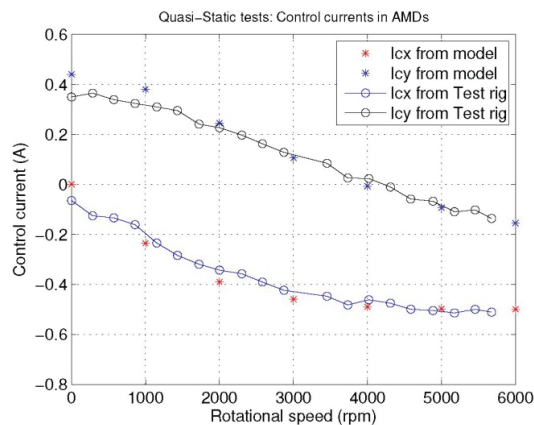
Figure 5:7 Control currents in the coils of one AMB with the rotor off-centered with 0.1mm eccentricity along +y direction. Comparison of simulation results and experimental ones shows good agreement.

The corresponding AMB forces are calculated with the linearized equation [1]. Consequently the values of EDB forces are obtained, which are plotted in Figure 5:8 to be compared with analytical results. The force comparison well validates the model. Figure 5:9 is plotted here with results obtained in the quasi-static identification of EDBs in Chapter 4 (The results are divided by 2.5, the factor between different values of eccentricities). The comparison between the two figures provides a cross validation.

It needs to mention that the current stiffness of the AMB ki is used to calculate the AMB forces in this test, thus the numerical value of ki can be adjusted from this test. Other parameters of the AMBs will be checked in the following section using Frequency Responses.
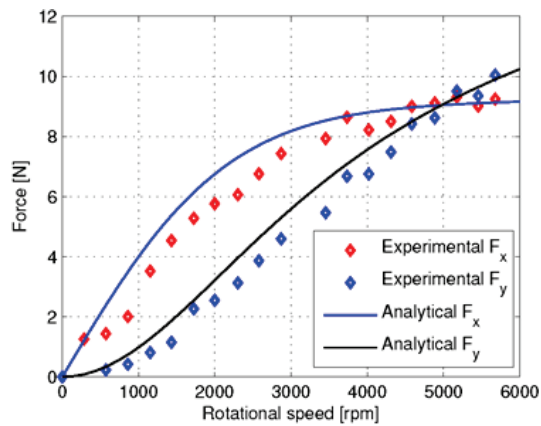
Figure 5:8 EDB forces developed by a single EDB unit when the rotor is rotating with a static eccentricity of 0.1 mm. Both analytical and experimental results are plotted to validate the analytical model.
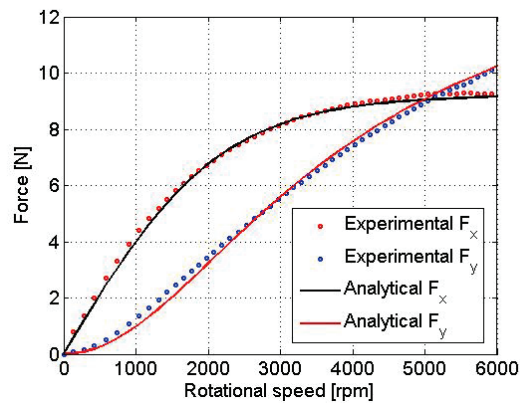
Figure 5:9 Results of EDB forces from quasi-static identification in Chapter 4.

Those results confirm the validity of the system model described in the previous chapter and demonstrate the potential of the EDB–AMD hybrid system.

5.3   Frequency response

To illustrate the dynamic performance of the system, measurements of frequency responses are carried out experimentally as well as with simulations. A disturbance current is input along one of the axes x_1, y_1, x_2, and y_2 of the two AMD action planes, the corresponding frequency response of displacement in the same direction is measured with a frequency sweep from 10 to 500 Hz. The scheme of this test is demonstrated in Figure 5:10.
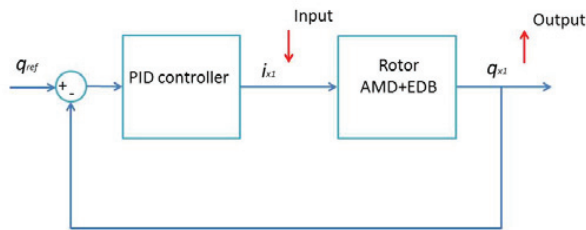
Figure 5:10 Scheme of the transfer function measurements along one of the AMD axis.
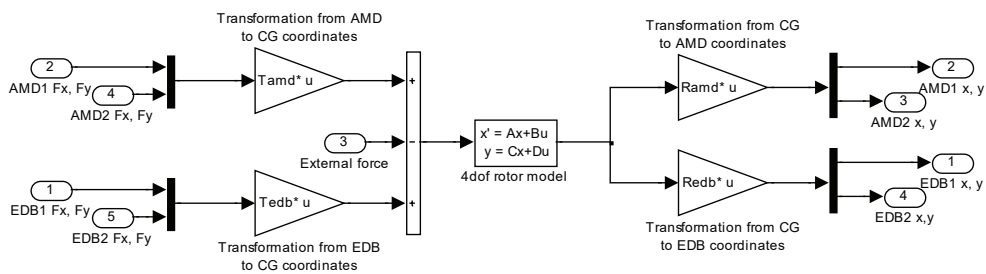
Figure 5:11 Block diagram of the EDB-AMD system

The block diagram of the complete system is provided (Figure 5:11) to help understand the present transfer function measurement tests. The transfer function between input current and output displacement in the same axis is obtained with the rotor levitated by AMDs and rotating at different spin speeds. The comparison of analytical and experimental results is shown in Figure 5:10, which shows good agreement. During the present tests, the parameters in the model has been checked and adjusted. Since the EDB coefficients and part of AMB parameters have been confirmed in the previous quasi-static test, they are confirmed again in this test. The adjusted parameters of the AMB are listed in Table 5:3.
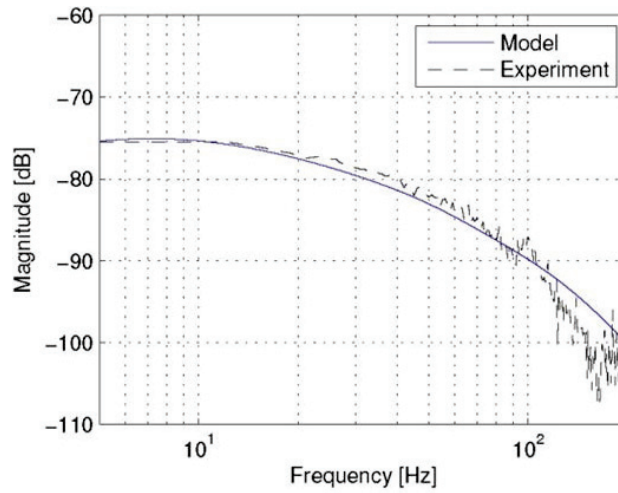
Figure 5:12 Frequency response plot along one axis of AMDs with input disturbance current and output displacement, where the rotor is levitated by AMD and rotates at zero speed.

Table 5:3 Adjusted Parameters of AMDs.

Parameter	Description	Value
k_x	Displacement stiffness	−30 N/mm
k_i	Current stiffness	9.5 N/A

The same transfer function is also obtained for higher speeds to show the effect of EDBs. Figure 5:13 shows the frequency response plots from numerical simulation respectively for Ω=1000 rpm, 3000 rpm and 6000 rpm based on the same control parameters of AMDs. It can be observed that with the increasing of rotational speed of the rotor, the gain between input current and output displacement at lower frequency moves downwards, which means the overall stiffness of the bearing system increases. It is due to the effect that EDB stiffness increases according to the rotational speed.
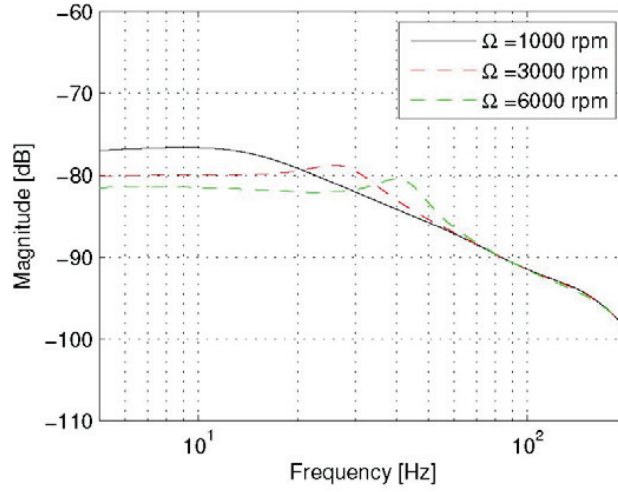
Figure 5:13 Frequency response plots for different rotational speeds.

5.4 PD control

In the preliminary tests, PID controller was applied to set up and validate the system. However, to relieve the load on AMDs, the integral term of PID controller should be disabled. Consequently PD control is used to allow EDBs work properly and to provide non-rotating damping to the rotor.

Here, the transfer function between position error and reference control currents in each direction of the AMD becomes:

$$\frac{i_{c\_AMD}}{\varepsilon_{\_AMD}} = K_p(1 + \frac{T_d \cdot s}{1 + \frac{T_d}{N} \cdot s}) \tag{5:3}$$

The corresponding non-rotating damping c_n is:

$$c_n = K_p \cdot T_d \cdot k_i \tag{5:4}$$

Bode plot of the PD controller is shown in Figure 5:14.
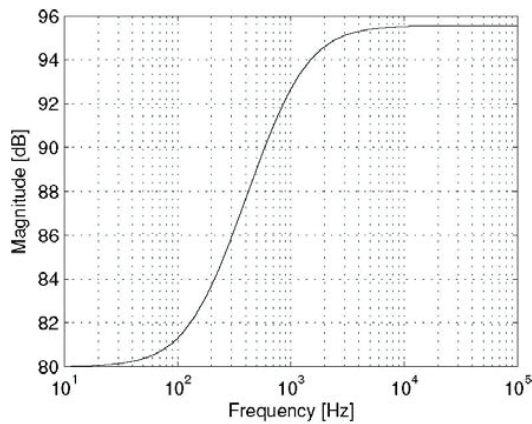
Figure 5:14 Bode plot of the PD controller

The control parameters of the PD controller are listed in Table 5:3

Table 5:3 Parameters of PD controller.

Parameter	Description	Value
K_p	Controller proportional gain	10 A/mm
T_d	Derivative time constant	0.005 s
N	Time constant of the first order derivative filter	5

With PD position control of AMDs, the rotor runs stably in the speed range of 0-6000 rpm. The displacements are measured in the speed domain (Figure 5:16). It should be noticed that the rotor is levitated from zero speed by AMDs, but not centered, because there is not integral effect in the controller. With the increasing of rotational speed, the restoring forces of EDBs increase. Therefore, the eccentricity of rotor reduces, which shows the contribution of EDBs. The difference in evolutions of displacements in *x* and *y* directions is related to the effect of EDB forces, which have different behaviors in the directions parallel and perpendicular to the eccentricity as shown in Figure 5:8.

Here the coordinates in the radial plane are shown in Figure 5:15, a cross section view of the rotor. The results (Figure 5:16) from the numerical model and the test rig are quite consistent, which validates again the numerical model of the system. The EDBs provide radial stiffness to the rotor and carries the main load at high speed. The feasibility of the hybrid EDB–AMD configuration has been demonstrated.
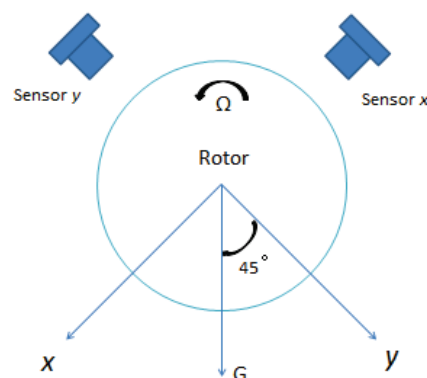
Figure 5:15 Scheme of the rotor in one AMD action plane
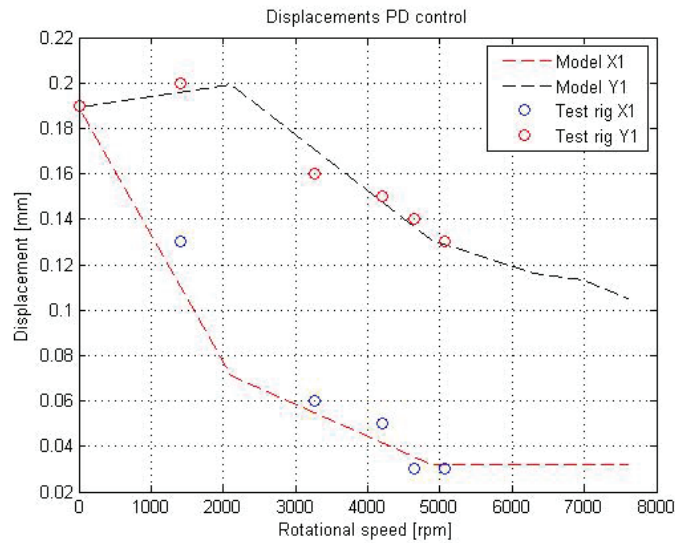
Figure 5:16 Displacements of the rotor according to rotational speed

5.4.1 Control currents comparison

The advantage of the hybrid configuration, as has been stated at the beginning of the present thesis, is to exploit the controllability of AMBs to stabilize the rotor supported by EDBs. Therefore, compared to standard AMBs, this system is expected to relieve the load on AMBs with EDBs' contribution. It means the possibility of downsizing AMB coils.

In this section, comparison analysis between PID and PD controls of AMDs in terms of control currents will be made to show the advantage of the hybrid bearing system. It is important to mention that with PID control to keep the rotor centered, the system is basically the same as a standard AMB system. Thus the comparison is between a standard AMB system and the present hybrid bearing system. The control currents in the AMDs are measured with the model in Simulink.

The AMD control currents in *x* and *y* directions of the AMD action plane using PID control and PD control are plotted respectively in the speed range (Figure. 5:17). With PID control, the levitation is mainly provided by AMDs. They work as pure AMBs since the rotor is kept centered by the actuators. Thus the control currents remain almost constant in the speed range. While using PD control of the AMDs, the rotor is not kept centered by the actuators. The restoring force is provided by EDBs. At low speed, the control currents are even higher compared to the case with PID control, which is due to the fact that with rotor eccentricity there is the contribution of negative displacement stiffness of AMD. Thus more control currents are required to compensate the effect of the negative stiffness. With the rotational speed increasing, the contribution of EDB restoring force increases accordingly. The eccentricity is getting smaller. The load on AMDs is also reduced, so that the AMD control currents reduce according to the rotating speed. The difference in evolutions of i_{Cx} and i_{Cy} is also due to the effect of EDB forces, which have different behaviors in the directions parallel and perpendicular to the eccentricity. Obviously the evolutions of control currents are consistent with the displacements variation in the speed range. At high operation speeds, the

amount of control currents in the actuator is significantly smaller compared to standard AMB system. The AMD actuators could be downsized in the hybrid configuration.
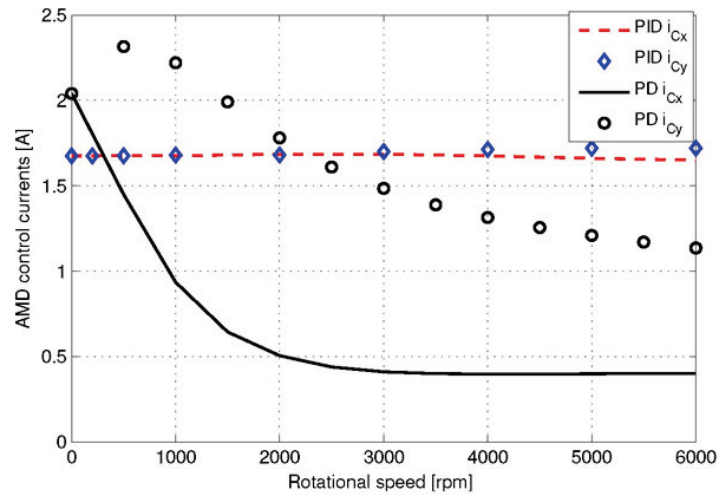
Figure 5:17 Comparison of AMD control currents according to rotating speed with PID control and PD control

5.4.2 Calculated Power consumption

Consequently, the total power consumption in the EDB–AMD system can be calculated. The power consumption in the EDB could be obtained with the product of torque and angular speed, where the torque is due to the EDB force and rotor eccentricity (Figure 5:18). The power consumption in the AMD is calculated directly with the obtained currents in the coils and the electrical resistances. This calculation does not include eddy current or windage losses in the actuators since they are relatively small in general. The total consumed power due to EDBs and AMDs in the system are plotted in Figure 5:19. The AMB power consumption is obtained by using PID position control of the actuators. It can be noticed that, the power consumption in EDBs is rather small compared to that in AMDs. At low speed, AMDs consume more power compared to standard AMBs, which is due to the effect of negative displacement stiffness in the actuators as explained in the previous section. At high speed, the sum of **power consumption in EDBs and AMDs can be reduced significantly compared to AMBs**.
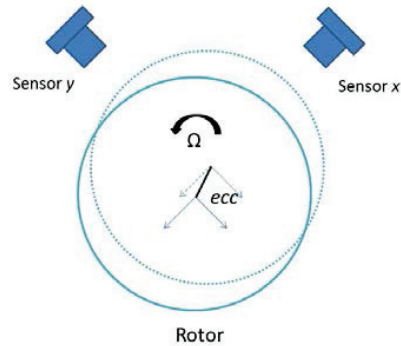
Figure 5:18: Scheme of the rotor rotates off-centered.
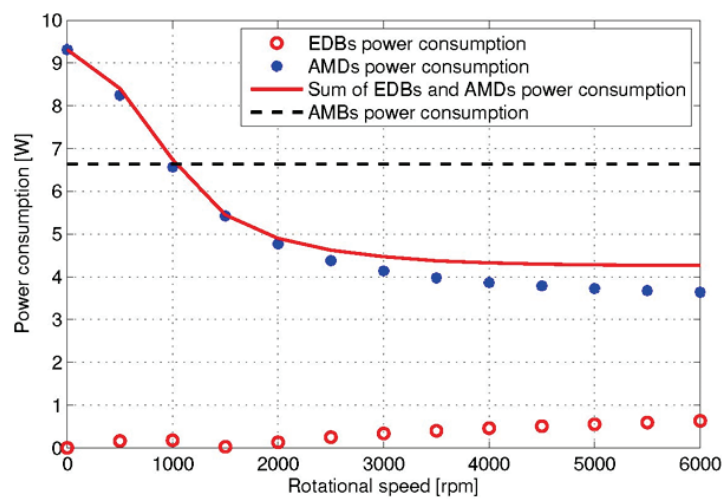
Figure 5:19 Calculated power consumption of the hybrid configuration

5.5   Conclusion of the results

These results demonstrate the effectiveness of the EDB–AMD solution. The instability issues of rotors supported by EDBs have been solved using active magnetic damping. This is an essential scientific novelty of the present work.

This solution not only overcomes the instability, but also allows tuning the amount of damping and even stiffness (if required) during operation. It shows the possibility of optimizing damping strategies.

The use of AMDs also allows the rotor to levitate from zero speed. It is also an advantage of this solution. In other existing works of EDBs, mechanical supporting structures are used to allow the rotor take off, which is not convenient.

The comparisons between PID and PD controls in terms of control currents and power consumptions show the advantage of this hybrid bearing system over standard AMBs. Compared to the standard AMB, the AMDs combined with the main load carrying EDBs will be much smaller, with significantly down-sized power electronics.

Additionally, at high speed, the EDB carries the rotor weight passively, in the sense that it does not depend on a controller or a sensor. This provides additional operational safety in critical applications.

The following chapter (Chapter 6) will be devoted to the control strategies of AMDs, which is to investigate the control approaches of the EDB-AMD system in order to find optimized control strategies.

In Chapter 7, the damping strategies of EDBs will be discussed and possible alternative solutions will be presented. The possibility of AMDs to realize a general viscous damper will also be discussed and demonstrated. It is the second essential novelty of the present work.

Chapter 6   Control strategies of AMDs

Control strategies of AMDs are discussed in this chapter. The parameters of PD position controller are decided according to the dynamics of the system to obtain stable and optimized performance. This study starts with the stability analysis of the rotor supported by EDBs. The target is to exploit AMDs to provide radial stiffness at low speed, when EDBs are not able to provide sufficient stiffness, whereas to introduce non-rotating damping in the whole speed range to achieve stable operation and optimal performance.

6.1   Rotordynamic Stability analysis

The rotordynamic stability analysis of the system is presented in the present section to show the dynamic behavior of the rotor supported by EDBs and AMDs.

Root locus plot is used to investigate the stability of the system. The stability analysis has also been made on the EDB-AMD system using the analytical model presented in Chapter 4. The approach was used to define proper parameters for the AMD controllers allowing stable operation of the system.

Figure 6:1 shows the stability of the rotor in the test rig within the rotational speed range 0 to 20000 rpm, where c_n is 465 Ns/m. The arrows indicate the directions of the evolution of the poles with increasing rotational speed. All the modes are stable in this case. Figure 6:2 is the plot of Campbell diagram. The first critical speed is 183 Hz, which is much higher than the speed range for experimental tests in the present work.

This method of stability analysis will be used in the following sections to search for the optimal control parameters of the AMD controllers, thus to find a proper control strategy of AMDs.
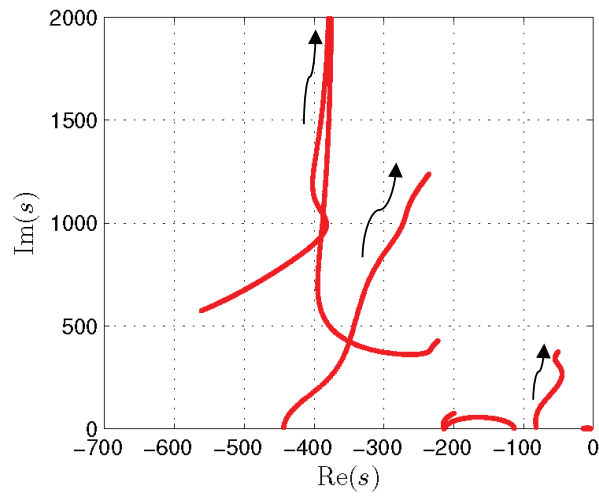
Figure 6:1 Root locus plot of the hybrid system with sufficient non-rotating damping
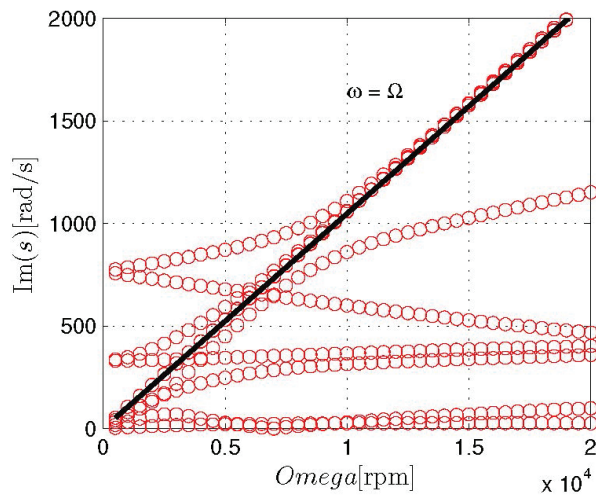
Figure 6:2 Plot of Campbell diagram

6.2 Control parameters of AMDs

Control of AMDs is performed utilizing the PD controller in the position control allowing proper function of the hybrid bearing system. The control strategies will be discussed in this section.

In the previous chapter, the feasibility of the hybrid system has been demonstrated. However, only a single set of control parameters was used to realize the system function. It is necessary to investigate the control strategies of AMDs, in other words, how to decide the amount of stiffness and non-rotating damping provided by AMDs.

6.2.1 Amount of non-rotating damping for stability

The first analysis is to see the stability range of the PD control parameters. Stability analysis of the system is utilized to understand the amount of non-rotating damping required to keep the rotor in stable operation. The tests have been completed in the speed range of 0-6000 rpm. The value of the derivative term *Td* in the PD controller was selected as high enough for stable operation (*Td*=0.005 here, which is the value used in Chapter.5) and kept as constant. The minimum values of proportional gain *Kp* for stability for different speeds have been investigated (Figure 6:3). Consequently the minimum amount of non-rotating damping is obtained ($c_n = K_p T_d k_i$).

Simulations with the validated model are used in this analysis. Figure 6:4 illustrates the minimum amount of non-rotating damping required from one of the AMD actuators to keep the rotor stable for different speeds. It can be noted that this plot shows similar fashion with the rotating damping developed in the EDB. The required damping value increases according to the rotational speed up to its maxima, which occurs around the electric pole of the EDBs. The maximum amount of non–rotating damping required for the rotor's stable operation is 371 Ns/m. This curve characterizes the damping demand in the EDB system and can be used to define the control parameters in the AMD.
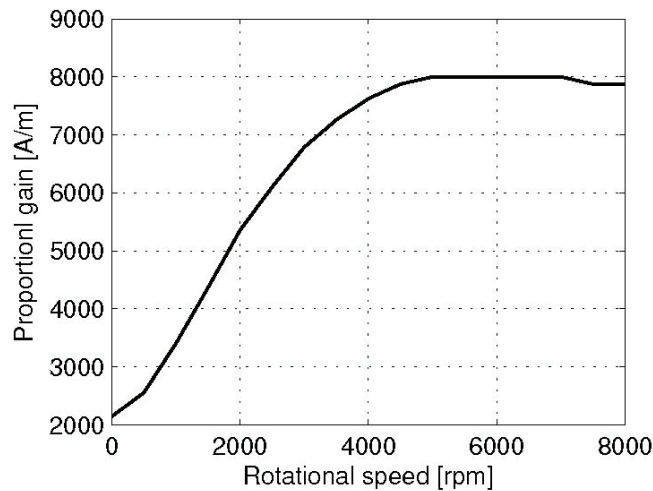
Figure 6:3 Minimum amount of proportional gain
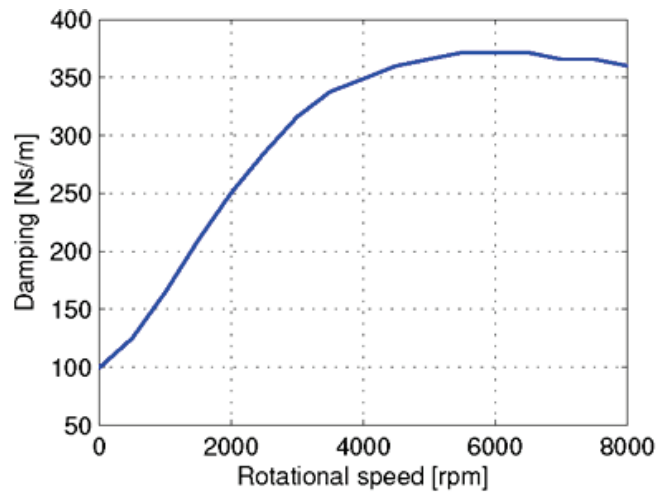
Figure 6:4 Minimum amount of non-rotating damping

It should be noticed that, in the present investigation, *Td* is fixed and *Kp* is variable. It is useful to decide the control parameters in the PD controller of AMDs for stable operation. The parameters are fixed during the whole speed range. Thus they are not guaranteed to be optimal in terms of efficiency.

6.3   Stability map with parameters

It is worth to see the amount of stiffness and non-rotating damping that are required from the AMDs to keep the system stable in the speed range. In the present analysis, the stiffness from AMD k_d and non-rotating damping c_n are variables that need to be decided.

6.3.1 Simplified model

A simplified mechanical model of the hybrid system has been built, as shown in Figure 6:5, where the AMDs are represented by a spring and damper connected in parallel. Stability analysis of such simplified mechanical model will be made to see the amount of k_d and c_n that are needed for stable operation.
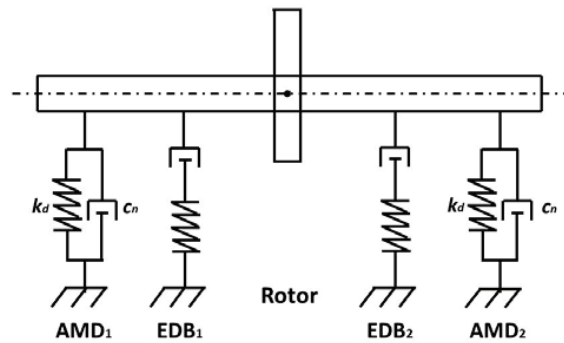
Figure 6:5 Scheme of the hybrid system, where AMDs are represented as a spring and a damper connected in parallel.

6.3.2 Stability map

The previous section focused on the fixed control parameters (it means the parameters do not change in the whole speed range of tests) in AMDs to ensure the system stability, especially the amount of required non-rotating damping was presented. However, the AMDs not only provide non-rotating damping, but also provide stiffness. The stiffness is essential for low speed levitation of the rotor. Besides, both damping and stiffness of AMDs affect the stability of the system. Thus it is important to see the stable zone of both variables.

A stability map (in the speed range of 0 to 6000 rpm) is plotted in Figure 6:6 in terms of the two variables k_d and c_n. The region above the stability line represents safe zone of k_d and c_n to keep the rotor stable in the testing speed range. This plot opens the possibility to choose the suitable values of stiffness and damping in the AMDs, consequently can be used to define the control strategies.
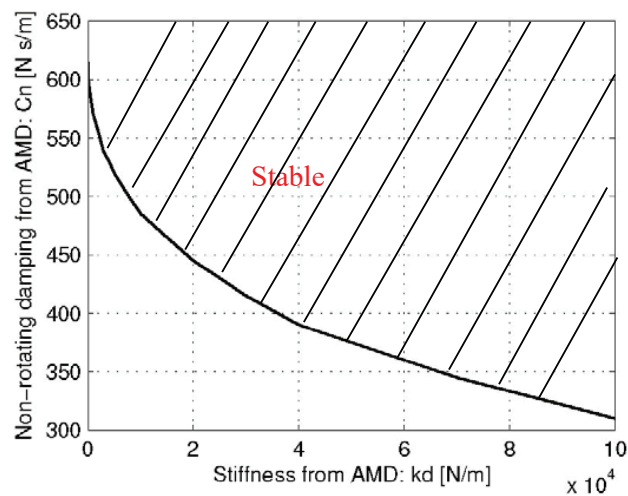
Figure 6:6 Stability map in terms of k_d and c_n

Chapter 7 Damping strategies

The feasibility of the proposed hybrid solution has been demonstrated in previous chapters. The control of AMDs has also been discussed. Based on the built model and obtained results, the general damping strategies for EDB systems will be presented in this chapter. Alternative solutions will also be discussed.

7.1 Adding non-rotating damping

As has been illustrated in Chapter 6, the rotor supported by EDBs presents instability. Thus non-rotating damping is demanded for stable operation. Different damping methods as well as their effectiveness and limitations have been presented in literature, which highly motivated the present work.

The hybrid solution has been demonstrated thoroughly in previous chapters. However, the present thesis is not only limited on the EDB-AMD solution. The target is to study damping strategies for EDB systems and to provide possible damping solutions. Thus further damping study, based on the validated EDB model adding non-rotating damping, will be made.

7.1.1 EDB-damper system

The analytical model of the test rig is used here for damping analysis. The AMDs in the model are replaced with simple viscous damper, that are able to provide non-rotating damping c_n to the rotor supported by the EDBs. Figure 7:1 shows the scheme of such a system. In general, the position of damper should be decided according to the rotordynamic behavior, especially for flexible rotors. The influence of damper positions was investigated in [41], where AMDs were used to control the vibration modes of a flexible rotor. While in the present study, only rigid mode is present in the speed range, thus the damper position influence on the rotordynamics is not under investigation.
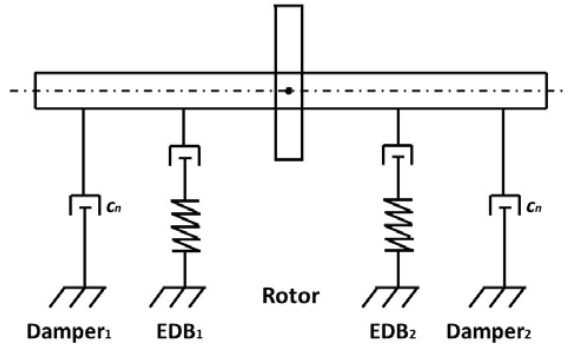
Figure 7:1 EDB-damper system

The analytical model of this system has been obtained based on modification of the EDB-AMD model. This model will be used to investigate the amount of non-rotating damping that is required from the dampers to keep the rotor in stable operation. The state-space model of the rotor coupled with dampers is:

$$
\begin{Bmatrix} \ddot{x} \\ \ddot{\phi}_y \\ \ddot{y} \\ \ddot{\phi}_x \\ \dot{x} \\ \dot{\phi}_y \\ \dot{y} \\ \dot{\phi}_x \end{Bmatrix} = \begin{bmatrix} -M^{-1}\Omega G - M^{-1}c_n T_{AMD} R_{AMD} & 0_{4\times4} \\ I_{4\times4} & 0_{4\times4} \end{bmatrix} \begin{Bmatrix} \dot{x} \\ \dot{\phi}_y \\ \dot{y} \\ \dot{\phi}_x \\ x \\ \phi_y \\ y \\ \phi_x \end{Bmatrix} + \begin{bmatrix} -M^{-1} \\ 0_{4\times4} \end{bmatrix} \begin{Bmatrix} F_x \\ M_y \\ F_y \\ M_x \end{Bmatrix} \quad (7:1)
$$

$$
\begin{Bmatrix} \dot{x} \\ \dot{\phi}_y \\ \dot{y} \\ \dot{\phi}_x \\ x \\ \phi_y \\ y \\ \phi_x \end{Bmatrix} = \begin{bmatrix} I_{8\times8} \end{bmatrix} \begin{Bmatrix} \dot{x} \\ \dot{\phi}_y \\ \dot{y} \\ \dot{\phi}_x \\ x \\ \phi_y \\ y \\ \phi_x \end{Bmatrix} + \begin{bmatrix} 0_{8\times4} \end{bmatrix} \begin{Bmatrix} F_x \\ M_y \\ F_y \\ M_x \end{Bmatrix} \quad (7:2)
$$

Where

$$\begin{Bmatrix} F_x \\ M_y \\ F_y \\ M_x \end{Bmatrix} = \begin{Bmatrix} F_{xEDB} + F_{x\_ext} \\ M_{yEDB} + M_{y\_ext} \\ F_{yEDB} + F_{y\_ext} \\ M_{xEDB} + M_{x\_ext} \end{Bmatrix} \qquad (7{:}3)$$

The analytical model of such a system will be obtained by coupling this model with EDB models (presented in Chapter 4).

Since the rotor is expected to be fully levitated during operation speed range, the damper should be able to introduce non-rotating damping without mechanical contact. Possible types of such a damper will be discussed later based on the desired damping characteristics.

7.1.2 The amount of non-rotating damping

To see the possibility of alternative damping solutions, it is essential to understand the stability of the rotor and how much damping is needed. Different from AMDs used in the test rig, which also introduce stiffness, in the present analysis, only non-rotating damping is introduced to the rotor supported by the EDBs. There's no additional stiffness to be considered. Therefore, the effect of the amount of non-rotating damping on the system stability can be investigated with stability analysis (root locus method).

The stability thresholds of rotational speed for different amounts of non-rotating damping have been calculated and plotted in Figure 7:2 for the experimental rotor as described in Chapter 3. This plot shows the relationship between the amount of non-rotating damping and the corresponding stability threshold of rotational speed. With this obtained characteristics, it is possible to design a damper in either active or passive way to keep the rotor in stable operation in the desired speed range. Of course, the damper is expected to be able to provide **contactless damping** to the rotor.
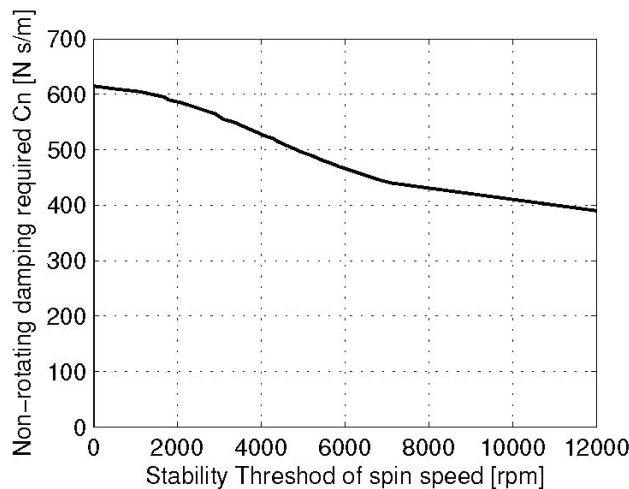
Figure 7:2 The amount of non-rotating damping introduced by each damper and the corresponding stability threshold of spin speed for the rotor in the test rig.

7.2   Realizing viscous dampers with AMDs

The previous section presents the strategies to add non-rotating damping to the rotor supported by EDBs. This work is based on the analytical model. Although the model has been validated and the investigation is useful, experimental results can always be a plus if possible. The aim of this section is to demonstrate the possibility of realizing viscous dampers with AMDs.

AMDs introduce k_d and c_n to the system. If make k_d equal to 0, AMDs provide only c_n. In this case, AMDs are able to simulate viscous dampers.

$$\frac{i_{cx\_AMD}}{\varepsilon_{x\_AMD}} = K_p(1 + \frac{T_d \cdot s}{1 + \frac{T_d}{N} \cdot s}) = K_p + \frac{K_d \cdot s}{1 + \frac{T_d}{N} \cdot s} \qquad (7:4)$$

The approach is to choose a proper value of Kp to make $k_d = 0$ (Equation 7:5). Then the damping estimation can be made using AMDs by tuning the values of K_d and T_d.

$$\begin{aligned} k_d &= K_p \cdot k_i + k_x \\ c_n &= K_d \cdot k_i \end{aligned} \qquad (7:5)$$

The same investigation of non-rotating damping as shown in Figure 7:2 can be made using the EDB-AMD model. Here T_d is fixed (0.005), the values of the derivative gain K_d to keep the rotor in stable operation are obtained. Consequently, the corresponding values of c_n are plotted in the speed range (Figure 7:3).

By comparing the two plots (Figure 7:2 and 7:3), which are quite consistent, it can be noticed that the AMDs can be used to achieve general viscous dampers that are used to introduce non-rotating damping to the EDB system.

This result is remarkable due to the fact that, in the EDB-AMD test rig, similar tests can be made experimentally to realize general viscous dampers using AMDs. It means that the EDB-AMD system can allow investigating in a controlled laboratory environment a damping strategy that could then find also a passive implementation.
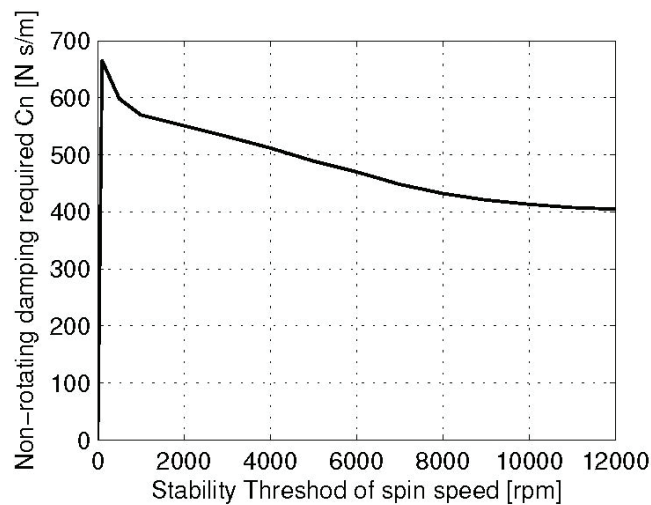
Figure 7:3 The same test as in Figure 7:2, but using AMDs

7.3 Damping solutions

Alternative damping solutions will be presented in this section. Based on the characterized minimum damping values for different spin speeds, proper dampers could be selected to meet the requirements. Possible solutions for such EDB system could be mainly electromagnetic dampers, both active and passive types. This does not exclude other possibilities such as electrorheological or magnetorheological dampers, which have been presented recently in rotordynamic applications.

In this section, the possibilities of using passive eddy current dampers and semi-active magnetic dampers will be discussed.

7.3.1 Eddy current dampers (ECDs)

Eddy current dampers (ECDs) introduce a damping effect exploiting the Lorentz forces due to the induced eddy currents in a conductor subject to a time-varying magnetic field, they are contact free. The eddy currents are induced by the relative motion between a conductor and a constant magnetic field or in a conductor experiencing a time-varying magnetic field. Therefore, ECDs can be passive (if using permanent magnetic field) or active (by modulating the current of an electromagnet). We study here an example of a passive (permanent magnet) damper.

77
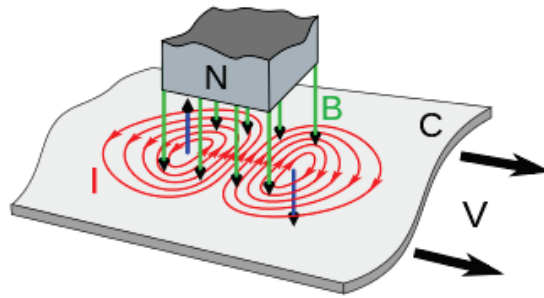
Figure 7:4 Eddy currents induced in motional conductor within a constant magnetic field: translational ECD.

For non-rotating damping, the permanent magnet must be on the rotor and the conductor on the stator. Figure 7:4 shows a possible configuration of ECD, where **the ECD is combined with a passive magnetic bearing**. The damping coefficients of the ECD depend on the magnetic field, the geometry and the conductivity of the conductor.
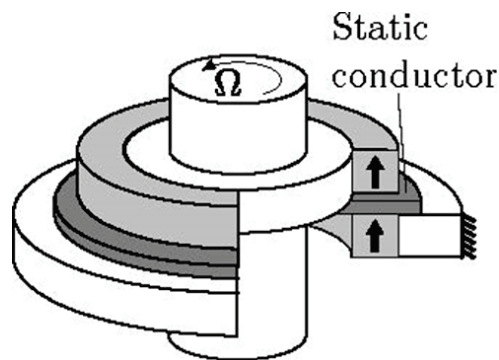
Figure 7:5 A eddy current damper implemented in rotordynamic application: this ECD is combined with a passive magnetic bearing.

Modeling of ECDs is a difficult task since the damping forces derive from a dynamic interaction between currents induced in a stationary conductor and a moving magnetic field. The calculation of the damping of ECDs has been conducted mainly using analytical equations or finite element (FE). However, existing analytical equations are not accurate enough [40]. While 3D time-stepping FE simulations are accurate but cost too much computational time, for example the analysis carried out in [42] required a total simulation time of 295 hours using a Pentium 4 3.0 GHz PC. Of course, the computational time could be reduced using more powerful computer.

A systematic approach of modeling and identification of ECDs in rotordynamic applications has been proposed by the author [40] [18]. It provides an accurate and efficient approach for identification of ECDs. This method employs an analytical dynamic model of the ECD (same as the EDB model in Chapter 4) and curve fitting with results of finite element (FE) models to obtain the parameters characterizing the ECD's mechanical impedance. The details of this approach are described in Appendix.

Utilizing this identification approach, the ECD could be designed properly and introduced to the ECD system to solve the instability problem. The possibility of a complete passive solution is very attractive due to the simplicity, reliability and lower cost. Since the space and cost are two critical factors that limits the application of magnetic bearings, EDBs combined with passive dampers, if proved to be fully effective, are really meaningful. This could be a future work.

7.3.2 Semi-active magnetic dampers

Semi-active magnetic dampers, also called transformer eddy current dampers, exploit transformer eddy currents. Different from active eddy current dampers, the coils in semi-active magnetic dampers are supplied with a constant voltage and generate the magnetic field linked to the moving element [43]. Figure 7:6 shows the sketch of a semi-active magnetic damper including two electromagnets. The motion of the moving element with speed $\dot{q}$ changes the reluctance of the magnetic circuit and produces a variation of the flux linkage. According to Faraday's law, the time variation of the flux generates a back electromotive force. Eddy currents are induced in the coils and generate damping force that act against the speed of the moving element. It has to be notice that there's also the fixed current due to the voltage supply in the coils which introduces negative stiffness.
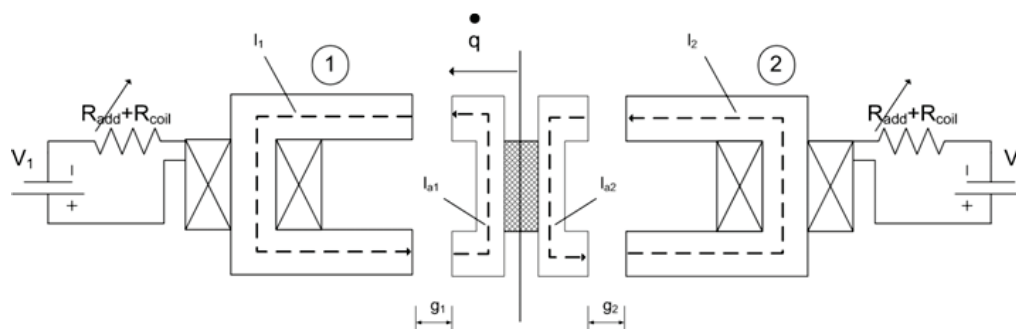
Figure 7:6 Sketch of a two electromagnet Semi-active magnetic damper [43]

Compared with AMDs or active eddy currents, the semi-active magnetic dampers have simpler architecture and smaller size. No feedback control is needed. Thus they could also be a solution for the EDB system in the present thesis.

Another appealing fact of the semi-active magnetic damper is the possibility to combine it with the axial-flux permanent magnet motor, which is used in the EDB test rig. Let's recall the configuration of the motor, as shown in Figure 7:7, it consists of the rotor with permanent magnets and the stationary coils.
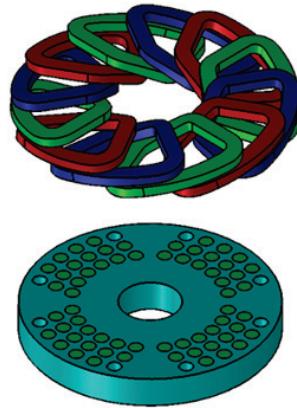
Figure 7:7 Configuration of the axial flux motor used in the EDB test rig. It shows the coils and the rotor with permanent magnets.

Therefore, it is possible to integrate the moving part of the semi-active damper in the rotor part of the motor, and put the coils of the damper on the stator of the motor, resulting a structure called Motor-Damper. Figure 7:8 shows a brief sketch of such structure, where (1) is permanent magnet and (2) is control coil of the motor, while (3) and (4) are the moving and stationary parts of the semi-active damper respectively.
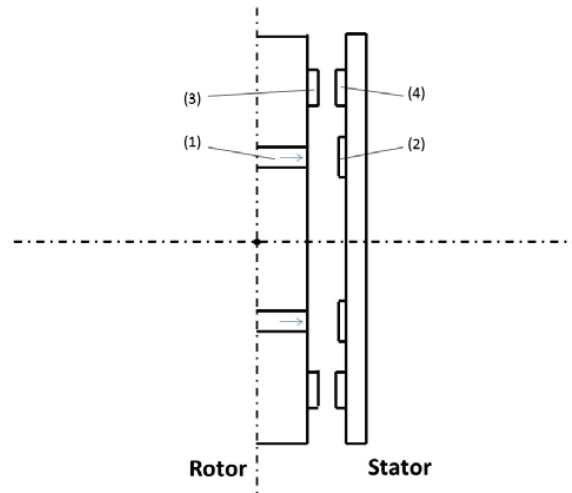
Figure 7:8 Sketch of the Motor-Damper structure.

Two possible configurations of EDB system using Motor-Damper structures could be built for different applications (Figure 7:9 and Figure 7:10). In configuration 1, two Motor-Damper structures are used to drive the rotor and to provide non-rotating damping. There are two radial EDBs, same as the test rig in the thesis. It may be interesting for long rotor applications. Configuration 2 uses single EDB with two Motor-Damper structures, it could be appealing for flywheel applications.
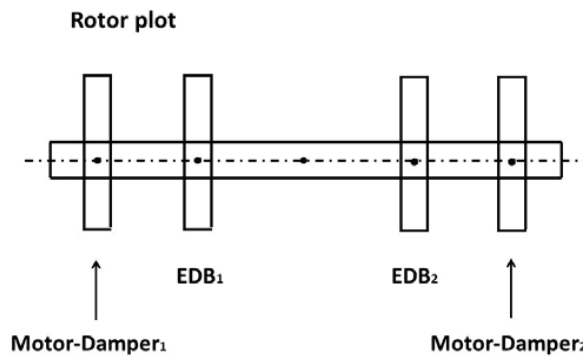
Figure 7:9 Configuration 1 using EDBs and the Motor-Damper structure.
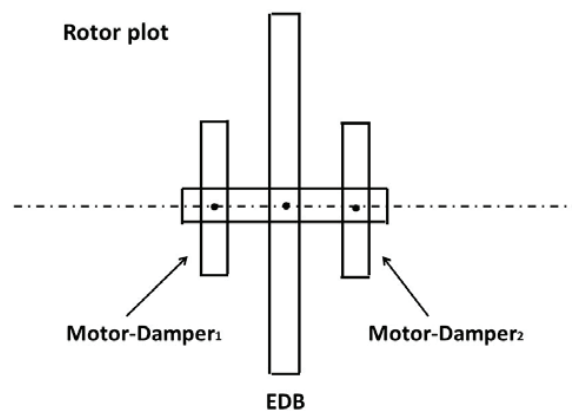
Figure 7:10 Configuration 2 using EDBs and the Motor-Damper structure.

7.4   Conclusion

The present chapter discussed about the damping strategies for EDB systems and also possible alternative damping solutions.

The EDB-AMD solution has been investigated in the present thesis and its effectiveness has been demonstrated. It is an ideal solution to overcome the instability of EDBs and also provides levitation from zero speed allowing the EDB's take off. However, it also increases the complexity and cost of the system, which also limits a bit the potential applications.

EDBs, as a type of passive magnetic bearings, show the possibility to achieve stable levitation using conductors and permanent magnets at room temperature, without introducing negative stiffness. Thus it would be very attractive if the instability issue of EDBs could be solved in passive ways.

That's another purpose of the present thesis, to investigate damping strategies and to see the possibility to reach stable levitation in a totally passive way.

Therefore, the EDB-damper model was built in the present chapter for stability analysis. Using this analytical model, the amount of non-rotating damping needed to keep the rotor in stable operation has been analyzed. It is useful to decide proper damping solution for EDBs.

The second contribution of the present chapter is that the possibility of using AMDs to realize general viscous dampers has been demonstrated. Therefore, the EDB-AMD system can be used to investigate possible passive damping solutions.

Besides, two possible damping solutions have also been presented. Passive eddy current damper could be very suitable, provided that the damper is properly designed and implemented, which opens the possibility of pure passive EDB suspension. A systematic approach for the modelling and identification of ECDs has also been proposed by the author, which makes the applications of ECD more convenient and efficient.

Semi-active magnetic dampers, using transformer eddy currents, present advantages over AMBs such as simplicity and lower cost. They also show the possibility to be combined with permanent magnet motors and then implemented in EDB systems. Thus semi-active magnetic dampers could be a possible solution for EDBs.

The work presented in this chapter could be very interesting for the future work in the field of EDB stabilization.

Chapter 8   Summary and Conclusions

8.1   Summary

The goal of the present thesis is to provide stabilizing solution to the rotor supported by Electro-dynamic Bearings (EDBs). It is well known that the rotating damping effect in EDBs causes instability issue, which limits the application of EDBs and thus has to be solved. Although some solutions have been presented by different researchers, the effectiveness of those proposed methods is still limited. This background highly motivated the present contribution.

The present thesis proposes a hybrid bearing configuration consisting of radial EDBs and radial Active Magnetic Bearings (AMBs). In this hybrid bearing system, AMBs are coupled to EDBs to provide stabilizing damping to the rotor, thus they work as Active Magnetic Dampers (AMDs). The aim of the research is to exploit the controllability of AMDs to stabilize the rotor supported by EDBs. At low speed, when the stiffness of EDB is not sufficient for levitation, the AMDs can also provide levitation and stabilization thus allowing stable levitation from zero speed, which can avoid complex mechanical structure to allow rotor take off as used in other EDB systems.

An analytical model has been built using a 4 DOF rotor model coupled with EDB and AMD models to study the rotordynamics and system stability. To validate the model, a dedicated test bench has been built. Experimental tests have been made to validate the numerical parameters and models. The effectiveness of AMDs has been demonstrated. Stable operation of the test rig is obtained with PD control in the AMDs. It confirms the feasibility of the EDB-AMD system. This is the first essential novelty of the present work: solving the instability issue of the rotor supported by EDBs with active magnetic damping.

 Based on the validated analytical model of the system, control strategies of AMDs have been discussed to set a reference of stability map, which is essential to define proper values of control parameters in AMDs.

Damping strategies for EDB systems are presented. Using the models of the rotor and EDBs of the test rig, the amount of non-rotating damping needed to keep the EDB system in stable operation has been obtained for different rotational speeds. It is useful to design and implement proper dampers for the EDB system. The same approach can be used to find damping solutions for a general EDB system. The EDB-AMD system has also been demonstrated to have the ability of realizing viscous dampers. Therefore, it can be used to investigate in a controlled laboratory environment a

damping strategy that could then find a passive implementation. This is another essential novelty of this work on the EDB-AMD system.

Two possible alternative damping solutions have been presented: eddy current dampers (ECDs) and semi-active magnetic dampers. ECDs can provide contactless damping in purely passive way. It can be implemented in EDB systems to provide stabilizing non-rotating damping and obtain stable levitation of rotors without active control. A systematic approach of modeling and identification of ECDs has been proposed by the author, which allows designing and identifying of ECDs in a more accurate and efficient way. Semi-active magnetic dampers are also able to introduce non-rotating damping to the rotors supported by EDBs. Compared to AMDs, semi-active magnetic dampers have simpler architecture and smaller size. The configuration of semi-active dampers shows possibility to be combined with permanent magnet motors (so called "Motor-Damper" structure), which is another important factor that makes them attractive for EDB systems. Two possible system configurations of EDB systems implemented with Motor-Damper structures have been presented, which show potential applications.

8.2   Outlook

At the end of the present thesis, based on the obtained results and solutions, some suggestions of future work are listed here:

1. "Smart control" of AMDs could be implemented. In the test rig of EDB-AMD system, a PD controller is used to control AMDs. The control parameters are fixed in the whole speed range during operation. However, it is clear that the stiffness from AMDs can be reduced with the increasing of rotational speed, because the stiffness contribution of EDBs increases accordingly. However, the required non-rotating damping increases when the rotor speeds up due to the increasing of rotating damping arising in the EDBs. Therefore, the control parameters could be changed in the speed range to obtain a more efficient control. This has been investigated in Chapter 6, which shows the stability map of the system in terms of stiffness and damping from AMDs. Therefore, the AMD stiffness and damping can be decided according to this stability map, the control parameters can be chosen accordingly.

2. Downsizing and simplifying of AMDs: as has been demonstrated in Chapter 5, the actuators in the AMDs can be downsized in this application. The whole architecture of AMDs could also be simplified. Since the AMDs are coupled with EDBs, which are a type of passive magnetic bearings, reducing of electronic components is meaningful. Thus further work on the EDB-AMD system could also be devoted in this aspect.

3. Realizing viscous dampers using AMDs experimentally: the possibility of this work has been discussed and demonstrated in Chapter 7. It can be very practical to investigate damping strategies for EDBs.

4. Optimization of supporting structure that allows EDBs to take off deserves some efforts. In EDB-AMD system, It is not an issue, since AMDs provides levitation from zero speed. However, if other

types of dampers are used in the EDB system, we have to face the fact that the rotor needs to be supported during its speed-up process. When the rotor arrives at a certain rotational speed, the supporting structure has to be disengaged. So far, in the existing radial EDB systems, the disen-gagement of the rotor supporting structure is performed manually. It is fine for laboratory proto-types but not acceptable for industrial applications. If this part of EDB systems could be improved, non-AMD dampers would become more appealing for EDBs. Thus EDBs may be more feasible for industrial applications.

References

[1] G. Schweitzer and E. Maslen, Magnetic bearings. Theory, design, and application to rotating machinery., Berlin: Springer-Verlag, 2009.

[2] S. Earnshaw, "On the nature of the molecular forces with regulate the constitution of the luminiferous ether," *Trans. Cambridge Phil. Soc.,* vol. 7, p. 97, 1839.

[3] P. Basore, "Passive stabilization of flywheel magnetic bearings," Master Thesis, Massachusetts Instisute of Techology, Cambridge, MA, 1980.

[4] R. Post and D. Ryutov, "Ambient-Temperature passive magnetic bearings: theory and design equations," *Proceedings of the Sixth International Symposium on Magnetic Bearings,* pp. 109-112, 1998.

[5] A. Filatov and E. Maslen, "Passive magnetic bearing for flywheel energy storage systems," *IEEE Transactions on Magnetics,* vol. 37, pp. 3913-3924, 2001.

[6] A. Tonoli, N. Amati, F. Impinna and J. G. Detoni, "A solution for the stabilization of electrodynamic bearings: Modeling and experimental validation," *Journal of Vibrations and Acoustics,* vol. 133, no. 2, p. 021004, 2011.

[7] J. G. Detoni, F. Impinna, N. Amati and A. Tonoli, "Stability of a four-degree-of-freedom rotor on homopolar electrodynamic passive magnetic bearings," *Proceedings of the Institution of Mechanical Engineers, Part I: Journal of Systems and Control Engineering,* vol. 230, no. 4, pp. 330-338, 2016.

[8] E. Laithwaite, "Electromagnetic levitation," *Electrical Engineers, Proceedings of the Institution of ,* no. 12, pp. 2361-2375, 1965.

[9] E. Laithwaite, «Linear electric machines- A personal view,» *Proceedings of the IEEE,* vol. 63, n° %12, pp. 250-290, 1975.

[10] "Maglev: How they're Getting Trains off the Ground," *Popular Science,* p. 135, 1973.

[11] L. Piggott and G. Nix, "Electromagnetic levitation of a conducting cylinder," *Proc IEE,* vol. 113, pp. 1229-1235, 1966.

[12] S. Iskierka, "Analysis of an induction bearing by the finite element method," *Arch fur Elektrotech,* vol. 6, pp. 375-380, 1984.

[13] J. Nikolajsen, "An AC electromagnetic bearing for flywhell energy storage in space," NASA Langley Research Center magnetic suspension technology workshop, Hampton, Virginia, USA, January 1993.

[14] J. Powell and G. Danby, "High speed transport by magnetically suspended trains," ASME Winter Annual Meeting, New York, 1966.

[15] J. Detoni, "Progress on electrodynamic passive magnetic bearings for rotor levitation," *Proc IMechE Part C: J Mechanical Engineering Science,* vol. 228, no. 10, pp. 1829-1844, 2014.

[16] R. Post, D. Ryutov, J. Smith et e. a. , «Research on ambient-temperature passive magnetic bearings at the Lawrence Livermore national laboratory,» Proceedings of the MAG'97 industrial conference and exhibition on magnetic bearings, Alexandria, Virginia, USA, August 1997.

[17] D. Eichenberg, C. Gallo and W. Thompson, "Development and testing of a radial Halbach array magnetic bearing," Technical Report NASA/TM 2006-214447, Cleveland, OH: NASA -Glenn Research Center, 2006.

[18] Q. Cui, M. Di Napoli, J. G. Detoni, N. Amati and A. Tonoli, "A systematic approach for modeling and identification of eddy current dampers in rotordynamic applications," *The 15th International Symposium on Magnetic Bearings,* pp. 797-804, 3-6

August 2016.

[19] R. Herzog, P. Buhler, C. Gahler and R. Larsonneur, "Unbalance compensation using generalized notch filters in the multivariable feedback of magnetic bearings," *IEEE Transactions on Control Systems Technology,* vol. 4, no. 5, pp. 580-586, 1996.

[20] C. Murakami and I. Satoh, "Experiments of a very simple radial-passive bearing based on eddy currents," Proceedings of the 7th international symposium on magnetic bearings, Zurich, Switzerland, August 2000.

[21] A. Filatov and E. Maslen, "A passive magnetic bearing," *Proceedings of the 7th international symposium on magnetic bearings,* pp. 147-152, Zurich, Switzerland, 2000.

[22] J. Pinkerton, "Magnetic bearing and method utilizing movable closed conductive loops". Patent US Pantent 5302874, 1994.

[23] A. Filatov, P. McMullen, K. Davey and e. a. , "Flywheel energy storage system with homopolar electrodynamic magnetic bearing," *Proceedings of the 10th international symposium on magnetic bearings,* pp. 326-331, Martigny, Switzerland, 2006.

[24] R. Hill, "Teaching electrodynamic levitation theory," *IEEE Transactions on Education,* vol. 33, no. 4, pp. 346-354, 1990.

[25] R. Post, "Passive magnetic bearings for vehicular applications," Technical Report UCRL-ID_123451, Livermore, CA: Lawrence Livermore National Laboratory, 1996.

[26] J. Sandtner and H. Bleuler, "Electrodynamic passive magnetic bearings with planar Halbach arrays," *Proceedings of the 9th international symposium on magnetic bearings,* p. 5, Lexington, Kentucky, USA. August 2004.

[27] J. Sandtner and H. Bleuler, "Passive electrodynamic magnetic thrust bearing especially designed for constant speed applications," *Proceedings of the 10th international symposium on magnetic bearings,* pp. 483-487, Martigny, Switzerland, August 2006.

[28] F. Impinna, J. Detoni and N. Amati, "Axial electrodynamic suspension for a vertical axis rotor: modeling and experimental validation," *AIAS 40th National Meeting,* p. 113, Palermo, Italy, September 2011.

[29] T. Lembke, "Induction bearings- a homopolar concept for high speed machines," in *Technical Report ISSN 1650-674X,* Stockholm, Sweden: KTH-Royal Institute of Technology, 2003.

[30] T. Lembke, "3D-fem analysis of a low loss homopolar induction bearing," *Proceedings of the 9th international symposium on magnetic bearings,* p. 34, Lexington,Kentucky, USA, August 2004.

[31] V. Kluyskens, B. Dehez and H. Ben Ahmed, "Dynamical electromechanical model for magnetic bearings," *IEEE Transactions on Magnetics,* vol. 43, pp. 3287-3292, 2007.

[32] V. Kluyskens and B. Dehez, "Parameterized electromachanical model for magnetic bearings with induced currents," *Journal of System Design and Dynamics,* vol. 3, no. 4, pp. 453-461, 2009.

[33] V. Kluyskens and B. Dehez, "Dynamical electromechanical model for magnetic bearings subject to eddy currents," *IEEE Transactions on Magnetics,* vol. 49, pp. 1444-1452, 2013.

[34] V. Kluyskens and B. Dehez, "Analysis of the stability and the consumption of an electrodynamic bearing for different operation conditions," in *The 13th International Symposium on Magnetic Bearings*, Arlington, Virginia, USA, 2012.

[35] N. Amati, X. De Lepine and A. Tonoli, "Modeling of Electrodynamic Bearings," *Journal of Vibration and Acoustics,* vol. 130, p. 061007, 2008.

[36] A. El-Shafei and A. Dimitri, "Controlling journal bearing instability using active magnetic bearings," *Journal of Engineering for Gas Turbines and Power,* vol. 132, p. 012502, 2010.

[37] A. Looser and J. Kolar, "An active magnetic damper concept for stabilization of gas bearings in high-speed Permanent-Magnet machines," *IEEE Transactions on Industrial Electronics,* vol. 61, no. 6, pp. 3089-3098, 2014.

[38] A. Bonfitto, G. Botto, M. Chiaberge, L. Suarez Cabrera and A. Tonoli, "A multi-purpose control and power electronic architecture for active magnetic actuators," in *EPE-PEMC 2012 ECCE*, Novi Sad, Serbia, 2012.

[39] A. Tonoli, "Dynamic Characteristics of Eddy Current Dampers and Couplers," *Journal of Sound and Vibration,* vol. 301, pp. 576-591, 2007.

[40] J. Detoni, Q. CUI, N. Amati and A. Tonoli, "Modeling and evaluation of damping coefficient of eddy current dampers in rotordynamic applications," *Journal of Sound and Vibration,* vol. 373, pp. 52-65, 2016.

[41] M. Kasarda, R. Kirk, H. Mendoza and A. Wicks, "A experimental investigation of the effect of an active magnetic damper on reducing subsynchronous vibration in rotating machinery," in *ASME Turbo Expo 2005: Power for Land, Sea and Air*, Reno-Tahoe, Nevada, USA, 2005.

[42] T. Yamaguchi, Y. Kawase, H. Kodama et et al, «Eddy current damping analysis of laser marker using 3-D finite element method,» *IEEE transactions on magnetics,* vol. 42, n° %14, pp. 1011-1014, 2006.

[43] A. Tonoli, M. Silvagni et N. Amati, Electromechanical dampers for vibration control of structures and rotors, INTECH Open Access Publisher, 2010.

Appendix

A systematic approach of modeling and identification of ECDs in rotordynamics applications has been proposed by the author. It has been published in [18] [40], where the complete introduction, explanation and experimental validation have been presented. Here is a brief introduction.

The proposed method uses an analytical model of the Lorentz forces arising in the conductor in combination with a 3D FE model to obtain the radial damping properties of the ECD. The solution of the FE model is obtained under quasi–static conditions, thus being simple to implement, and fast to solve, in a variety of commercial FE software. Finally, the proposed method is validated experimentally showing very good accuracy for the calculation of electromechanical parameters and modelling of dynamic behaviour of an ECD.
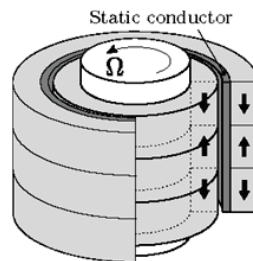

Figure A1 ECD with passive magnetic bearing

The analytical model of eddy current forces due to the relative motion of a conductor and a magnetic field has been discussed in Chapter 4. In this case the interaction can be studied with two reference frames, one fixed to the magnets, the other to the conductor.
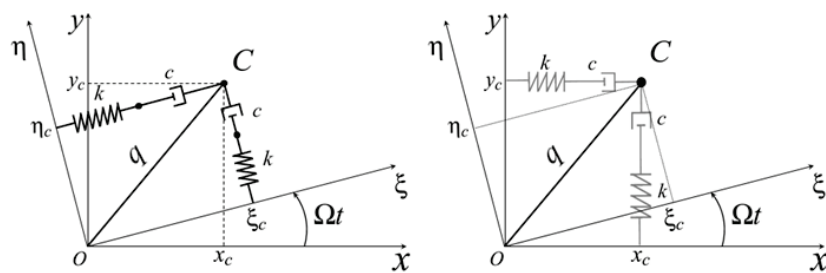
Figure A2 Equivalent mechanical representation of the eddy current force model in a conductor in relative motion about an axisymmetric magnetic field.

(a) The general model for a spinning conductor, usually used for electrodynamic bearings; (b) model for ECDs, where the magnetic field rotates whereas the conductor is static.

The schematic representation of this physical system is shown in Figure A2a. Points O and C give, respectively, the position of the axes of magnetic field and conductor. The reference frame (O, x, y) is fixed whereas (O, ξ, η) is a rotating reference frame that rotates with the same spin speed Ω as

the conductor. The pairs (x_c, y_c) and (ξ_c, η_c) are the coordinates of point C in the fixed and rotating reference frames, respectively. In Figure A2b, the magnetic field rotates whereas the conductor is fixed to the stator, which shows the specific model of an ECD.

Applying the method introduced in Chapter 4.2, the dynamic behavior of the eddy current forces generated by the conductor's spin and relative motion can be expressed as:

$$\dot{F} = k(\dot{q} - j\Omega q) - F(\omega_{RL} - j\Omega) \tag{A:1}$$

where Ω is the spin speed of the conductor and q represents its complex displacement. Equation (A:1) is linear and has constant parameters. It allows modeling dynamically the resistive and inductive effects on the eddy currents. Therefore the forces can be calculated provided that the equivalent electromechanical parameters k and c are known. For dynamic modeling of the forces produced by the ECD, Equation (A:2) must be rewritten for the non-spinning conductor ($\Omega=0$):

$$\dot{F} = k\dot{q} - F\omega_{RL} \tag{A:2}$$

For quasi-static condition, which means constant relative displacement ($q=q_0$=constant) and constant spin speed Ω, the force produced by eddy currents becomes:

$$F = \frac{k}{1+(\frac{\omega_{RL}}{\Omega})^2}q_0 - j\frac{c\Omega}{1+(\frac{\Omega}{\omega_{RL}})^2}q_0 \tag{A:3}$$

This force is proportional to the displacement and depends on the rotor spin speed. It can be observed that for values of Ω much lower than the frequency of the electric pole the real component of the force vanishes, and the imaginary component assumes the value:

$$F = -jc\Omega q_0 \tag{A:4}$$

Figure A3 shows how the forces evolve with increasing spin speeds and how the characteristics of their real and imaginary components can be exploited for the purpose of identification. The frequency of the electric pole ω_{RL} is clearly shown and can be used to identify the bandwidth of the damper. It shall be noted that the real component has an asymptote equal to kq_0 that represents a perfectly elastic force. This behavior can only be exploited at values of spin speed much higher than the electric pole frequency, and is of particular interest in the field of electrodynamic bearings. At low speeds, the slope of the imaginary component near zero is given by Equation (A:4). This equation can be used for the identification of the damping coefficient of the ECD, which behaves as a simple viscous damper for speeds much lower than the electric pole frequency.
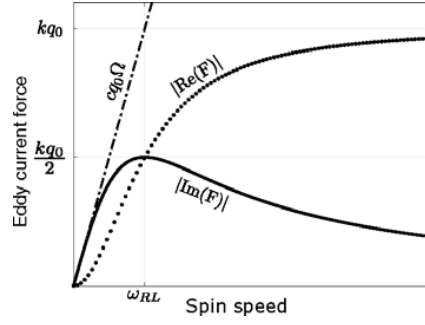
Figure A3 Eddy current forces with increasing the spin speed.

The solid line is the modulus of the force along x (real) and the dotted line is the modulus of the force along y (imaginary). The dash-dot line grows with the same slope as the imaginary component for $\Omega \ll \omega_{RL}$.

Quasi-static calculation with FE method is used to obtain the eddy current forces in ECDs. The same approach was used in Chapter 4 for the identification of EDBs. The quasi-static simulation was performed for a given Ω and by introducing a small eccentricity ε between the ECD magnets domain Γ_m and conductor domain Γ_c on the x direction, where $q_0 = \varepsilon$. Here q_0 is a real number, thus the Lorentz forces calculated by the FE can be directly compared to the forces of Equation (A:3). The real component gives the force along x whereas the imaginary component gives the force along y.
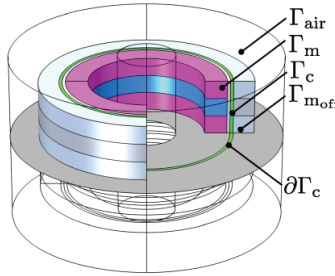

Figure A4 Three dimension model of a permanent magnet bearing equipped with an ECD.

The arrows indicate the different domains considered for simulation: Γ_{air} is the air surrounding the system, Γ_m are the rotor permanent magnets, Γ_c is the copper sleeve that acts as ECD, $\Gamma_{m_{off}}$ are the stator permanent magnets that are turned off for simulation, $\partial\Gamma_c$ boundary of the sleeve domain

For the identification of the ECD electromechanical parameters, it is necessary to calculate the Lorentz forces for n different values of conductor spin speed Ω. The identification of parameters k and c is performed using a curve fitting procedure. The errors between values calculated with Equation (A:3) and the FE model are minimized using the least squares approach. The function to be minimized is stated as:

$$S(k,c) = \sum_{i=1}^{n} \left(F_{Ltz_x i} - \mathrm{Re}(F_i) \right)^2 + \left(F_{Ltz_y i} - \mathrm{Im}(F_i) \right)^2 \quad (A:5)$$

Equation (A:5) is used to search for values of *k* and *c* that minimize the error between data and model for the forces in *x* and *y* directions contemporaneously. For the present analysis this nonlinear problem was solved using the MATLAB function fminimax.

If the frequencies of the lateral vibrations of the rotor are expected to be much lower than the electric pole frequency, it is reasonable to model the ECD as a simple viscous damper. Thus the damping coefficient *c* can be obtained from the results of the FE model using Equation (A:4) as:

$$c_s = -\frac{F_{Ltzy}}{\varepsilon\Omega} \qquad (A:6)$$

Using this equation, it is possible to calculate the damping coefficient from a single FE solution obtained for a low value of *Ω*. It is a very convenient method to obtain the damping coefficient.

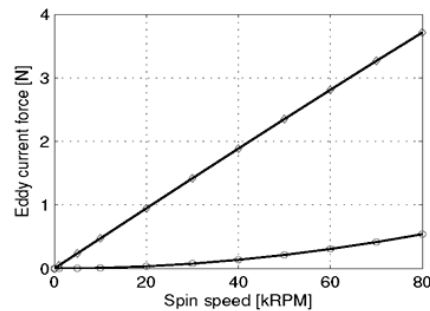Figure A5 shows the plot of eddy current force identification as presented in [18].

Figure A5 Eddy current force identification, comparison between identified model (solid lines) and finite element results (circular and diamond markers).

The present approach was validated experimentally with two different eddy current dampers in [40] [18].

.

Curriculum Vitae

PERSONAL INFORMATION & CONTACT

Name: Qingwen CUI

Date of Birth: December 13th, 1987

Place of Birth: Jiangsu, China

Nationality: Chinese

EDUCATION

2013— 2016   PhD in Robotics, Control, and Intelligent Systems,
               Swiss Federal Institute of Technology Lausanne (EPFL)

2010— 2012   Master of Science in Mechanical Engineering,
               Politecnico di Torino, Italy

2006— 2010   Bachelor of Engineering in Mechanical Engineering,
               Southeast University, Nanjing, P.R. China

2003— 2006   Jiangsu Hai'an Senior High School, Jiangsu, P.R. China

PROFESSIONAL EXPERIENCE

2013/09— 2015/01 Research Assistant in Laboratory of Robotic Systems, EPFL, Switzerland
               Research on magnetic bearings:
               Electrodynamic bearings, diamagnetic levitation and magnetic bearing system
               stabilizing methods.

2012/10— 2013/08 Research Assistant in Mechatronics Lab of Politecnico di Torino, Italy
               Research on magnetic bearings, 3D rotordynamics analysis and mechatronic
               systems.

PUBBLICATIONS

1. G. Genta, M. Silvagni, C. Qingwen, *Dynamic Analysis Of Rotors: Comparison Between the Simplified One-Dimensional Results and Those Obtained Through 3-D Modeling.* In: XXI Congresso nazionale AIMETA, Torino, September 2013.
2. Cui Q., Sandtner J., Bleuler H., *Whirl Imposer --- Proposal for a Novel Passive Magnetic Rotor Bearing System.* Proceedings of ISMB14, Linz, Austria, August 11-14, 2014.
3. J. G. Detoni, Q. Cui, N. Amati, A. Tonoli, *Modeling and evaluation of damping coefficient of eddy current dampers in rotordynamic applications.* Journal of Sound and Vibration(2016).

4. Q. Cui, F. Impinna, J. G. Detoni, N. Amati, A. Tonoli and H. Bleuler, *Simulations and experimental tests of electrodynamic bearings combined with active magnetic dampers*. AIM2016, Bormio, Italy, April14-16, 2016.
5. Q. Cui, F. Impinna, L. D. Suarez Cabrera, J. Detoni, N. Amati, A. Tonoli and H. Bleuler, *Dynamic characterization of electrodynamic bearings combined with active magnetic dampers*. The 15th International Symposium on Magnetic Bearings, August 3-6, 2016, Mojiko Hotel, Kitakyushu, Japan. pp 706-716.
6. Q. Cui, M. Di Napoli, J. G. Detoni, N. Amati and A. Tonoli, *A systematic approach for modeling and identification of eddy current dampers in rotordynamic applications.* The 15th International Symposium on Magnetic Bearings, August 3-6, 2016, Mojiko Hotel, Kitakyushu, Japan. pp 797-804.

AWARDS

2014   Best Presentation Award, 2014 GMSI (the Graduate Program for Mechanical Systems Innovation) and GSDM (the Global Leader program for Social Design and Management) Summer Camp, University of Tokyo, Japan

2008   Third Prize of the Mechanical Design Contest of Southeast University

2007   Excellent School Student Leader of Southeast University

SCHOLARSHIP

2016   Research Scholarship from DIMEAS Politecnico di Torino

2010   Scholarship from China Scholarship Council

2007   The Chinese National Scholarship for undergraduates